SEMIEMPIRICAL AND PROCESS-BASED GLOBAL SEA LEVEL PROJECTIONS

John C. Moore,[1,2,3] Aslak Grinsted,[1,4] Thomas Zwinger,[1,5] and Svetlana Jevrejeva[1,6]

Received 19 July 2012; revised 4 June 2013; accepted 6 June 2013.

[1] We review the two main approaches to estimating sea level rise over the coming century: physically plausible models of reduced complexity that exploit statistical relationships between sea level and climate forcing, and more complex physics-based models of the separate elements of the sea level budget. Previously, estimates of future sea level rise from semiempirical models were considerably larger than those from process-based models. However, we show that the most recent estimates of sea level rise by 2100 using both methods have converged, but largely through increased contributions and uncertainties in process-based model estimates of ice sheets mass loss. Hence, we focus in this paper on ice sheet flow as this has the largest potential to contribute to sea level rise. Progress has been made in ice dynamics, ice stream flow, grounding line migration, and integration of ice sheet models with high-resolution climate models. Calving physics remains an important and difficult modeling issue. Mountain glaciers, numbering hundreds of thousands, must be modeled by extensive statistical extrapolation from a much smaller calibration data set. Rugged topography creates problems in process-based mass balance simulations forced by regional climate models with resolutions 10–100 times larger than the glaciers. Semiempirical models balance increasing numbers of parameters with the choice of noise model for the observations to avoid overfitting the highly autocorrelated sea level data. All models face difficulty in separating out non-climate-driven sea level rise (e.g., groundwater extraction) and long-term disequilibria in the present-day cryosphere-sea level system.

Citation: Moore, J. C., A. Grinsted, T. Zwinger, and S. Jevrejeva (2013), Semiempirical and process-based global sea level projections, *Rev. Geophys.*, *51*, doi:10.1002/rog.20015.

1. INTRODUCTION

[2] Sea level rise is interdisciplinary both in terms of its causes and with respect to users of projections. An early adopter of semiempirical sea level prediction was General Dwight Eisenhower who relied on tidal predictions from a mechanical computer for setting the dates of the D-Day landings on beaches in Normandy in 1944 [*Parker*, 2011]. Considerably earlier, the Chinese used empirical predictions of tidal bores in the Qiantang River that were based on correlations between water level and lunar and solar positions for navigation purposes. They are considered accurate to the day; originally carved on stone, they were later copied and published in 1252 [*Yang et al*., 1989]. In this paper, we are dealing with much more difficult and long-term projections than these pioneers—the projected impact of warming on glaciers and ice sheets and hence on sea level over the coming century.

[3] The majority (about 84%) of energy increase of the planet over the last 40 years has been absorbed by the oceans, with a further 7% absorbed by ice [*Levitus et al*., 2005]. Thus, the linked ocean-cryosphere system is by far the largest heat reservoir associated with global climate change. Sea level is a useful diagnostic of this system and is also an important climate impact, since hundreds of millions of people live within 1 m of high tide [*Anthoff et al*., 2006].

[4] To date, there are two methods of estimating sea level rise as a function of climate forcing. The conventional approach, used in Intergovernmental Panel on Climate Change (IPCC) climate assessments, is to use "process-based" models to estimate contributions from the sea level components such as thermal expansion and melting from glaciers and the dynamics of ice sheets, and then simply sum them up [*Meehl et al*., 2007a, 2007b; *Pardaens et al*., 2011; *Solomon et al*., 2009]. Semiempirical models, in contrast, extract statistical relationships using physically plausible

[1]State Key Laboratory of Earth Surface Processes and Resource Ecology, College of Global Change and Earth System Science, Beijing Normal University, Beijing, China.
[2]Arctic Centre, University of Lapland, Rovaniemi, Finland.
[3]Department of Earth Sciences, Uppsala University, Uppsala, Sweden.
[4]Centre for Ice and Climate, Niels Bohr Institute, University of Copenhagen, Copenhagen, Denmark.
[5]CSC-IT Center for Science Ltd., Espoo, Finland.
[6]National Oceanography Centre, Liverpool, UK.

Corresponding author: J. C. Moore, State Key Laboratory of Earth Surface Processes and Resource Ecology, College of Global Change and Earth System Science, Beijing Normal University, 19 Xinjiekou Wai St., Beijing 100875, China. (john.moore.bnu@gmail.com)

8755-1209/13/10.1002/rog.20015
Paper number 2012RG000411

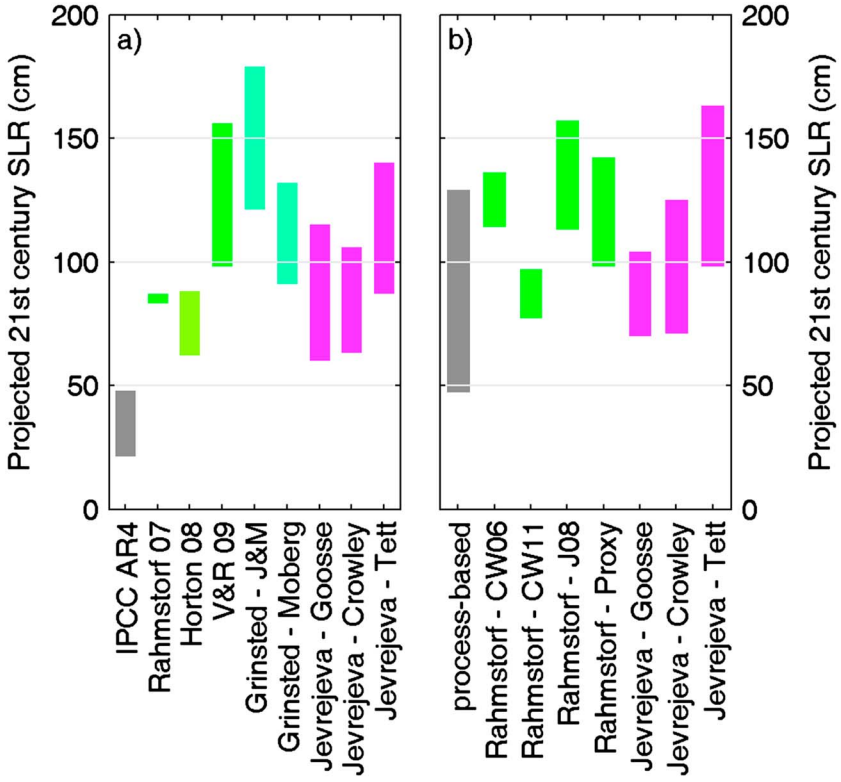

Figure 1. (a) Sea level projections (5–95%) by 2100 for semiempirical models driven by the A1B SRES scenario compared with the IPCC AR4 projection without ice sheet discharge (gray bar) [*Meehl et al*., 2007a, 2007b, Table 10.7]. Differences between semiempirical models are due to differences in both the forcing used to drive some models, and the calibration data sets of past forcing used to derive the model parameters. Green-hued bars are from semiempirical models with global surface temperature as forcing and pink-hued bars use radiative forcing. The data sets from left to right: *Rahmstorf* [2007a] based on projections in IPCC TAR, only central value is available; *Horton et al*. [2008] the *Rahmstorf* [2007a] model forced with input from 11 IPCC AR4 climate models; *Vermeer and Rahmstorf* [2009]; *Grinsted et al*. [2010] with *Jones and Mann* [2004] temperature reconstruction for calibration; *Grinsted et al*. [2010] with *Moberg et al*. [2005] as calibration; *Jevrejeva et al*. [2010] with *Goosse et al*. [2005] radiative forcing for calibration; *Jevrejeva et al*. [2010] with *Crowley et al*. [2003] as calibration; *Jevrejeva et al*. [2010] with *Tett et al*. [2007] as calibration. (b) Sea level projections (5–95%) by 2100 for semiempirical models driven by the RCP8.5 scenario compared with the process-based projections. Process-based (gray bar) includes estimates for thermal expansion of 28 cm [*Yin*, 2012]; 18–21 cm for glaciers [*Radic and Hock*, 2011; *Marzeion et al*., 2012]; −3 to 14 cm for Antarctica [*Bindschadler et al*., 2013]; 4–66 cm for Greenland [*Bindschadler et al*., 2013]. Semiempirical estimates are (left to right) for *Rahmstorf et al*. [2011] with *Church and White*, [2006] sea level data for calibration; *Rahmstorf et al*. [2011] with *Church and White* [2011] sea level data for calibration; *Rahmstorf et al*. [2011] with *Jevrejeva et al*. [2006] sea level data for calibration; *Rahmstorf et al*. [2011] with *Kemp et al*. [2011a] sea level proxy data for calibration; *Jevrejeva et al*. [2012a] with *Goosse et al*. [2005] radiative forcing for calibration; *Jevrejeva et al*. [2012a] with *Crowley et al*. [2003] radiative forcing data for calibration; *Jevrejeva et al*. [2012a] with *Tett et al*. [2007] radiative forcing for calibration.

models of reduced complexity where sea level responds to histories of global temperature [*Rahmstorf*, 2007a; *Vermeer and Rahmstorf*, 2009; *Grinsted et al*., 2010; *Kemp et al*., 2011a] or radiative forcing [*Jevrejeva et al*., 2009; *Jevrejeva et al*., 2010]. By physically plausible, we mean that the models rely on formulations that relate a forcing from climate to a proportionate response of the sea level system with some characteristic response time(s). All semiempirical models project higher sea level rise for the 21st century than those from the last generation of process models summarized in the IPCC Fourth Assessment Report (AR4; Figure 1). We would have much better confidence in sea level rise projections if the two approaches could be reconciled—and as can be seen in Figure 1b that has been achieved, though obviously much of the agreement is now because of large uncertainties as well as an upward shift in estimates from process-based models.

[5] The need for a better understanding of causes of sea level rise was illustrated in the IPCC Fourth Assessment Report (AR4): "Dynamical processes related to ice flow not included in current models but suggested by recent observations could increase the vulnerability of the ice sheets to warming, increasing future sea level rise. Understanding of these processes is limited and there is no consensus on their

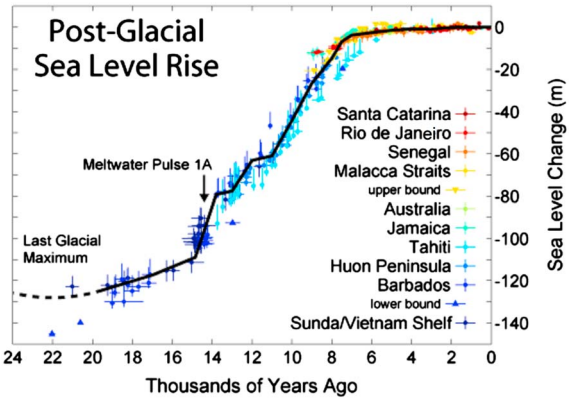

Figure 2. History of sea level rise since the Last Glacial Maximum from paleo sources [*Fleming et al*., 1998; *Milne et al*., 2005] downloaded from http://upload.wikimedia.org/wikipedia/commons/1/1d/Post-Glacial_Sea_Level.png.

magnitude." [*Intergovernmental Panel on Climate Change* (*IPCC*), 2007]. There is clearly a time lag between climate change and response of the cryosphere-sea level system. *Douglas* [1992] argued that *acceleration* in observed global sea level rise needed at least 50 years of observations to be significant; otherwise, it was merely short-term variation. Hence, if we were to rely purely on sea level observations to diagnose an accelerating climate impact on the cryosphere, it would require decades before it becomes unequivocal. Thus, it is very important that we have reliable process-based models of sea level rise that can be used by policy makers. This led to the European Union (EU) and U.S. funding initiatives on sea level rise (ice2sea: www.ice2sea.eu and SeaRISE: websrv.cs.umt.edu/isis/index.php/SeaRISE_Assessment) that focus primarily on ice sheet dynamical contributions to sea level rise.

[6] While sea level change relative to coastline has long been obvious (e.g., through features such as raised beaches or drowned terrestrial environments), separating the relative vertical movement of the land from a change in the mean global sea level was, and remains, a significant challenge [*Thomas et al*., 2011]. It is now known from evidence such as coral reefs that sea levels have risen globally by about 130 m since the Last Glacial Maximum some 20,000 years B.P. [*Lambeck and Chappell*, 2001; *Peltier and Fairbanks*, 2006, *Rohling et al*., 2009]. The isostatic adjustment of the land that followed the removal of the continental ice sheets produced large vertical motions over much of the planet. Some of that change occurred rapidly following deglaciation, but the high viscosity of the mantle means that isostatic rebound will be significant for at least another 10,000 years [*Peltier*, 1998]. The global pattern of vertical land movement is required to adequately describe the overall picture of historical sea level rise and is also of great significance in determining the regional impact of continued deglaciation and sea level rise in the future [*Milne et al*., 2009]. In this paper, we do not discuss changes in sea level caused by the changing shape of the oceans. While this was important during deglaciation (e.g., in the formation of the Baltic Sea), the changes in geometry of the ocean basins today cannot significantly affect global sea level on timescales of centuries [*Lambeck and Chappell*, 2001]. Hence, a conversion of ocean mass to sea level rise change requires, to a good approximation, only the density structure of the oceans to be determined.

[7] For much of the last 6000 years, the rate of sea level rise (Figure 2) has been steadily reducing [*Fleming et al*., 1998] as the result of isostatic adjustment [*Lambeck and Chappell*, 2001] and the approach toward an equilibrium ice volume for Holocene temperatures [*Rohling et al*., 2009]. Evidence from salt marsh proxies spanning up to the last 2000 years [*Kemp et al*., 2011a] suggests that global sea level passed through a minimum at the end of the Little Ice Age (LIA, 1350–1850). The LIA was a period of generally widespread cooling [*Le Treut et al*., 2007] when many glaciers were at their greatest extent (the Neoglacial) of the Holocene [*Oerlemans*, 2005]. Indeed, there is observational evidence from long-duration tide gauge records such as Amsterdam [*van Veen*, 1945], Stockholm [*Ekman*, 1988], Liverpool [*Woodworth*, 1999], and global-reconstructed sea level [*Jevrejeva et al*., 2008] that sea level once again began rising following the ending of the LIA around the middle to late nineteenth century. Since sea level inevitably lags behind climate forcing due to the considerable response time of the ocean and ice system, it is clear that in a sustained period of rising temperatures, sea level will continue to react to the past accumulated temperature rises until it reaches a new equilibrium. Hence, we are clearly committed to ongoing sea level rise—the important questions are how fast the rise will be, and what can be done to mitigate long-term sea level rise.

[8] Sea level varies on all time and space scales over which it has been measured: The highest-resolution tide gauge data exist at subminute resolution, and satellite altimetry has a spatial footprint of about 10 km. Much of the high-frequency and fine-scale variability is not related to climate change. The dominant multiannual variations are due to the El Niño–Southern Oscillation (ENSO), with roughly 2.2–5 year band of variability which can impact global sea level by about 10 mm [*Nerem et al*., 1999; *Jevrejeva et al*., 2006; *Church et al*., 2004]. Decadal variability in sea level contribution is possibly associated with the hydrological cycle [*Grinsted et al*., 2007], observational errors, and non-climate-driven changes in continental water storage contribution [*Wada et al*., 2010; *Chao et al*., 2008]. There is evidence that longer period variations also exist [*Unal and Ghil*, 1995; *Jevrejeva et al*., 2004, 2006, 2008; *Chambers et al*., 2012], though at much lower amplitude. It has also been postulated that the largest volcanic eruptions such as Krakatau (1883) caused multidecadal impacts on the heat content of the deep ocean that would have led to sea level falls [*Gleckler et al*., 2006]. These natural variations in sea level imply that the sustained global sea level rise of 3 mm yr^{-1} may, over periods of say 20 years or so, be dominated or reversed by ENSO or volcanic impacts. The cumulative effect of volcanic eruptions is to lower the sea level through their cooling effect, and *Jevrejeva et al*. [2009] estimated that sea level during the twentieth century was about 7 cm lower because of eruption activity than it would have been in its absence.

[9] As we have seen, our understanding via models has led to notable successes in explaining both broad features glacial-interglacial swings in sea level and the transient impacts

TABLE 1. Sea Level Budget for the Period Since 1955 From Different Studies

	Rate (mm/year)		
Contributors	IPCC AR4, 2007 (1961–2003)	*Moore et al.* [2010] (1955–2005)	*Church et al.* [2011] (1972–2008)
Thermosteric	0.42 ± 0.12	0.32	0.80 ± 0.15
Mountain glaciers	0.50 ± 0.18	1.0	0.67 ± 0.03
Greenland ice sheet	0.05 ± 0.12	0.28	0.12 ± 0.17
Antarctica ice sheet	0.14 ± 0.41	N/A	0.30 ± 0.20
Land water storage	N/A	N/A	-0.11 ± 0.19
Sum	1.1 ± 0.5	1.6	1.78 ± 0.36
Observed	1.8 ± 0.5	1.72	1.83 ± 0.18 (tide gauge only)

of volcanic eruptions; however, simulating the specific rates of change of sea level when driven by climate forcing expected in this century remains challenging. Here we discuss shortcomings in both process-based and semiempirical models and examine the ongoing and future lines of progress that can be made in identifying and modeling the key processes. Process-based model limitations include sparse observational data on grounding-line migration, the lack of realistic calving models, the largely unknown subshelf melting/aggregation distribution, and the poorly constrained basal drag and its spatiotemporal variability. Semiempirical difficulties include potential overfitting to limited observations and long-term nonclimate-related sea level rise contaminating the calibration—an analogous situation to the spin-up issue in ice sheet models. Both types of models may be adversely affected by climate regime change in different ways: Semiempirical models rely on the future being similar as the past, while process models need to include physical processes that may become important in the future. First, we summarize the components of the sea level budget and the observational constraints that determine key parameters in the models, then we introduce process and semiempirical models. Finally, we discuss specific model issues and opportunities for future advances in understanding.

2. OBSERVED COMPONENTS OF SEA LEVEL

[10] We can describe the total sea level budget as a sum of contributions from various terms. However, since there is no unique reference level for sea level, S, it is common to describe the rates of change of budget components which then sum to the total rate of sea level change over time, $\mathrm{d}S/\mathrm{d}t$. Total sea level is then given as an integral over time with an arbitrary integration constant. We then have

$$\frac{\mathrm{d}S}{\mathrm{d}t} = \frac{\mathrm{d}(S_T + Mg + Gis + Ais + S_{nc})}{\mathrm{d}t}, \qquad (1)$$

where S_T is the contribution from thermosteric expansion of ocean water, Mg is from mountain glaciers and ice caps, Gis from Greenland ice sheet, and Ais from Antarctic ice sheet mass losses. S_{nc} is a nonclimate source of sea level rise, for example, from building dams and extracting groundwater.

[11] The global sea level budget has been analyzed for 1910–1990 in the IPCC Third Assessment Report (TAR) [*Church et al.*, 2001] and for 1961–2003 in the IPCC AR4 [*Bindoff et al.*, 2007], and the individual contributions sum to less than the observed rate of sea level rise. For example, the AR4 assessed the mean observational rate for 1961–2003 as $1.8 \pm 0.5\ \mathrm{mm\ yr^{-1}}$ and the sum of the budget terms as $1.1 \pm 0.5\ \mathrm{mm\ yr^{-1}}$ [*Bindoff et al.*, 2007; *Hegerl et al.*, 2007]. However, the quoted uncertainties for these estimates are large enough that the differences are not significant at the 95% level.

[12] Over the past few decades, there has been considerable progress in quantifying the contributions from these components using various in situ and satellite data sets. The observed budget of sea level change can be conveniently separated into the modern observational period spanning the last 50 years (since ~1955–1960) and the overlapping satellite era (beginning in 1993). Most recent studies [e.g., *Cazenave and Llovel*, 2010; *Church et al.*, 2011] show that the sea level budget since 1993 can be closed within uncertainties, explaining an observed sea level rise of $3.2\ \mathrm{mm\ yr^{-1}}$ with contributions from glaciers melting, thermal expansion of the ocean, melting of the Greenland and Antarctic ice sheets, and the land water storage (groundwater mining combined with storage in artificial reservoirs). For the period since 1955, the sea level budget could be closed by climate-related contributors alone [*Moore et al.*, 2011], and since 1971 with a small -0.1 ± 0.2 mm/yr contribution from change in land water storage [*Church et al.*, 2011], as shown in Table 1.

[13] Thermosteric sea level change is estimated from various historical shipboard measurements (ocean station data, expendable bathythermographs, etc.) since 1955 [*Levitus et al.*, 2009; *Ishii and Kimoto*, 2009] and by the Argo profiling floats after 2000 [*Roemmich et al.*, 2010]. Although both data sets have suffered from issues related to instrument calibration [*Gouretski and Koltermann*, 2007], time series of corrected thermosteric sea level change since 1955 show that upper ocean warming accounts for about $0.54 \pm 0.05\ \mathrm{mm\ yr^{-1}}$ of sea level rise for the 0–2000 m layer and $0.41 \pm 0.04\ \mathrm{mm\ yr^{-1}}$ for the 0–700 m layer [*Levitus et al.*, 2012]. Due to lack of data in the Southern Hemisphere and in the deep ocean (below 700 m), this estimate is likely a lower bound. *Domingues et al.* [2008] estimated the thermosteric rate to be $0.5 \pm 0.1\ \mathrm{mm\ yr^{-1}}$ since 1960, while *Church et al.* [2011] estimated it to be $0.7 \pm 0.2\ \mathrm{mm\ yr^{-1}}$ for 1961–2008 including the updated deep ocean contribution from *Purkey and Johnson* [2010]. Since 1993, thermosteric sea level accounts for $\sim 1.0 \pm 0.3\ \mathrm{mm\ yr^{-1}}$, hence about 30% of the observed sea level rise [*Cazenave and Llovel*, 2010; *Church et al.*, 2011].

[14] The AR4 estimated that the glacier and ice cap contribution to sea level rise is $0.50 \pm 0.18\ \mathrm{mm\ yr^{-1}}$ over the period

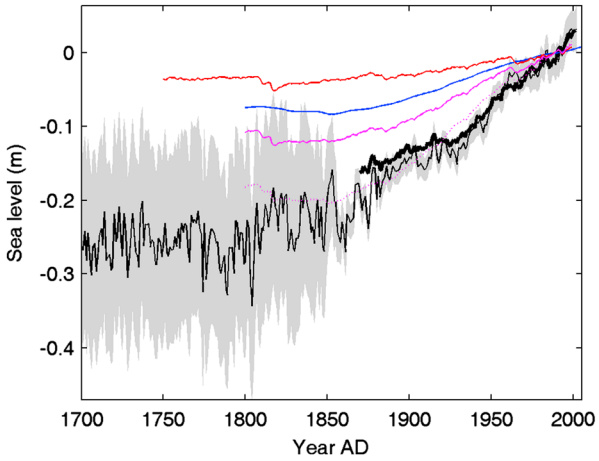

Figure 3. Sea level rise since 1700 (thin black line) reconstructed from tide gauges with 95% confidence interval (gray band) [*Jevrejeva et al.*, 2008]; sea level reconstruction from *Church and White* [2011] (thick black line); steric sea level simulated by AOGCM (red) [*Gregory et al.*, 2006]; contribution from melting from glaciers (blue) [*Leclercq et al.*, 2011] steric + contribution from glaciers (magenta). The dotted magenta line is calculated as (steric + 2 times glaciers). The curves are all referenced to the mean 1980–1999 sea level used as the reference.

1961–2003 and $0.77 \pm 0.22\,\mathrm{mm\,yr^{-1}}$ over the period 1993–2003 [*Lemke et al.*, 2007]. More recent estimates include $1.0 \pm 0.2\,\mathrm{mm\,yr^{-1}}$ for 2001–2004 [*Kaser et al.*, 2006], $1.4 \pm 0.2\,\mathrm{mm\,yr^{-1}}$ for 2001–2005 [*Cogley*, 2009], and $0.41 \pm 0.08\,\mathrm{mm\,yr^{-1}}$ for 2003–2010 excluding the Greenland and Antarctic peripheral glaciers and ice caps [*Jacob et al.*, 2012].

[15] Knowledge of the contribution of the Greenland and Antarctic ice sheets to sea level change comes from a variety of sources. For the last two decades, different remote sensing techniques (radar and laser airborne and satellite altimetry, interferometric synthetic aperture radar, and GRACE satellite gravity) have allowed systematic monitoring of the mass balance of the ice sheets [e.g., *Velicogna*, 2009; *Sørensen et al.*, 2011]. The Greenland and Antarctic contributions to sea level rise are estimated at $0.11 \pm 0.17\,\mathrm{mm\,yr^{-1}}$ and $0.25 \pm 0.20\,\mathrm{mm\,yr^{-1}}$, respectively, over 1961–2008, and $0.31 \pm 0.17\,\mathrm{mm\,yr^{-1}}$ and $0.43 \pm 0.20\,\mathrm{mm\,yr^{-1}}$ over 1993–2010 [*Church et al.*, 2011].

[16] Due to a lack of observations, estimates of land water storage changes over the past two decades rely on global hydrological models. Model-based studies [*Milly et al.*, 2003; *Ngo-Duc et al.*, 2005] found no long-term climatic trend in total water storage. In addition, several studies have discussed how direct human intervention on land water storage has induced sea level change [*Gornitz*, 2001; *Huntington*, 2008; *Milly et al.*, 2010, *Lettenmaier and Milly*, 2009]. *Wada et al.* [2010] suggest a contribution of $0.8 \pm 0.1\,\mathrm{mm\,yr^{-1}}$ to sea level rise since 1960. *Milly et al.* [2010] and *Konikow* [2011] provide a considerably lower value of 0.2–0.3 $\mathrm{mm\,yr^{-1}}$ for the sea level rise at recent years. *Church et al.* [2011] estimated the net effect of land water storage contribution of $-0.2 \pm 0.2\,\mathrm{mm\,yr^{-1}}$ over 1972–2008.

[17] Prior to 1955, physical processes which could account for sea level rise are not well documented [*Church et al.*, 2001; *Moore et al.*, 2011; *Gregory et al.*, 2012]. Reconstructions of glacier melting contributions extend to the 1800s [*Cogley*, 2009; *Oerlemans et al.*, 2007; *Leclercq et al.*, 2011]. Steric sea level is available from coupled ocean-atmosphere climate model (AOGCM) runs since 1750 [e.g., *Gregory et al.*, 2006] or even longer [*Von Storch et al.*, 2008]. Using the mountiain glacier and thermostric estimates now available for the sea level budget since the 1850s, *Moore et al.* [2011] suggested a large, residual sea level rise component of about 0.6 $\mathrm{mm\,yr^{-1}}$ or 40% of observed global sea level rise. This may be due to a nonclimate-related trend or alternatively, an ice sheet contribution correlated with, and of the same magnitude, as small glaciers, as illustrated in Figure 3. Support for a long-term ice sheet contribution comes from *Mitrovica et al.* [2001] who estimated a contribution from Greenland of 0.6 $\mathrm{mm\,yr^{-1}}$ through the twentieth century on the basis of the regional pattern of global sea level rise from tide gauge stations in comparison with models of regional patterns expected from mass loss from Antarctica and mountain glaciers.

3. OBSERVATIONAL CONSTRAINTS ON MODELS

[18] The models of future sea level rise that we will discuss in detail in sections 4 and 5 rely on estimating parameters that must be constrained by observational data based on present-day sea level and its record of change over timescales as long as glacial cycles. Additionally, models that predict the future state of the cryosphere should be capable of producing a realistic pattern of its evolution over the last few centuries. Ensuring that models match present-day ice sheet geometries and velocity patterns through inversion or ensemble culling will not ensure a realistic future response. A better approach would be to calibrate/invert models to match the temporal evolution rather than enforcing a match to a present-day snapshot.

3.1. Total Sea Level Rise

[19] Constraints on total sea level are relevant primarily for semiempirical models in that they limit the range of parameter space that can be explored. This is crucial in extracting maximum information from the inherently highly autocorrelated sea level observations. The constraints include the following:

[20] 1. Only positive response times (v) are meaningful and causal; that is, temperature must drive sea level not vice versa.

[21] 2. Sea level over the twentieth century was rising so we are already out of equilibrium with forcing (Figure 3).

[22] 3. In the Last Interglacial (LIG), polar temperatures inferred from deep ice cores were 3–5°C warmer than present and sea level was 6–10 m higher [*Kopp et al.*, 2009]. While the LIG climate was different from that expected in the future, there are sufficient similarities for it to be a partial analogue: Polar amplification caused polar temperatures to rise 2–4°C more than the global average, while increased seasonality increased summer melt in the Arctic. Polar amplification is observed in the Arctic, and the presence of anthropogenic aerosols is also contributing to increased summer melt [*Ramanathan and Carmichael*, 2008]. Hence, a weak

constraint is that climate stabilization at present-day temperatures results in an equilibrium response of less than 10 m.

[23] 4. The sensitivity (or long-term equilibrium response to a unit change in forcing) must covary with total ice volume since the fluxes in and out of an ice sheet are dependent on the ice area (though of course, distance to precipitation source and many other conditions affect mass flux). Present-day ice volume is only one third of that in the Last Glacial Maximum and so the value that is applicable for the present ice sheet configuration is probably significantly smaller than that derived from glacial cycles, and the sensitivity derived from glacial-interglacial values can provide an upper bound. *Rohling et al*. [2009] estimated a glacial sensitivity of about $11\,m\,°C^{-1}$ using paleoproxies for sea level from Red Sea and Antarctic temperatures, and about half that sensitivity for interglacial climate.

[24] 5. A naïve estimate of sensitivity can be obtained by considering that over the last 150 years, there has been ~0.3 m of sea level rise (Figure 3) and ~0.8°C warming [e.g., *Jones and Mann*, 2004; *Moberg et al*., 2005], giving ~0.4 m/°C. This must be considered a lower limit as sea level has not yet fully responded to the recent warming. The equilibrium sea level change from thermal expansion alone has been estimated to be ~0.2–0.6 m/°C [*Meehl et al*., 2007b].

[25] 6. Constraints from millennial-scale sea level variability include Mediterranean archaeological data [*Sivan et al*., 2004], salt marsh records from New England [*Gehrels et al*., 2005], and corals from South Cook Islands [*Gehrels et al*., 2011] that suggest sea level has been falling for much of the last millennium. Differences between sites on these timescales can be attributed to glacial isostatic adjustment (GIA). Looking at sites with well-constrained GIA shows that centennial variations in North Atlantic sea level have not exceeded ±0.25 m from 2000 to 100 years before present. For the Mediterranean, sea level may have fallen 0.5 m over the last 1000 years [*Toker et al*., 2012]. *Kemp et al*. [2011a, 2011b], in contrast, shows a salt marsh record from North Carolina that indicates a continuous rising trend over the last 2000 years, with an acceleration over the past 300 years, although GIA correction appropriate for the site is disputed [*Grinsted et al*., 2011; *Kemp et al*., 2011b]. Globally, sea level has been more stable over the last 3000 years than during much of Holocene (Figure 2), with sea level at 2000 B.P. probably slightly lower than at present, but within 0.5 m of present-day levels [*Lambeck et al*., 2004]. The long-term stability in the preindustrial limits the plausible range of equilibrium sensitivities and thus acts as a particularly important constraint.

[26] Constraints 3–5 on the equilibrium response to a temperature change cannot be directly applied to models that use radiative forcing without a conversion of units. The additional uncertainty involved in this conversion weakens these constraints considerably. However, the sensitivity in the *Jevrejeva et al*. [2009] semiempirical model is efficiently constrained by constraint 6 alone.

3.2. Individual Component Observational Constraints

[27] The traditional method of estimating sea level rise relies on accurate estimates of each component that should sum to match the observed total sea level rise rate from satellites and tide gauges.

3.2.1. Steric Sea Level

[28] The steric sea level component has been well constrained by hydrographic observations of temperature and salinity since 1955 [*Levitus et al*., 2009; *Ishii and Kimoto*, 2009]. However, the data are mainly from the upper ocean, generally the upper 700 m. The average ocean depth is nearly 4 km, and few observations extending to the abyssal ocean below 4000 m depth have been made [*Purkey and Johnson*, 2010]. They estimate that the abyssal ocean contributes about $0.05\,mm\,yr^{-1}$ to sea level rise since 1990, but the pattern of warming is variable and some parts of the abyssal ocean are cooling [*Purkey and Johnson*, 2010]. The highest warming rate is from the deep ocean (1000–4000 m depth) south of the southern convergence and amounts to $0.09\,mm\,yr^{-1}$, though the Nordic Seas have also warmed in recent decades [*Karstensen et al*., 2005]. Hence, a minimum from the deep and abyssal ocean is $0.15\,mm\,yr^{-1}$. The much better data coverage over the upper ocean provides a total steric contribution of $0.54\,mm\,yr^{-1}$ over 1955–2010 [*Levitus et al*., 2012]. Glacial age data on noble gas concentrations in ice cores show that the mean global ocean temperature during the Last Glacial Maximum (LGM) was 2.7°C cooler than during the preindustrial [*Headly and Severinghaus*, 2007]. This corresponds to a steric rise of about 2 m, out of a total sea level rise change of 120 m since the LGM.

[29] The large inertia of the ocean system means that even if no further surface temperature increase occurred, sea level would continue to rise. *Yin* [2012] reports that even under Representative Concentration Pathway (RCP) 2.6 with almost immediate reductions in radiative forcing, sea levels rise by 13 and 21 cm by 2100 and 2300, respectively. Using the possibly more realistic scenarios RCP 4.5 and RCP 8.5 leads to 18 and 28 cm under at 2100, which then increases and to 52 and 119 cm by 2300 under the two scenarios [*Yin*, 2012]. A doubling of CO_2 over preindustrial levels leads to an eventual sea level rise of 0.5–2 m, while a $4 \times CO_2$ increase leads to twice that [*Church et al*., 2001] in Earth System Models of Intermediate Complexity, where perhaps only half the eventual full steric sea level rise occurs in the first 500 years. Comparing these rises with totals in Figure 1 shows that the steric contribution is known with reasonable confidence and contributes about 15–50% of the total by 2100.

3.2.2. Greenland

[30] Figure 4 illustrates the processes important to the mass balance of Greenland. Recent observations by satellite altimetry and gravity have revolutionized understanding of the state of balance of the polar ice sheets. Prior to that time, only sporadic and sparse field campaigns enabled only approximations of ice sheet mass balance [*Bjørk et al*., 2012] and the only estimates of the dynamic state of the ice sheet come from retreat rates of outlet glaciers. Most outlets in Greenland and essentially all in Antarctica are marine-terminating tidewater systems whose front positions do not have a simple relationship with climate forcing [*Cuffey and Paterson*, 2010]. Attempts at a leveling across Greenland were made in the

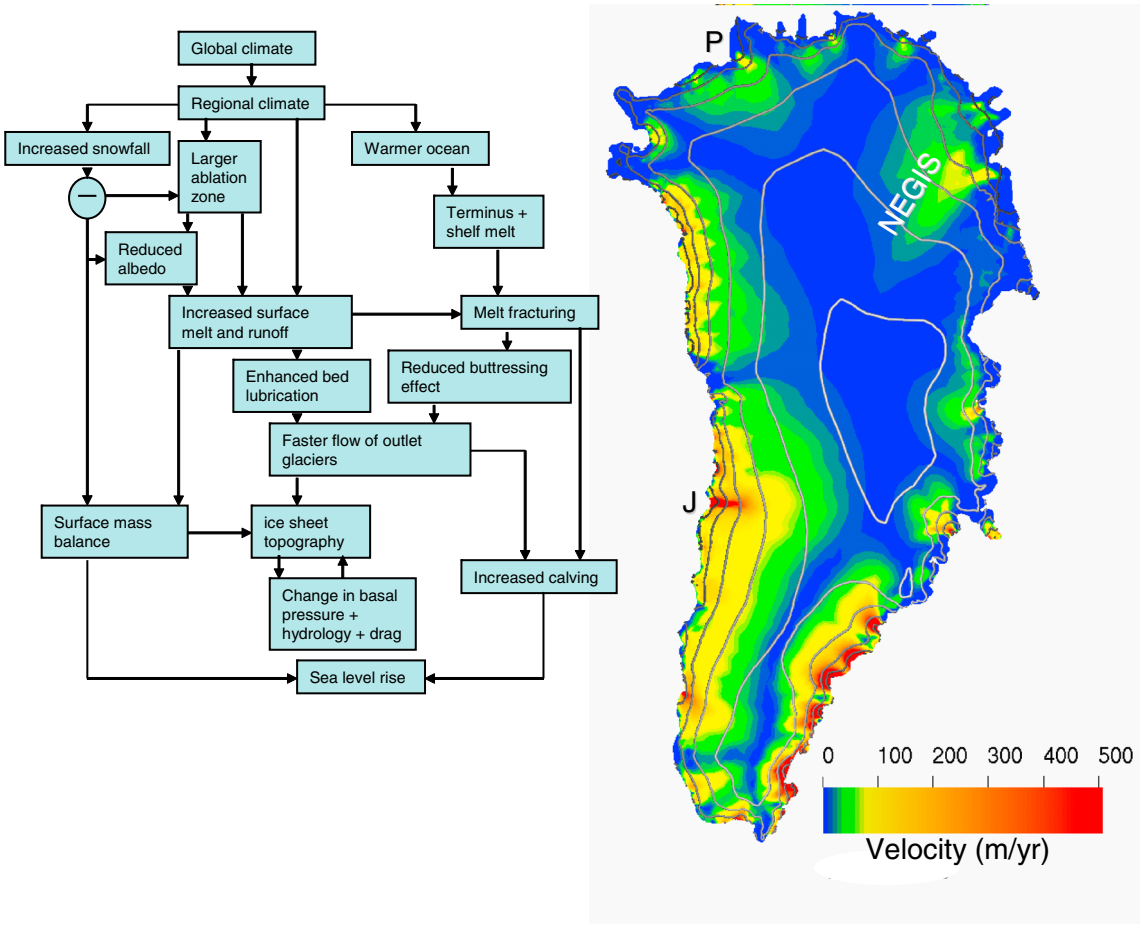

Figure 4. Greenland ice sheet showing velocity distribution from *Joughin et al.* [2010] with gaps filled by balance velocities of *Bamber et al.* [2001] J: Jakobshavn Isbræ, NEGIS: Northeast Greenland Ice Steam, P: Petermann glacier. Summary of factors affecting the Greenland ice sheet contribution to sea level rise based on *Cuffey and Paterson* [2010]. Note the relative importance and complexity of surface mass balance processes and the lesser importance of ocean warming relative to the Antarctic contribution in Figure 6.

1950s and 1960s and used to compute differences in ice sheet elevation across northern Greenland [*Paterson and Reeh*, 2001]. They report that the eastern side had experienced only small changes, while the west side had undergone significant thinning from 1954 to 1995. Surface mass balance estimates were commonly made by early expeditions but are considered to be of too short duration and affected by contamination from melt [*Ohmura and Reeh*, 1991] to be of great value in our context. Data became much more continuous and of higher quality following the International Geophysical Year in 1957–1958. Surface mass balance estimates were summarized by *Rignot et al.* [2008] and span the period from 1958 to the present. Estimates of mass balance based on reanalysis and regional climate models [*Wake et al.*, 2009] extend back to 1865 and estimates of glacier frontal position to 1933 [*Bjørk et al.*, 2012].

[31] Satellite and airborne laser altimetry provide a snapshot of the elevation of the ice sheet. To convert this to a mass balance change, a model of the density profile in the upper layers of the ice sheet must be made [*Sørensen et al.*, 2011]. Furthermore, the density profile must account for seasonal changes and any long-term changes perhaps due to rising temperatures [*Li and Zwally*, 2011]. Results tend to show thickening of the ice sheet above 1500 m elevation and thinning at lower elevations [*Johannessen et al.*, 2005; *Zwally et al.*, 2011]. More direct estimates of ice sheet mass balance come from the GRACE satellite [e.g., *Velicogna*, 2009]. *Khan et al.* [2010] showed mass loss spreading from southeast to northwest Greenland since 2003 with a doubling of mass loss rate by 2009. However, the mass loss estimate relies on having accurate measurements of crustal motion, which was done using precise GPS receivers on bedrock along the ice margin.

[32] Measurements of ice velocity using synthetic aperture radar imagery can be used to determine changes in flux through the marginal glaciers around Greenland. Several glaciers were shown to have speeded up by considerable fractions between 1995 and 2005 [*Rignot and Kanagaratnam*, 2006], with the pattern of mass loss through acceleration seeming to move northward over the decade of measurements. More recently, *Moon et al.* [2012] extended the analysis to more than 200 glaciers, finding a complex pattern of behavior with accelerating flow observed for marine-terminating glaciers, steady flow for ice shelf-terminating

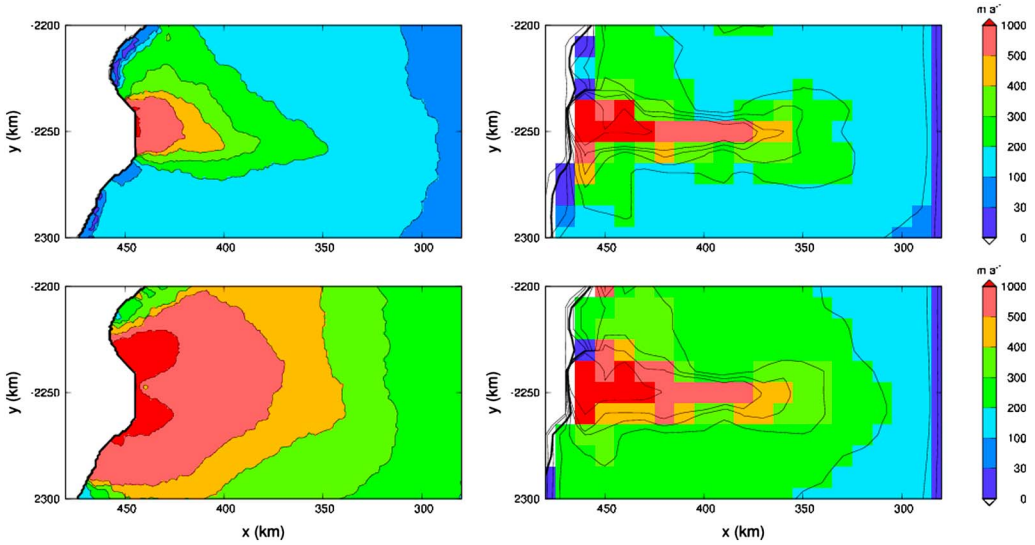

Figure 5. Surface velocities in the area of Jakobshavn Isbræ computed with a (top) surface climate forcing by the scenario A1B climate and (bottom) combined A1B forcing with doubled basal sliding year after 100 model years from present. (left) Elmer/Ice Full Stokes model and (right) SICOPOLIS, a SIA model. Note the stronger impact of basal sliding than surface mass balance, and the more focused velocities in the SIA model than FS due to lack of longitudinal stresses in the SIA model. The dynamical response to reduced basal drag is much stronger in the FS model than the SIA. The ELMER model grid is an unstructured mesh and has much high resolution than the uniform rectangular SICOPOLIS mesh in the fast flow region. Extracted from *Seddik et al*. [2012].

glaciers, and slowdown for the land-based ice tongues. There was a speedup observed for northwest glaciers, while southeast glaciers showed more variability between 2000 and 2010. This seems to be consistent with the observations of accelerating and northwestward spreading of mass loss from the GRACE data between 2003 and 2009 [*Khan et al*., 2010]. Interaction with the warming ocean has been postulated as the cause of this acceleration—based on the simultaneous increase in ocean temperatures along west Greenland in 1997 and acceleration of Jakobshavn Isbræ [*Holland et al*., 2008]. Projected changes in ocean temperatures during the 21st century [*Griffies et al*., 2011], showing that waters around Greenland will warm by about double the global mean, suggest that Greenland will become more sensitive to ocean-driven change than may be expected given the scenario in Figure 5.

[33] Evidence on long-term change in Greenland is crucial both to understand long-term response to climate forcing and to determine if long period responses to past climate change are presently important in the mass balance. The long-term response to deglaciation on Greenland [*Vinther et al*., 2009] demonstrates that the summit of Greenland lost elevation over the last 1500 years by about 30 m. The behavior is consistent with a marginal retreat of at least 100 km since the LGM. *Mitrovica et al*. [2001] suggested a continuous contribution from Greenland of 0.6 mm yr^{-1} during the twentieth century, equivalent to 6 cm in total or about 30% of total sea level rise during that time (Figure 3). This suggests that Greenland is still reacting to climate change millennia ago, and we may ask how much sea level rise we may eventually expect from Greenland in a warming world. The total sea level rise during the Eemian interglacial (115 kyr B.P.) was about 6 m [*Kopp et al*., 2009]. Analysis of Sr, Nd, and Pb isotopes in sediments indicates that southern Greenland was not completely deglaciated and only about 1.6–2.2 m of the global sea level rise came from Greenland [*Colville et al*., 2011], a result consistent with ice sheet elevation change inferred from an ice core to bedrock in north Greenland [*Dahl-Jensen et al*., 2013].

3.2.3. Antarctica

[34] Figure 6 shows the major processes involved in the mass balance of Antarctica. In contrast with Greenland, surface melting of the ice sheet is almost negligible, though for the peripheral ice caps and glaciers along the peninsula, it is significant [*Hock et al*., 2009]. The colder conditions on Antarctica mean that warming within the next century would, in a simplistic analysis, be expected to lead to a net lowering of sea level since warmer air can contain more moisture leading to greater precipitation over the ice sheet, while surface melting would remain negligible. However, this neglects any impact of warming on the dynamic interaction between ocean and ice which can, and has, led to large mass loss in some drainage basins over recent decades [*Wingham et al*., 2009]. Furthermore, ocean-ice interaction can occur via multiyear fast ice (that is, sea ice that is tens of meters thick), and which has been shown to be both changeable on short timescales and to influence ice shelves [*Massom et al*., 2010].

[35] *Velicogna* [2009] presented evidence from GRACE of increased mass loss rate from Antarctica, but the uncertain GIA casts much doubt on these conclusions. Subsequently, attempts were made to combine data from GRACE with ICESat elevation data [*Riva et al*., 2009] or ocean bottom pressure data [*Wu et al*., 2010] to constrain both GRACE

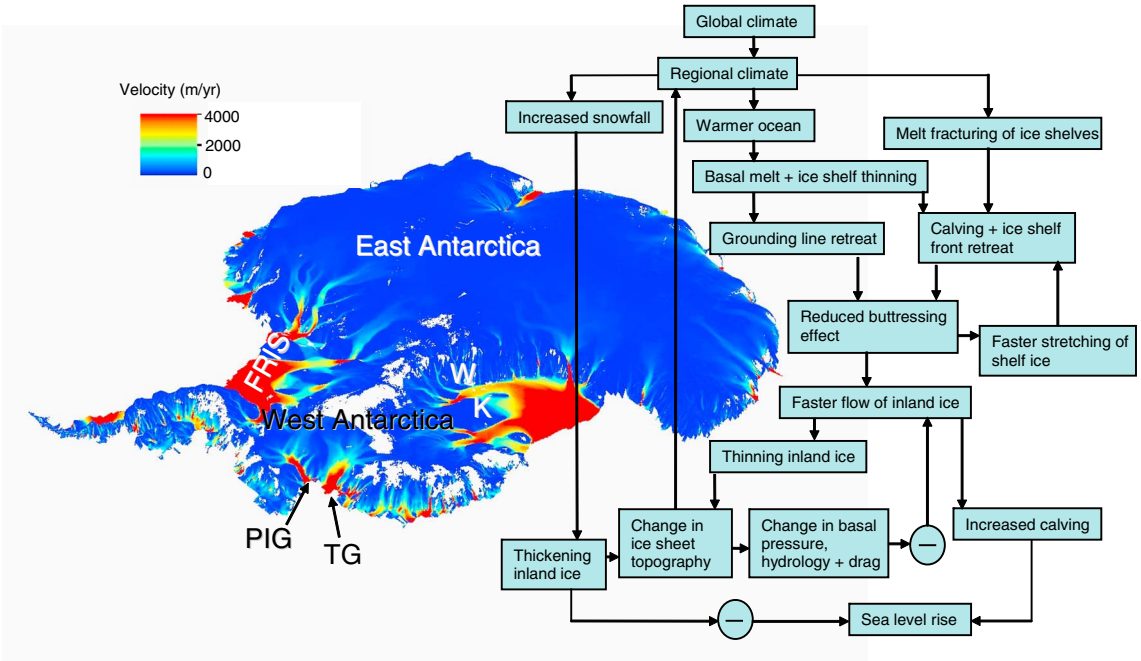

Figure 6. Antarctic ice sheet showing various features discussed in the text with flow velocity [*Rignot et al*., 2011] as color scheme (white is no data), surface elevation with 100 times vertical amplification from *Bamber et al*. [2009a]. FRIS: Filchner-Ronne Ice Shelf, W: Whillans Ice Stream, K: Kamb Ice Stream, PIG: Pine Island Glacier, TG: Thwaites glacier. Summary of factors based on *Cuffey and Paterson* [2010] affecting the Antarctic ice sheet contribution to sea level rise. Note the relative simplicity of surface mass balance processes and greater importance and complexity of ocean warming processes relative to Greenland contribution in Figure 4. Antarctic picture courtesy of G. Durand.

and GIA and produce quite different mass loss estimates both spatially and in total. *Thomas et al*. [2011] used a GPS network extending to 1995 to directly measure crustal motion. The most obvious feature is the elastic response to loss of several Antarctic Peninsula ice shelves, especially the loss of Larsen B in 2002. These elastic responses make establishing accurate GIA corrections for GRACE estimates difficult. *King et al*. [2012] applied the *Whitehouse et al*. [2012b] GIA model to the GRACE data to estimate mass balance in 26 independent drainage basins with techniques designed to minimize bias and contamination from non-Antarctic mass change and infer a net sea level contribution from Antarctica of 0.19 ± 0.05 mm yr^{-1} (2-sigma errors). Considerable mass loss is found for the Pine Island and Thwaites glacier drainage basins, but that is partly offset by mass gains in East Antarctica. The *King et al*. [2012] net mass balance estimate for Antarctica is much closer to the satellite altimetry estimates [*Zwally and Giovinetto*, 2011] than previous GRACE studies and with much smaller acceleration of mass loss than found by *Velicogna* [2009], essentially due to the newer GIA model used.

[36] Despite the considerable uncertainty, the present net balance of Antarctica is likely to be negative [*Shepherd et al*., 2012] as shown in Table 1. Given this, it is then very hard to see how it could become positive in a warming world. The modest increases in surface mass balance expected with rising temperatures are likely to be offset by the various nonlinear dynamic responses to warming that all result in accelerated mass loss as is discussed further in section 5.

[37] One of the most notable features of the sea level curve during deglaciation (Figure 2) was the rapid rise in sea level known as Meltwater pulse 1a [*Bard et al*., 1996]. Sea level rose by about 20 m in 340 years (14,310–14,650 B.P.) [*Deschamps et al*., 2012] and was coincident with the Bølling warm period. Fingerprinting the coral records of sea level rise from different regions suggests Antarctica as a likely contributor to sea level rise [*Bassett et al*., 2005]. However, data-constrained modeling studies of the last deglaciation indicate that the total Antarctic contribution to ocean-induced sea level rise from 20,000 to 9000 B.P. is likely to be in the range 6–17 m [*Philippon et al*., 2006; *Pollard and DeConto,* 2009; *Ritz et al*., 2001; *Whitehouse et al*., 2012a]. The contribution of Antarctica to rapid sea level rise during Meltwater pulse 1a supports the theory of marine ice sheet instability [*Weertman*, 1974] in the West Antarctic ice sheet. Section 5.3 discusses the present understanding of ideas on marine ice sheet instability. This may also be the cause of the large negative mass balance in West Antarctica on the Pine Island and Thwaites glaciers (Figure 6) [*King et al*., 2012; *Wingham et al*., 2009; *Thomas et al*., 2004; *Jacobs et al*., 2011].

3.2.4. Mountain Glacier Length Records

[38] The response of small glaciers to climate has been investigated in several ways. Recently, *Leclercq et al*. [2011] used glacier length records from 349 glaciers to construct a globally representative signal and estimate the mass balance change over time. The results indicate that the glaciers were in equilibrium with climate forcing sometime in the early

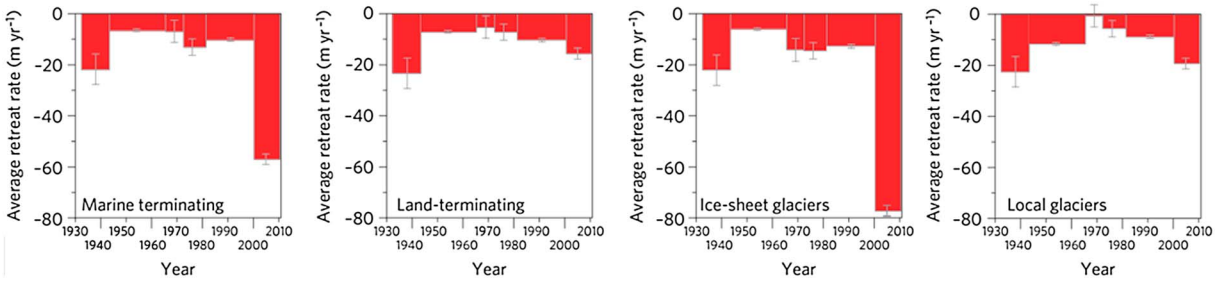

Figure 7. Frontal glacier changes around the southeastern part of the Greenland ice sheet shown as aggregated frontal retreat rates during six observation periods from 1933 to 2010. Error bars reflect the measuring uncertainty for each observational period. Extracted from *Bjørk et al*. [2012]. Reprinted by permission.

nineteenth century and that they contributed 9.1 ± 2.3 cm between 1850 and 2005 to global sea level. This information together with the total volume of ice in the small glaciers can be used to estimate a response time for the glacier contribution. In these types of estimation, the representativity of data is a key uncertainty, especially as in earlier times, observations were limited to a small geographical region (mostly the Alps). *Hock et al*. [2009] used local mass balance estimates based on reanalysis data and surmised that the high-latitude small glaciers contributed relatively larger amounts to sea level than temperate latitude glaciers over the twentieth century. This is somewhat confirmed by *Bjørk et al*. [2012] where the southeastern part of the Greenland ice cap shows a correlated response from the ice sheet and small glaciers, except in recent years when a dynamical response of marine-terminating glaciers from the ice sheet dominates the retreat rate (Figure 7).

[39] In summary, mountain glacier length records provide the longest observation record on the state of the cryosphere as in several regions (especially Europe), particular glaciers have been readily accessible. However, there are considerable issues related to the extent that these few glacier records can be regarded as representative of the general behavior of both glaciers in the same glaciated range, and for mountain glaciers and ice sheets in general.

4. MODELS

4.1. Introduction

[40] Although the sea level budget has many components, here we focus on the role of the ice sheets. This is because they seem to have the largest potential for unexpected contributions to sea level in the coming centuries [*IPCC*, 2007]. This is not to say that other components are satisfactorily understood at present, and we briefly go through the models of the steric and terrestrial sea level contributions.

[41] *Griffies and Greatbatch* [2012] in their comprehensive review of the factors involved in the ocean contribution to sea level show that there is a net positive tendency to global mean sea level, largely due to low-latitude heating and because the thermal expansion coefficient of sea water is much larger in the tropics than high latitudes. However, sea level rise through low-latitude heating is largely compensated by a sea level drop from poleward heat transport and ocean mixing. Processes involving density via salt transfer from melt and freezing of sea ice are several orders of magnitude smaller than the dominant impacts of energy balance, river flow, precipitation, and evaporation. The steric component as simulated by different AOGCMs is not very well constrained on decadal timescales [*Gregory et al*., 2006], nor through the 21st century. For example, *IPCC* [2007] gives a 5–95% confidence interval (17 estimates) of 0.13–0.32 m for steric sea level rise by 2100 under the A1B scenario, and this disagreement between models under the same forcing is only slightly reduced with Coupled Model Intercomparison Project Phase 5 models [*Yin*, 2012]. Coupled atmosphere-ocean models are known to have issues such as substantial differences among state-of-the-art models in ocean heat [*Yin*, 2012; *IPCC*, 2007; *Meehl et al*., 2007a, 2007b; *Raper et al*., 2002; *Sokolov et al*., 2003], mixing [*Goosse et al*., 1999], and lack of deep and abyssal ocean model components. *Yin* [2012] gives multimodel ensemble mean estimates of sea level rise by 2100 of 13, 18, and 28 cm in RCP 2.6, RCP 4.5, and RCP 8.5, respectively.

[42] The terrestrial contributions (see section 2) are related to human development. The net contribution to sea level has been usually thought to be close to zero [*Lettenmaier and Milly*, 2009; *Wada et al*., 2012]. *Pokhrel et al*. [2012] find far larger groundwater depletion than other estimates, but this estimate seems to be an upper bound as they assume unlimited and instantaneous water supply to match any demand. In the future, it is predicted that ground water extraction will dominate water storage behind dams, leading to net sea level rise. There are few publications on the potential contribution to sea level rise from groundwater mining and reservoir impoundment [*Konikow*, 2011; *Wada et al*., 2012] and these estimates are not very dependent on climate scenario. *Wada et al*. [2012] using land surface hydrology models and the Special Report on Emissions Scenarios (SRES) suggested a net contribution up to 0.07 m (0.05–0.09 m, 5–95% interval) by 2100. *Konikow* [2011] estimated the contribution from groundwater extraction to be 0.04 m by 2100, which could be partly canceled by negative sea level contribution of 0.02 m from water storage in reservoirs (assuming a constant rate of -0.2 ± 0.05 mm yr^{-1}) [*Chao et al*., 2008]. Uncertainties in these estimates are large due to limited information on future groundwater extraction, building of reservoirs, changes in global population, and water demand. It is, however, quite clear that all these estimates form only a small fraction of the total sea level rise expected by 2100 (Figure 1).

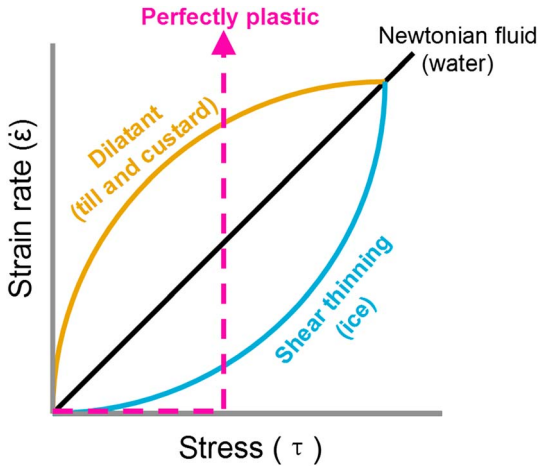

Figure 8. Stress and strain rate relationships for various fluid types—note that till may be closer to plastic under many subglacial conditions.

4.2. Dynamic Ice Sheet Models

[43] Glaciers and ice sheets are systems that at first sight appear simple and hence amenable to modern computer modeling. Ice has been disparagingly called a monomineralic rock, while the boundary conditions at the atmosphere, ocean, and lithosphere are all elements in Earth System Models. However, as we shall show, this simplicity hides many problematic details, not only in the details of the boundary conditions but also in the closeness of ice on Earth to its melting point; hence, the liquid water phase is often intimately mixed with the solid phase. Ice is also a complex non-Newtonian fluid with enormous anisotropy and with mechanical properties very sensitive to temperature. In addition, the continuum mechanics used to describe ice on macroscopic scales breaks down when the brittle nature of real glaciers becomes important—most obviously as a glacier calves icebergs into the ocean.

[44] Several good introductions to ice flow modeling have recently been published [*Blatter et al.*, 2011; *Kirchner et al.*, 2011]. Standard literature on ice flow modeling has been contributed by *Hutter* [1983], *van der Veen* [1999], and more recently, by *Greve and Blatter* [2009]. The full set of equations used to describe ice flow need to acknowledge that ice is a nonisotropic, incompressible, nonlinear-viscous, heat-conducting fluid with strong temperature dependence. In that respect, ice resembles custard (Figure 8). However, unlike custard or a mixture of water and cornstarch which is dilatant or shear thickening (http://www.youtube.com/watch?v=BN2D5y-AxIY), the viscosity gets lower as ice flows, making it a pseudoplastic or shear-thinning fluid. This favors the formation of narrow and fast-flowing ice streams from large slow-moving ice plains as the ice drains toward the ocean. In some locations such as beneath Whillans Ice Stream, the subglacial till is thought to be dilatant [*Alley et al.*, 1986], which may lead to formation of common features such as drumlin fields marking a previously glaciated landscape [*Clark*, 2010].

4.2.1. Basic Equations of Ice Flow

[45] The flow of ice is governed by equations that conserve mass, linear momentum, and energy. Mass conservation is equivalent to volume conservation for ice which, if considering long timescales, can be modeled as a nearly incompressible fluid of density ρ (910 kg m^{-3}), and is expressed by the vanishing divergence of the three-dimensional velocity field, $\mathbf{u}$:

$$\nabla\cdot\mathbf{u} = 0, \tag{2}$$

which at the same time is the first invariant of the strain rate tensor

$$\boldsymbol{\varepsilon} = \frac{1}{2}\left[\nabla\mathbf{u} + (\nabla\mathbf{u})^T\right], \tag{3}$$

[46] The Navier-Stokes equation is the continuum formulation of conservation of linear momentum for a fluid under a specific force (in our case, density times gravity), $\rho\mathbf{g}$:

$$\underbrace{\rho\left(\frac{\partial\mathbf{u}}{\partial t} + (\mathbf{u}\cdot\nabla)\mathbf{u}\right)}_{\to 0} = \nabla\cdot\boldsymbol{\sigma} + \rho\mathbf{g}, \tag{4}$$

[47] In three dimensions, the stress tensor $\boldsymbol{\sigma}$ is a 3 × 3 matrix with the leading diagonal composed of normal stresses and the other six terms being shear stresses. It is usually split into two parts $\boldsymbol{\sigma} = \boldsymbol{\tau} - p\mathbf{I}$, where p is pressure, and $\mathbf{I}$ is the identity matrix so that $p\mathbf{I}$ denotes the stress in an isotropic state (or hydrostatic equilibrium). Hence, $\boldsymbol{\tau}$ denotes the deviatoric stress tensor. Since any fluid deforms only if the stress deviates from an isotropic state, the spatial variability of the velocity defined as the strain rate, $\dot{\boldsymbol{\varepsilon}} = \frac{1}{2}(\nabla\mathbf{u} + \nabla\mathbf{u}^T)$, depends on the deviatoric stress tensor $\boldsymbol{\tau}$. In case of large values of the viscosity, the Reynolds number (expressing the relative importance between inertia and viscous forces) is small and the inertial terms on the left-hand side of (4) may be set to zero, leaving the Stokes equation. This equation is in need of a constitutional law for expressing the deviatoric stress tensor in terms of the strain rate tensor:

$$\boldsymbol{\tau} = \boldsymbol{\eta}(\dot{\boldsymbol{\varepsilon}}_{\mathrm{E}})\ \dot{\boldsymbol{\varepsilon}}, \tag{5}$$

where the viscosity, $\boldsymbol{\eta}(\dot{\boldsymbol{\varepsilon}}_{\mathrm{E}})$, can be a general function of the second invariant of the strain rate tensor $\dot{\boldsymbol{\varepsilon}}_E = \sqrt{\frac{1}{2}\mathrm{trace}\left(\dot{\boldsymbol{\varepsilon}}\dot{\boldsymbol{\varepsilon}}^T\right)}$. Field observations and laboratory experiments show that the relation between $\dot{\boldsymbol{\varepsilon}}$ and $\boldsymbol{\tau}$ follows a power law for the range of stresses in ice sheets (50 to 150 kPa) [*Cuffey and Paterson*, 2010]:

$$\dot{\boldsymbol{\varepsilon}} = A{\tau_E}^{n-1}\boldsymbol{\tau}. \tag{6}$$

[48] The coefficients A and n are estimated from observations (summarized in *Cuffey and Paterson* [2010]), and usually n is taken as 3, while A can be described by an Arrhenius law having different activation energy above and below −10°C such that as ice approaches the pressure melting point, the ice gets softer increasingly rapidly likely because of sliding between grains on a quasi-liquid pre-melted layer. The relationship between the stress on ice and its deformation is a flow law and is influenced by a wide range of physical processes including dislocation creep at high stress, grain boundary sliding, and diffusional creep at low stresses.

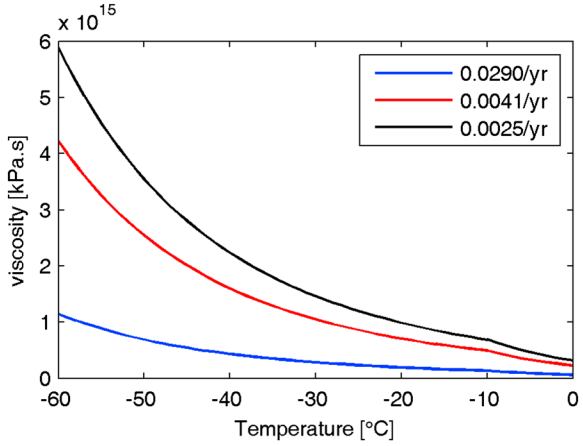

Figure 9. Plots of viscosity as a function of temperature for different strain rates ($\dot{\boldsymbol{\varepsilon}}_E$) taken from measurements on Agassiz ice cap (blue), Law Dome (red), Dye 3 (black). The higher activation energy at temperatures above −10°C can be seen as a kink in the curves. We take $n=3$ and $E=1$; changing the enhancement factor would reduce the viscosity by that factor. We took values of $A=A_0\ \exp[-Q/(RT_m)]$ where T_m is absolute temperature (K); if $T_m<-10°C$ then $A_0=3.985\times10^{-13}\,s^{-1}\ kPa^{-n}$ and $Q=60\,kJ\,mol^{-1}$ and if $T_m>-10°C$ then $A_0=1.916\times10^{3}\ s^{-1}\ kPa^{-n}$ and $Q=139\,kJ\,mol^{-1}$. R is the gas constant ($8.314\,J\,mol^{-1}$).

Therefore, there is still some debate on what the optimal representation of A and n is for real ice sheets (Figure 9) [e.g., *Cuffey and Paterson*, 2010].

[49] A nonlinear relation for the viscosity based on inverting the flow law [see, e.g., *Greve and Blatter*, 2009] leads to

$$\eta=\frac{1}{2}[EA]^{-1/n}\,\dot{\boldsymbol{\varepsilon}}_E{}^{(1-n)/n}. \tag{7}$$

[50] In this formulation, the enhancement factor, E, is an empirical factor that, if larger than unity, represents "softening" of ice relative to that expected by equation (6). It is not an inherent property of the ice but altered to values deviating from unity to account for various physical processes. One important factor that may be included in a simplified way [e.g., *Seddik et al.*, 2011] into E is the ice crystal anisotropy. In ice sheets, the ice grains begin in a disorderly mixed state which on a macroscopic scale makes the ice behave isotropically, but the processes of ice deformation themselves lead to reorganization of the ice crystal structure producing, over time, ice with preferred crystallographic orientations. Hence, there is coupling between ice flow history and viscosity through evolution of the grain fabric which in turn affects ice rheology. Typically, E can take a value of 3 for ice sheets where large thicknesses of glacial ice are expected [*Cuffey and Paterson*, 2010].

[51] Conservation of energy in a fluid such as ice may be expressed as a function of ice temperature, T:

$$\rho c\left(\frac{\partial T}{\partial t}+\mathbf{u}\cdot\nabla T\right)=\nabla\cdot(k\nabla T)+\Phi, \tag{8}$$

[52] The ice heat capacity c and the heat conductivity k are functions of temperature, and Φ is an internal source rate of heat per unit volume due to ice deformation or friction known as strain heating ($\dot{\boldsymbol{\varepsilon}}:\boldsymbol{\tau}=\mathrm{trace}(\dot{\boldsymbol{\varepsilon}}\boldsymbol{\tau}^T)$), ice melt, and refreezing. Diffusion of heat in ice is very slow compared with the dynamic response of the ice sheet; this means that the temperature recorded in boreholes [*Dahl-Jensen et al.*, 1998] contains information on climate history extending well into the last glaciation. This also implies that setting up the correct temperature distribution with an ice sheet model requires many tens of thousands of model years—"spin-up" time.

4.2.2. Approximations to Full Stokes

[53] Full Stokes (FS) models are a system of four unknowns (the three dimensional components of **u** and p) that form a "saddle point" system that is numerically challenging to solve. Therefore, models are restricted to spatiotemporal domains covering hundreds of square kilometers and hundreds of years only. Routine simulations of coupled paleo ice shelf/ice sheet systems are, to date, not possible with FS models.

[54] Therefore, a series of approximation are commonly used to describe the ice dynamics of the large Greenland and Antarctic ice sheets. The most common Stokes approximations all make the assumption of hydrostatic stress in the vertical. From here, the next level down is the "higher order" system (also known as "first-order" or "Blatter-Pattyn," e.g., *Pattyn et al.* [2012]), which is for the most part, accurate everywhere except in places of steep and/or highly variable bedrock topography over short distances, or at other rapid flow transitions (e.g., grounding lines). For other parts of the ice sheet, other further simplifications may apply. The higher-order linear momentum can be written in component form as

$$\begin{aligned}\frac{\partial\sigma_{xx}}{\partial x}+\frac{\partial\sigma_{xy}}{\partial y}+\frac{\partial\sigma_{xz}}{\partial z}&=0,\\ \frac{\partial\sigma_{yx}}{\partial x}+\frac{\partial\sigma_{yy}}{\partial y}+\frac{\partial\sigma_{yz}}{\partial z}&=0,\\ \frac{\partial\sigma_{zz}}{\partial z}&=\rho g.\end{aligned} \tag{9}$$

[55] These higher-order models are systems of equations with only two unknowns (the horizontal velocity components) and can quite skillfully simulate ice streams.

[56] For slow (or no) sliding and flow at slow velocities dominated by vertical shear, the SIA (shallow ice approximation) may apply [*Hutter*, 1983]. The SIA assumes all shear stress components except in the vertical direction to be zero, sets the vertical normal stress equal to zero, and hence obtains a hydrostatic pressure distribution so that

$$\frac{\partial\sigma_{xz}}{\partial z}=\rho g\frac{\partial s}{\partial x},\frac{\partial\sigma_{yz}}{\partial z}=\rho g\frac{\partial s}{\partial y}, \tag{10}$$

where s is the surface elevation. From these relations, the vertical profile of the horizontal velocity components is obtained by integrating with respect to height. This is a computationally easy task and does not demand the solution of a matrix-vector system. The vertical velocity component is then found from the horizontal terms using equation (2). On the other hand, for flow where the basal surface is essentially in free slip, vertical shear is negligible and horizontal stretching dominates, leading to the SSA (shallow shelf approximation)

[*Muszynski and Birchfield*, 1987; *MacAyeal*, 1989]. The SSA formulation neglects only the vertical shear, so is applicable to areas with negligible vertical shear stress such as floating ice shelves:

$$\frac{\partial \sigma_{xx}}{\partial x} + \frac{\partial \sigma_{xy}}{\partial y} = \frac{\partial \sigma_{yx}}{\partial x} + \frac{\partial \sigma_{yy}}{\partial y} = 0, \frac{\partial \sigma_{zz}}{\partial z} = \rho g. \qquad (11)$$

[57] SSA and SIA can both be derived as the "end-members" of the FS system. For ice streams with fast sliding flow over low-friction beds, an extra basal boundary condition is added, often in the form $\tau_b = \beta^2 \times \mathbf{u}$, where τ_b is the basal shear stress and β^2 is a friction parameter ($\beta^2 = 0$ in ice shelves). This type of "hybrid" model (e.g., SSA for sliding + SIA for deformation) is popular in models such as Parallel Ice Sheet Model [*Bueler and Brown*, 2009] and often referred to as "shelfystream". Equations (10) and (11) for the SIA and SSA are very fast to solve, but are only applicable to flow situations that match their initial assumptions, either the grounded ice parts of an ice sheet (SIA) or the floating parts (SSA). Indeed, the SIA is not applicable to many parts of the land-based ice: the centers of ice flow where ice cores are often drilled (domes, ridges), ice streams including the transition from the grounded ice to floating ice, and margins with "steep" bedrock slopes. These limitations exclude many areas that are critical for understanding ice dynamics. In particular, this applies to the grounding line where the land-based ice begins to float forming ice shelves (see section 5 for more discussion).

4.2.3. Boundary Conditions

[58] The governing equations of every model presented here are completed by boundary conditions, usually applied on the free surface (coupling to atmosphere) and the bedrock (traction and isostasy). Either the state variable values (defining a Dirichlet boundary condition) or their gradients (a Neumann condition) can be specified in a model. The case of a sliding law combines both into one, forming a Robin boundary condition. In addition to the geometry of bed and surface (which can be part of the solution themselves), the geothermal heat flux (or basal ice temperature) and any heat sources and sinks from either refreezing or melting as well as surface temperature are always required. Additionally, if the bed is at the pressure melting point, then a sliding law needs to be provided (or deduced).

[59] Neither the FS, higher-order, SIA, nor SSA equations have time as an explicit variable, so represent steady state solutions. In other words, the Stokes equations and its approximations describe an instantaneous response to a given viscosity distribution (mostly influenced by temperature and crystal fabric) and a geometry at a certain time. Time dependence of the thermomechanically coupled systems lies completely within those viscosity determining advected and diffused variables, such as the temperature field (equation (8)) and the kinematic boundary condition,

$$\frac{\partial s}{\partial t} + u\frac{\partial s}{\partial x} + v\frac{\partial s}{\partial y} - w = b_{\perp}, \qquad (12)$$

at the free surface that links the volume surface balance to a given (local) surface mass balance, $b_{\perp}$.

4.2.4. Dynamical Estimates for the Ice Sheet Contributions

[60] Dynamical estimates for the future Greenland sea level rise contribution come from ice sheet models with prescribed changes in boundary conditions to illuminate the envelope of possible ice loss by various mechanisms. For example, *Seddik et al*. [2012] used a full Stokes finite element flow model to examine SeaRISE group scenarios for the difference in ice loss if the basal drag coefficient in three Greenland outlet glaciers is reduced by a factor of 2 (Figure 5). They found an additional 13 cm of sea level rise by 2100. In contrast, *Price et al*. [2011] used a higher-order flow model to examine the impact of perturbations to the marine terminations (to simulate calving) of the same three large Greenland outlets and estimated a dynamical contribution of 0.6–4.5 cm by 2100. Similar process studies are being attempted in Antarctica [*Winkelmann et al*., 2012] and, while still at an early stage, appear to show that ice sheet history and not just instantaneous configuration is an important factor in present-day response to forcing. *Bindschadler et al*. [2013] using an ensemble of models suggest a range of 4–66 cm for Greenland and −3 to 14 cm for the Antarctic ice sheet by 2100 (Figure 1b).

4.3. Mountain Glacier Models

[61] Mountain glaciers and small ice caps in general are not amenable to modeling using shallow ice approximations since the form factor (ζ) may be close to unity. Full Stokes models may be used on individual glaciers [*Zwinger et al*., 2007; *Zwinger and Moore*, 2009] where detailed geometry data (both surface and bedrock) exist. These glaciers are a very small fraction of the total number of mountain glaciers worldwide. However, dynamical simulation of small glaciers is less important with respect to sea level rise estimates than surface mass balance simulation. This is because mountain glaciers tend to have relatively large snow accumulation rates in their upper reaches and corresponding large melt rates in their ablation areas. At the same time, the dynamical advection of ice through the glacier is relatively slow due to the shallow thickness, and proximal lateral and basal friction forces.

[62] Ideally, mountain glacier surface mass balance (SMB) would be modeled using very high resolution meteorological input data sets with equally high resolution topographic data. This is very important because of steep topography causing shading in ablation areas and turbulence effects on snowfall. Regional climate models are limited to about 20 km at present, and it is probable that only microclimate modeling will be suitable for such process-based modeling of mountain glaciers. So in practice, parameterizations have been used that are tuned to a small number of selected glaciers where surface measurements have been taken [e.g., *Radic and Hock*, 2011]. In IPCC AR4 [*Bindoff et al*., 2007], simple scaling relations between global temperature and ice volume change were used (see AR4, Appendix 10. A2). However, the model parameters are not purely empirically calibrated but the sensitivity is calibrated by both observations and SMB models.

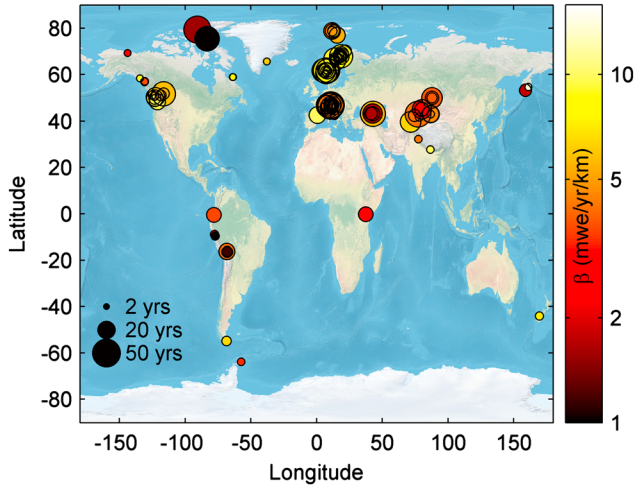

Figure 10. Geographical distribution of glaciers with mass balance records (length of record indicated by circle size). The color bar shows the vertical mass balance gradient, β, in meters of water equivalent per km, indicating the very large differences that can exist even for glaciers within the same mountain group. Data from *World Glacier Monitoring Service* [2009].

[63] More sophisticated approaches are available that account for differences in regional mountain climates. Regional parameterizations are desirable since maritime glaciers are known to be more sensitive to both changes in temperature and precipitation than continental glaciers. In other words, given the large annual temperature cycle, interannual variability, and low precipitation typical of a continental climate, a continental glacier must be relatively insensitive to climate in order to survive. In many models, ablation is calculated using a "positive degree-day" method [e.g., *Braithwaite*, 1990] whereby the sum of positive daily temperatures is multiplied by the number of days with positive temperatures, so that 1 day with a temperature of 5°C produces the same ice melt as 5 days with a 1°C temperature. *Radic and Hock* [2011] used reanalysis data (at typically 300 km resolution—though weather stations tend not to be homogeneously distributed in mountain regions) to derive lapse rates for temperature and precipitation as a function of altitude. The equilibrium line elevation (ELA) was set to the mean glacier elevation, so that as the glacier retreats, the ELA will move up the mountain. In all, seven model parameters were calibrated on observed data sets from 36 glaciers to set the degree-day melt rates for snow and ice, the lapse rates for temperature and precipitation, and correction factors that statistically downscale the reanalysis data. *Radic and Hock* [2011] find that only three variables could be determined by statistical downscaling the meteorological fields; the others were taken to be the means of the calibration glaciers or an optimization to find the best fit over each glacier region. Their key finding is expressed as a mass balance sensitivity to changes in precipitation or temperature. Typically, this is taken as the average change in mass balance over the whole glacier (B) per 1°C of temperature increase, C_T, or for a 10% change in precipitation, C_P:

$$C_T = \frac{B(T+1) - B(T-1)}{(T+1) - (T-1)}, \tag{13}$$

$$C_P = \frac{B(P+10\%) - B(P-10\%)}{(P+10\%) - (P-10\%)}. \tag{14}$$

[64] Attempts have also been made to find a simple estimate of these sensitivities based on gridded climate data. *Giesen and Oerlemans* [2012] calibrated sensitivities using data from nine glaciers having automatic weather stations. They find that C_T increased with increasing precipitation and was highest for New Zealand, Scandinavia, and northeastern Russia. However, where both surface melting and accumulation can occur in the same season (such as in Tibet), the model did not perform as well as elsewhere. In general, the lack of any significant relationship between precipitation lapse rate and other simple meteorological fields such as gridded precipitation or latitude makes finding general relationships for glacier mass balance problematic (Figure 10).

[65] Other approaches have been rather simpler and parameterized regional mountain glacier mass balance sensitivity to temperatures and precipitation [*Slangen and van der Wal*, 2011; *Marzeion et al.*, 2012]. The change in glacier mass balance over time can then be forced by regional temperatures and precipitation. The resulting volume change may then used to characterize a new glacier area using a volume-area scaling law introduced by [*Bahr et al.*, 1997]

$$\text{Volume} = \kappa\,\text{Area}^{\chi}. \tag{15}$$

[66] This relation may be used to specify how area changes over time as the glacier shrinks, and hence, how large the integrated surface mass balance translates into a volume change.

[67] A purely statistical estimate of mountain glacier contributions to sea level can also be directly based on volume-area scaling relations [*Bahr et al.*, 1997] if an estimate of the ratio of accumulation area to total area (AAR) of each glacier can be found [*Bahr et al.*, 2009; *Mernild and Lipscomb*, 2012]. The idea behind the method is that there is a value, AAR_0 where the glacier exists in equilibrium with climate, which was estimated as 0.4–0.8 with an average, for 86 glaciers, of 0.57 ± 0.01. In contrast, the presently observed worldwide AAR is 0.44 [*Bahr et al.*, 2009]. Using the scaling relationship to calculate a volume loss requires that about 27% of present ice volume be lost to achieve an average AAR of 0.57. It can be argued that this approach is very simplistic; however, *Bahr et al.* [2009] claim that a more detailed calculation with AAR_0 estimated for individual glaciers leads to only a 10% difference from the simple approach in ice loss required under present-day climate to reach equilibrium. *Mernild et al.* [2013] estimated that 140 glaciers and ice caps were even further from equilibrium in the first decade of the 21st century, and they would need to lose 38 ± 8% of their volume. In this method, no time constant is available, so no timescale of ice loss can be found without further assumptions (such as exponential decay).

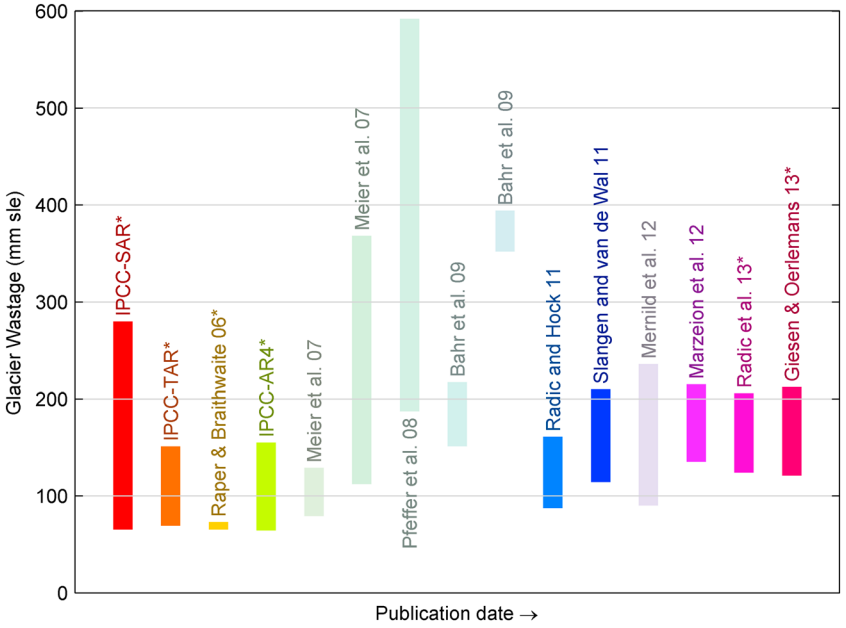

Figure 11. Regularized projections of sea-level rise as a function of source (labels), due to small-glacier mass balance from 2001 to 2100. Bar height represents range of estimates. Lighter shading indicates scenario independent projections. Sources from left to right: IPPC SAR—*Warrick et al.* [1996], IS92a; IPCC TAR—*Church et al.* [2001], IS92a; *Raper and Braithwaite* [2006], A1B; IPCC AR4—*Meehl et al.* [2007a], 6 SRES; *Meier et al.* [2007], constant rate; *Meier et al.* [2007], constant trend; *Pfeffer et al.* [2008], upper bound; *Bahr et al.* [2009], steady climate; *Bahr et al.* [2009], evolving climate; *Radic and Hock* [2011], A1B; *Mernild et al.* [2013], steady climate; *Marzeion et al.* [2012], RCP6; *Giesen and Oerlemans* [2013], A1B.

[68] *Cogley* [2012] summarized the various sea level rise estimates by 2100 due to small glaciers from various methods, and we added some of the latest numbers (Figure 11). Total glacier volume estimates (in global sea level equivalent) from *Huss and Farinotti* [2012] of 43 cm, *Marzeion et al.* [2012] of 37 cm, and *Grinsted* [2012] of 34 cm are significantly smaller than the *Radic and Hock* [2010] estimate of 60 cm. *Marzeion et al.* [2012] claim to have the only cross-calibrated and validated mass balance model of global mountain glaciers and predict a range of glacier contribution to sea level from 42.4 ± 4.6 cm under RCP 8.5 to 14.8 ± 3.5 cm under RCP 2.6; these estimates are significantly larger than those of *Radic and Hock* [2011]. The projected loss under RCP 8.5 is larger than the total volume estimated by *Grinsted* [2013] and almost equal to the volume estimate by *Huss and Farinotti* [2012]. Thus, the mountain glacier contribution must clearly be sensitive to the initial ice volume distribution contrary to the conclusions of *Slangen and van de Wal* [2011].

4.4. Semiempirical Total Sea Level Models

[69] Projections by semiempirical models are based on the assumption that sea level in the future will respond as it has in the past to imposed climate forcing. This may not hold in the future if potentially nonlinear physical processes, such as marine ice sheet dynamics or thermal expansion, do not scale in the future as they have in the past. However, the models are based on physically plausible ideas and are not merely statistical fits of sea level to forcing. Furthermore, the sea level system tends to respond in a linear fashion to radiative (or temperature) forcing [W*inkelmann and Levermann*, 2012; *Good et al.*, 2011]; that is, the individual components of sea level (Greenland, Antarctica, and steric sea level) when considered separately produce a sum that is very similar than when all are forced simultaneously. Another example of linearity is seen when considering the impact on sea level of changing surface mass balance and basal sliding separately or together [*Bindschadler et al.*, 2013; *Levermann et al.*, 2012]. This linearity suggests that the semiempirical method of considering the response of the whole sea level system to forcing is a good approximation to a component-by-component set of models.

[70] *Gornitz et al.* [1982] presented the first "semiempirical" model of sea level related to temperature change by fitting a simple linear relationship between sea level and global temperature:

$$S = aT + b, \tag{16}$$

where a and b are constants. Using the data that existed from tide gauge stations to that date, they estimated that sea level rise would amount to 20–30 cm from thermal expansion and increase to perhaps 40–60 cm with increased ice melt by 2050. Using a lag correlation approach, they found that sea level was best fitted with an 18 year delayed response relative to forcing. This approach was never used by IPCC

to project future sea level because there was little physical basis for the relationship found by correlation.

[71] *Oerlemans* [1989] developed a model of rates of sea level rise as function of the major components of the sea level budget. Each component of the model was designed to capture the physics of the sea level component in the simplest way possible. For example, thermal expansion was estimated assuming a simple column ocean with a diffusion scheme using realistic time constants. The mountain glacier contribution rate was linked exponentially to the global mean temperature with a single time constant and a finite ice volume. In this model, the ice sheet contributions were linked to temperature and Greenland melt essentially canceled Antarctic growth.

[72] Rather than model each contributor to the sea level budget separately, *Rahmstorf* [2007a] developed a model based on the rate of sea level rise dependent on global mean temperature. While this may seem a step toward lower complexity compared with the *Oerlemans* [1989] approach, there is the considerable advantage that the observations of sea level rise can be directly fitted to historical observations of global temperature. The second advantage of this approach is the sea level budget does not need to be balanced or closed in order to produce a useful projection and avoids the structural uncertainties in the process models. The model fits two constants to the observational data, a sensitivity relating sea level rise rate per degree temperature change, and an equilibrium temperature where sea level is in balance with global temperature. Inherent in the formulation is that the response of the major components must be much longer than the observational period—expected to be of the order 10^3 years:

$$\frac{\mathrm{d}S}{\mathrm{d}t} = a(T - T_0), \tag{17}$$

where S is the global mean sea level, T is the mean global temperature, T_0 is the reference temperature at a time when sea level was in equilibrium, and a is the sensitivity. The model was criticized by some groups concerning the statistical fitting of the constants derived from the observations [*Holgate et al*., 2007; *Schmith et al*., 2007]. *Rahmstorf* [2007a] low-pass filtered the sea level rate data and binned prior to fitting. Since sea level data are already highly autocorrelated, this filtering reduced the available degrees of freedom further. However, since only two constants are fitted, this procedure arguably makes no practical difference to the model [*Rahmstorf*, 2007b].

[73] In an effort to introduce some high-frequency variability to the *Rahmstorf* [2007a] model, *Vermeer and Rahmstorf* [2009] invented a new term in the equation that mimics short-term (actually instantaneous, but then filtered to decadal scales) contributions. This term is proportional to the rate of change of temperature. Physically, this represents fast processes such as the heat content of the oceanic surface mixed layer. The model also attempts to remove the non-climate-forced component of reservoir building before fitting the forcing to sea level. The latest development of the model [*Kemp et al*., 2011a] added an intermediate response time term, making a total of five parameters to be fitted. The model is

$$\frac{\mathrm{d}S}{\mathrm{d}t} = a_1\big(T(t) - T_{0,0}\big) + a_2(T(t) - T_0(t)) + b\frac{\mathrm{d}T}{\mathrm{d}t}, \tag{18}$$

where

$$\frac{\mathrm{d}T_o}{\mathrm{d}t} = \frac{T(t) - T_0(t)}{v}. \tag{19}$$

[74] In this formulation, there is an instantaneous response governed by the sensitivity b, an infinite response determined by a_1, a variable response with time constant v, and sensitivity a_2. $T_{0,0}$ is a constant as is T_0 in equation (17). $T_0(t)$ is a moving reference "base temperature" that represents the equilibrium temperature at the instantaneous sea level at time t, neglecting the infinite and instantaneous terms; this is not found from the regression analysis directly but from a_2 and v. Finally, an arbitrary offset, or constant of integration (in equation (18)), for sea level is determined to produce sea level rise relative to any given reference period. Since all models of sea level do not predict absolute sea level relative to the center of the Earth, but rather its change over a specified time period, this integration constant is not a fitted parameter.

[75] In 2010, Grinsted et al. introduced a different semiempirical model that made use of a response time to be determined by the data that represent the presumed centennial- or millennium-scale response of oceans and ice sheets and which avoid either the infinite or instantaneous formulations. *Jevrejeva et al*. [2009] used radiative forcing as the forcing variable in a semiempirical formulation based on *Grinsted et al*. [2010]—the respective published dates do not match their formulation history. The idea of using radiative forcing rather than temperature has several pros and cons. It removes the conversion from prescribed radiative forcing (as given for example in the RCP or SRES formulations of climate change drivers) to model dependent temperatures. On the other hand, snow, ice, and ocean thermal expansion are mainly driven by surface temperatures; hence, there is still an implied conversion and perhaps another time delay as temperature lags radiative forcing. While radiative forcing is prescribed in IPCC, it is still, of course unknown how it will actually vary in future—since emission scenarios are simply estimates based on expert assessment economic scenarios. In the model training period, it is debatable which is better known—temperature data from sparse instrumental and proxy sources or radiative forcing from indirect estimates (such as volcanic indices and solar irradiance). Hence, use of radiative forcing versus temperature as a driver for semiempirical models is a trade-off between climate model bias (expressed, e.g., as climate sensitivity) and accuracy of the historical record of forcing.

[76] Assuming that for a given mean global radiative (or surface temperature) forcing (F), there is an equilibrium sea level (S_{eq}), *Grinsted et al*. [2010] argue that the relationship between S_{eq} and F must be nonlinear for large changes in sea level such as those that occur on glacial-interglacial timescales [*Rohling et al*., 2009]. However, for interglacial climate, the relationship is nearly linear, with a considerably lower sensitivity than during glacials [*Rohling et al*., 2009].

Therefore, a linearization that should be valid for global temperatures up to several degrees warmer than present is

$$S_{eq} = aF + b, \tag{20}$$

where a is the sensitivity of sea level to a forcing (F) change and b is a constant. Potential sea level rise is the result of changes in global ice volume and global ocean heat content, both of which are modeled as reacting to changes in radiative forcing with some single response time of the climate system (v). Global ocean heat content and ice volume will have different response times; however, both are plausibly centennial [*Grinsted et al*., 2010], and therefore, sea level will approach S_{eq} with response time as follows:

$$\frac{\mathrm{d}S}{\mathrm{d}t} = \left(S_{eq} - S\right)/v. \tag{21}$$

[77] To obtain sea level (S), equation (21) is integrated over time using the 1000 years of available forcing (F) and knowledge of the initial sea level at the start of integration (S_0). As a consequence, the model required three parameters to be fitted (and an arbitrary integration constant), which was challenging with only historical observations. Therefore, paleodata were used extensively to constrain the parameters (see section 3.1) and also extend the range of data to include the full 300 year extent of tide gauge observations. No data pre-filtering was done, and a Monte Carlo procedure was used to determine the probability density distribution of the model parameters so that confidence intervals on the sea level projections can be made.

[78] A source of confusion in the interpretation of the models that make use of different calibration data sets is the sometimes nonoverlapping confidence intervals on projections that arises. For example, in *Grinsted et al*. [2010], there are three calibration data sets: a relatively short historical record of instrumental temperature and two longer reconstructions based on various proxies using different methodologies. The confidence interval for projections based on the historical forcing does not overlap the other two. However, the historical model is clearly constrained by the prior rather than the data and thus the results for that simply cannot be trusted. What this means is that there is simply not enough information in the calibration data set to reliably constrain all parameters. The symptoms are evident in the probability distributions of the b parameter and discussed in the paper: "The simple conclusion is that the calibration time series is too short relative to the response time." The confidence intervals based on the two proxy-based reconstructions are obviously conditional on their respective climate reconstructions being correct. So if they happen to have a high degree of overlap, then they are actually allowed to be incompatible because the temperature reconstructions cannot both be correct. The whole point of doing the calibration with different temperature reconstructions is to gauge how much additional uncertainty in projections comes from assuming a given temperature history.

[79] Comparing the *Kemp et al*. [2011a] and the *Jevrejeva et al*. [2009] formulations of semiempirical sea level is not easy. It is tempting to compare the intermediate response term in equation (18) with equation (21); however, the response times will not be the same unless the a_1 and b parameters are set to zero in equation (18). Furthermore, there are differences in the units of the a_2 in equation (18) and a in equation (20), with the units being m/K/yr and m/K, respectively. There is no equilibrium sea level for any given temperature in the *Kemp et al*. [2011a] model since there is an infinite response term that will lead to eventual infinite sea level rise. In the original formulation [*Rahmstorf*, 2007a], this term was justified as simply a device that in practice, could be approximated by a linear approximation to the initial response of sea level rise. This term is quite important as it does allow for very long period variability in sea level (say on millennial timescales), which the *Jevrejeva et al*. [2009] model lacks having typically a response time of a few centuries, and may account for the somewhat lower projections of sea level when using the *Jevrejeva et al*. [2009] model (Figure 1). *Jevrejeva et al*. [2012] experimented with various nonclimatic (that is, sea level trends, or millennial-scale time constant) processes on estimates of future sea level rise simply by removing trends from the target calibration tide gauge records, then performing a model simulation, then adding in the trend again to produce a total projection. *Church et al*. [2001] suggested 2.5 cm per century could come from a long-term dynamic response of the ice sheets since the Last Glacial Maximum, which would also be consistent with uncertainties within the tide gauge record (Table 1 and Figure 3). Compensating for this trend in the modeling leads to a 6 cm lowering of projected sea level at 2100. It is clear that there are more parameters to be fitted or constrained by observational priors in the *Kemp et al*. [2011a] model than the *Jevrejeva et al*. [2009] model, and this requires careful examination of the observational record and assumptions on the noise characteristics of the sea level data (section 5.9) [*Rahmstorf et al*., 2011].

5. MODEL SHORTCOMINGS

[80] In this section, we highlight important features of the cryosphere-sea level system, which are difficult to incorporate into models, or lack good theoretical understanding, and hence are hindering progress. We do not touch on features that are reasonably well understood—such as surface mass balance projections over the ice sheets. Rather, the key issues are related to the breakdown in continuum mechanics approaches, the limits of observational data, limited computing power, numerical convergence issues, and lack of fundamental physics.

5.1. Ice Shelf Melt

[81] Most of the mass loss from Antarctica is from calving of floating ice to the ocean [*Rignot et al*., 2008]. The marine-based part of West Antarctica could potentially contribute 3.3 m to global sea level [*Bamber et al*., 2009b]. This estimate will however be revised upward as ever-improving radar mapping of the bedrock topography reveals previously unknown areas of reverse sloping bedrock along ice streams that drain significant areas of West Antarctica [*Ross et al*., 2012].

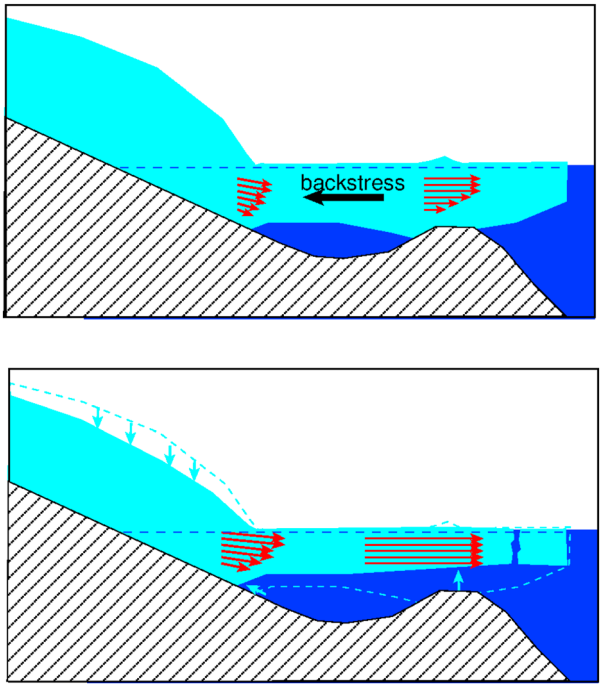

Figure 12. Cartoon of dynamic impact of ice shelf loss on land based glaciers due to removal of the buttressing effect. (top) Ice shelf contact points on sub-shelf bedrock highs or along side walls dominate the buttressing force. (bottom) If the ice shelf thins, typically via bottom melting then the ice shelf looses restraining force, allowing ice to flow faster off land (red arrows) and then contributing to sea level rise. Once the ice shelf loses contact, it typically rapidly breaks up and retreats.

[82] The floating ice fringing the continent is directly connected to the ocean beneath it, and hence strongly influenced by changes in its temperature or currents [*Massom et al*., 2011]. The issue of coupling the ice sheet to the ocean will be mentioned in section 5.7. The importance of variation in ice shelf melt over geological time periods has been demonstrated by models such as *Pollard and DeConto* [2009], but the impacts over centennial scales are only just being approached in models. *Pritchard et al*. [2012] find thinning caused by basal melt on 20 of 54 ice shelves, with the most widespread and rapid losses (up to 7 m/yr) on the coast of West Antarctica, where warm waters have access to thick ice shelves via deep bathymetric troughs. Though this ice loss does not contribute to sea level rise directly as it is already floating, the ice shelves provide significant buttressing force on the inland ice [*Gagliardini et al*., 2010]. This acts via longitudinal stresses where shelves ground on pinning points and as a result of shear stress where shelves make contact with embayment sides—both of which will decrease if and when ice thins as a result of increased melting (Figure 12). This thinning then allows acceleration of feeder ice streams and glaciers [*Dupont and Alley* 2005; *Scambos et al*., 2004; *Berthier et al*., 2012]. *Pritchard et al*. [2012] note that wherever ocean-driven ice shelf thinning occurred, it was coupled with dynamic thinning of grounded tributary glaciers, which together account for about 40% of Antarctic ice discharge and the majority of Antarctic ice sheet mass loss [*Rignot et al*., 2008]. The importance of ice shelf buttressing demands the use of models that can handle the boundary layer problem at the ice shelf grounding line (see section 5.3).

[83] *Hellmer et al*. [2012] showed that a coupled regional sea ice-ocean model, forced by a global atmospheric model driven by emissions scenarios, could simulate a dramatic increase in basal melting beneath the Filchner-Ronne ice shelf. The basal melting induced rises to about 80% of the total surface mass balance of Antarctica by the later part of the 21st century due to a projected inflow of warmer water into the sub-ice shelf cavity. In this model, the sub-ice shelf geometry remains fixed throughout the model run which is clearly an unrealistic assumption as projected melt rates imply rapid disintegration of a large part of the ice shelf (Figure 13). This would be expected to lead to increased ice flow off the continent leading to sea level rise as discussed earlier (Figure 12). *Timmermann et al*. [2012] use the same model setup with two different ocean model modules to examine present-day melt rates between many ice shelves around Antarctica and show the importance of the Bellingshausen Sea ice shelves and the apparent insensitivity of the large ice shelves under present climate conditions. However, many of the smaller fringing ice shelves cannot be well represented despite the high resolution of the models. Two different high-resolution models give total melt rates that differ by about a factor of 2, though for the largest 10 ice shelves, the differences are about 30%.

[84] Circumpolar Deep Water (CDW), or slightly modified CDW, lies just off the continental shelf break in many areas of Antarctica (closer to the ice in some areas, e.g., Pine Island Glacier, than in others, e.g., Ross and Filchner-Ronne ice shelves). Progress has been in made in understanding how CDW may travel up onto the continental shelf and into cavities beneath ice shelves. *Pritchard et al*. [2012] postulate that for many ice shelves, this is likely caused by changes in wind forcing leading to divergence and local upwelling increasing oceanic supply of warm water [*Thoma et al*., 2008; *Jacobs et al*., 2011; *Dinniman et al*., 2012]. *Hellmer et al*. [2012] suggest that the reduction in sea ice cover as the temperatures rise allows its drift speed northward to increase and allows momentum to be transferred offshore. The enhanced surface stress, which is not related to an increase in atmospheric wind stress, directs the coastal current southward toward the Filchner-Ronne ice shelf front. Prior to the recent observational and modeling work, the presence of warm water beneath ice shelves was thought to be reliant on high salinity shelf water (formed by brine rejection during sea ice formation) at the surface freezing temperature (about −1.89°C) fueling a sub-ice shelf circulation that brings heat to the southern ice shelf grounding line. The need for a dense water mass to transport heat to the grounding line was used as an argument for reduced subshelf melting in a warmer climate [*Nicholls*, 1997] via reduced sea ice formation.

[85] Thus, it now seems that the processes that caused the loss of Larsen A and B ice shelves, those which now dominate the thinning of Larsen C [*Pritchard et al*., 2012], and

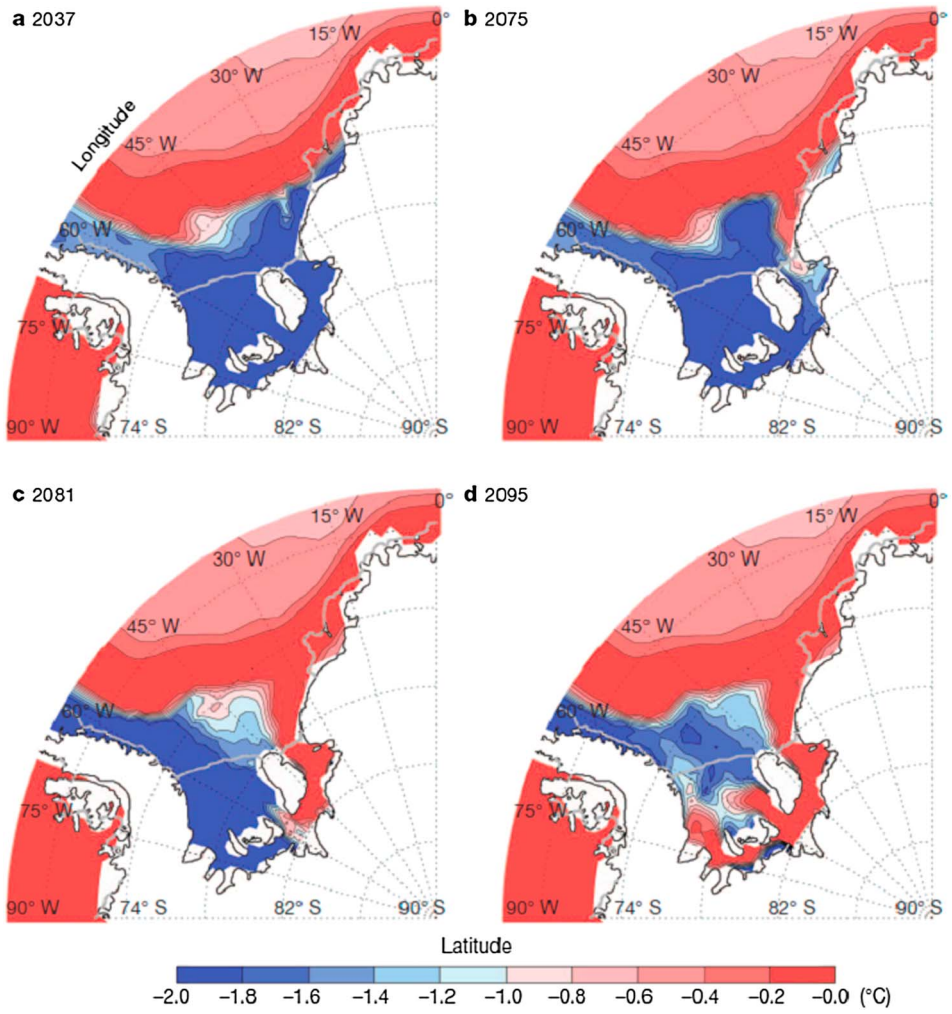

Figure 13. Simulated evolution of near-bottom temperatures in the Weddell Sea and beneath the Filchner-Ronne Ice Shelf. Values are from 60 m above bottom for the period 2030–2099 of the HadCM3-B/A1B scenario. (a) Warm pulses into the Filchner Trough (2037) are followed by a return of the shelf water masses to the cold state typical for present conditions; (b) by 2075, the tongue of slightly modified warm deep water reaches the Filchner Ice Shelf front. (c) It fills the deeper part of the Filchner Ice Shelf cavity and enters the Ronne Ice Shelf cavity near the grounding line south of Berkner Island in 2081. (d) By 2095, warm water fills most of the bottom layer of the Filchner-Ronne Ice Shelf cavity, reaching a quasi-steady state. The solid gray line off the coastline indicates the ice shelf front (see Figure 6 for location). From *Hellmer et al*. [2012]. Reprinted by permission.

those postulated to cause the demise of the Filchner-Ronne ice shelf [*Hellmer et al*., 2012] are driven by the atmospheric warming, loss of sea ice, and encroachment of warm water into the sub-ice shelf cavities. Hence, both surface melting and subshelf melt processes are driven by the atmospheric conditions and linkages to the global climate system. These mechanisms imply that Antarctic ice shelves can respond to atmospheric forcing on timescales much shorter than the millennial response times that were expected from earlier generations of ice sheet models. Furthermore, the West Antarctic region and the Antarctic Peninsula have warmed faster than almost anywhere else on Earth between 1958 and 2010 [*Bromwich et al*., 2013], including a significant warming trend during the summer melt season. Investigation of the possible causes of this trend suggests exclusion of effects such as Antarctic ozone trends, but is probably caused by a tropically forced atmospheric Rossby wave train [*Ding et al*., 2012], and hence is directly related to global warming [*Schneider et al*., 2011; *Steig et al*., 2012]. It should however be noted that *Yin et al*. [2011] suggest that ocean warming around Antarctica during the 21st century will only be half the global average. Clearly, the high-resolution coupled ocean-ice shelf models being pioneered by *Timmermann et al*. [2012] and *Hellmer et al*. [2012] will need development and incorporation within the framework of larger ice sheet models to accommodate the potentially rapid warming of Antarctic waters in this century.

5.2. Calving

[86] Calving has been relatively little studied, perhaps because the statistical nature of the work requires long-term monitoring. In the regions where it has been documented,

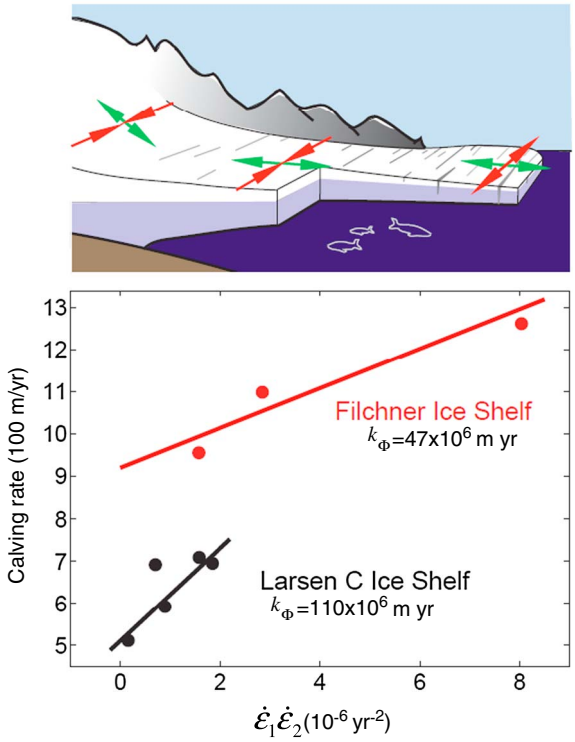

Figure 14. Concept of *eigencalving*. (a) Schematic illustrating proposed kinematic calving law: the calving rate is proportional to the spreading rates in both eigendirections of the flow which generally coincide with directions along (green arrows) and perpendicular to (red arrows) the flow field. In the confined region of the ice shelf, e.g., in the vicinity of the grounding line, convergence of ice flow perpendicular to the main flow direction yields closure of crevasses, inhibits large-scale calving and stabilizes the ice shelf. Near the mouth of the embayment, the flow field expansion occurs in both eigendirections and large-scale calving impedes ice-shelf growth onto the open ocean. (b) The observed calving rate determined as the ice flow at the calving front increases with the product of the two eigenvalues. Adapted from *Levermann et al*. [2012a].

however, calving constitutes up to 40–50% of mass loss on marine-terminating small glacier ice fronts [*Burgess et al*., 2005; *Dowdeswell et al*., 2008; *Walter et al*., 2010; *Thomas et al*., 2004]. Calving from marine-terminating glaciers accounts for almost all mass loss from Antarctica and about 50% from Greenland [*Rignot et al*., 2008; *Jacob et al*., 2012]. At present, no process-based ice sheet model incorporates calving as a function of atmospheric and oceanic forcing. Indeed, no formulation for calving has yet been agreed as suitable for models, though several have been proposed [*Benn et al*., 2007b; *Nick et al*., 2010; *Bassis et al*., 2011; *Levermann et al*., 2012]. Various models may be suitable for different applications such as ice shelves [e.g., *Levermann et al*., 2012] or basin-scale studies [e.g., *Nick et al*., 2011].

[87] Two fundamentally different relationships can be postulated for calving: (1) the case of a grounded terminus such as a tidewater glacier that advances on a platform of its own sediment into deeper water and (2) the situation in a freely and essentially unconstrained ice shelf. The two mechanisms produce radically different types of calving: small ice blocks that fall off the calving cliff in typically warm tidewater glacier settings and large flat-topped bergs that can be tens of kilometers across from the colder ice shelves or ice streams of the ice sheets.

[88] For mountain glaciers in Svalbard and Alaska, a simple relationship has long been known between water depth at the terminus, H_w, and calving rate,

$$\dot{c} = k_c H_w, \tag{22}$$

with k_c found to be 17 year^{-1} [*Brown et al*., 1982]. *Benn* [2007a] proposed a physically based model with the rate of calving depending on the depth of penetration of surface crevasses which in turn depends on the longitudinal strain rate. A modification suggested was to increase crevasse depth by the filling of crevasses by surface meltwater which is common occurrence in summer even on ice sheets, and certainly typical of many marine-terminating smaller glaciers. *Nick et al*. [2010] introduced a further modification by including basal crevasses with a calving criterion when surface crevasses reach basal crevasses. Basal crevasses can be much more incised than surface air-filled crevasses, hence inducing fracturing much farther from the terminus. The existence of huge tabular icebergs originating in floating ice shelves provides ample motivation for incorporating this effect..

[89] *Alley et al*. [2008] proposed that the calving rate $\dot{c}$ depends on longitudinal strain rate ($\dot{\boldsymbol{\varepsilon}}_{xx} = \frac{\partial u}{\partial x}$), H_m the ice thickness at the calving front, and also the width of the ice shelf, Y. However, *Hindmarsh* [2012] showed that rather than the calving rate, this formulation instead determines the ice velocity at the calving front. If the calving position is stationary then the calving rate will equal the ice velocity. This explains why the Alley calving law has no dependence on oceanographic factors such as ice shelf geometry and sub-ice shelf ocean circulation as may be expected.

[90] Incorporation of calving into ice models has been problematic. The resolution of many models simply does not include small ice cliff failure. *Cuffey and Paterson* [2010] summarized the situation as most models either let ice shelves advance to the edges of the model grid, or assume that ice shelves terminate at a prescribed water depth (H_w = 400 m typically). For marine-terminating glaciers that are not fully floating, most models either assume that calving rate increases with water depth (equation (22)), or constrain the ice front thickness H_m instead of the calving rate.

[91] *Amundson and Truffer* [2010] proposed a calving "framework" that allows any thickness-based calving relationship to be incorporated, with calving rate governed by ice thickness, thickness gradient, strain rate, mass-balance rate, and backward melting of the terminus. Key parameters to be determined in this approach are the critical thicknesses of the terminus before and after calving—which are variable from glacier to glacier and reflect both intrinsic strength of the ice shelf, and external forcing factors. *Bassis* [2011] examined the statistical mechanics of a one-dimensional calving front, and while "a universal calving law" was found, its applicability in ice sheet models is not clear. A similar issue

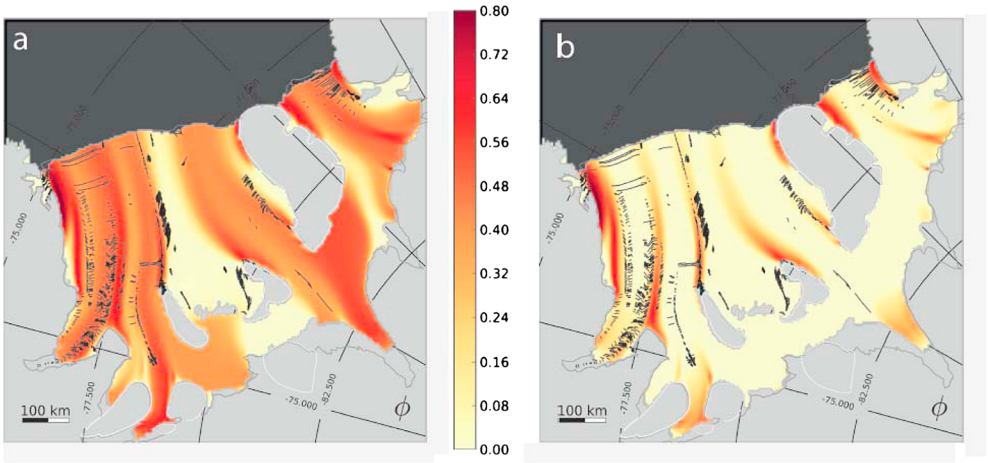

Figure 15. Steady-state fracture density (color bar) for Filchner-Ronne ice shelf (Antarctica, Figure 6) simulated with a shallow shelf approximation but with parameterized fracture mechanics. (a) Without healing of fractures and (b) with healing due to overburden pressure and accumulation. The critical threshold stress for fracture initiation was set to 70 kPa. Observed visible surface fractures are overlaid in black. The high-density fracture regions should match observations, though it is possible that snow cover could hide crevassing in some locations, and crevassing formed on grounded ice is not simulated in the model. From *Albrecht and Levermann* [2012a]. Reprinted with permission.

arises in applying a discrete particle model that requires supercomputing resources [*Astrom et al.*, 2013] to produce realistic distributions of calving fragments based on fundamental elastic deformation, granular flow, and viscotic cohesion.

[92] To accommodate the unique features of individual calving fronts, a statistical continuum damage approach may yield better results in models of ice shelves [e.g., *Levermann et al.*, 2012a; *Borstad et al.*, 2012] or to mountain glacier calving [e.g., *Jouvet et al.*, 2011]. This can be illustrated by, for example, *Levermann et al.* [2012a] where the vertically averaged ice strain rate tensor yields eigenvalues ($\dot{\boldsymbol{\varepsilon}}_1$, $\dot{\boldsymbol{\varepsilon}}_2$), which can be determined from the spatial derivative of the remotely sensed velocity pattern. When $\dot{\boldsymbol{\varepsilon}}_1 \geq \dot{\boldsymbol{\varepsilon}}_2$ the ice is locally undergoing expansion, while if $\dot{\boldsymbol{\varepsilon}}_1 < \dot{\boldsymbol{\varepsilon}}_2$ the ice is contracting (Figure 14). Under expansion a calving rate can be formulated as product of the two eigenvalues and a constant k_Φ (in m s evaluated at the calving front):

$$\dot{c} = k_\Phi \; \dot{\boldsymbol{\varepsilon}}_1 \; \dot{\boldsymbol{\varepsilon}}_2. \tag{23}$$

[93] The constant k_Φ depends on the fracture density field that can be matched with remote sensing observations of crevassing (Figure 15). Once the model is tuned to observations, there are no other observations needed for the model to "carry itself forward" into the future. That is, it can "predict" calving without any other observations inputs (the necessary inputs would all come from the model dynamic ice sheet model). However, this may not produce reasonable future simulation given the importance of sub-ice shelf process affected by changing ocean regime such as influx of CDW as discussed in section 5.1. Over broad areas of an ice shelf, the viscosity is reduced by crevasses (e.g., along the flow units coming from different tributary ice streams and glaciers), or the ice may be strengthened by the presence of sub-ice shelf freeze-on of ocean water. The crevasses can be readily seen in imagery, and these images can be used to tune models for ice viscosity and fracture initiation stress in specific ice shelves or tributary ice streams to give similar patterns of both crevassing and velocities as observations [*Albrecht and Levermann*, 2012a, 2012b].

5.3. Grounding Line

[94] The grounding line is the transition region where land-based ice begins to float as it is carried to the calving front. As mentioned in section 3.2.3, the West Antarctic ice sheet is a marine ice sheet where significant parts are grounded below sea level. The area is suspected as a candidate for the rapid sea level rise of Meltwater pulse 1a. Furthermore, the Pine Island and Thwaites glacier catchments that drain along reverse sloping bedrock troughs have been losing ice mass over recent decades. Questions over the stability of marine ice sheets (see the review by *Vaughan* [2008]), and most especially, the grounding line where they reach floatation is an active research topic. In the late 1990s, the first systematic investigations (EISMINT) [*Huybrechts*, 1998] on the representation of grounding line migration in numerical models showed a high dependency of the results on the numerical implementation, the grid resolution, and the applied simplification of the governing Stokes equations. The most prominent finding at this time was the irreversibility of grounding line position on a sloping bedrock if a perturbation in terms of sea level rise was applied and reset thereafter. This result led to the conclusion that the state-of-the-art numerical ice sheet models were not able to correctly predict the behavior of marine ice sheets [*Vieli and Payne*, 2005] and, consequently, were explicitly excluded from IPCC prognostic projections of sea level rise [*Bindoff et al.*, 2007].

[95] Recently, a deeper understanding of the mechanics around the grounding line has been provided [*Schoof* 2007a; 2007b; *Schoof*, 2011] that allows the use of the "matched asymptotic expansion technique" [*van Dyke*, 1964; *Kevorkian*

and Cole, 1981; *Schoof and Hindmarsh*, 2010]. This results in a set of boundary conditions (for the thickness as well as the flux at the grounding line) that enable the treatment of marine ice sheets as a moving boundary problem [e.g., *Pollard and DeConto*, 2009] in the SIA. However doubts have been raised about the applicability of the Schoof approximation in three dimensions, and also when the grounding line changes rapidly [*Drouet et al*., 2012] such as the decadal period accelerations observed at Pine Island glacier. A comprehensive report on the behavior of different combinations of approximations to the governing equations and treatment of the grounding line problem is given in *Docquier et al*. [2011]. *Gladstone et al*. [2010] investigated how the subgrid cell treatment of the ice thickness profile from the last grounded to the first floating grid point impacts the required resolution of a model, they show that a wise choice of parameterization could give similar model performance as doubling resolution with simpler parameterization schemes.

[96] The alternative to using the Schoof boundary layer formulation is to resolve the grounding line at horizontal resolutions significantly smaller than the ice thickness at the grounding line. Additionally at the grounding line, all stress components should be accounted for to resolve the dynamics of this boundary layer. These demands have been studied within two-dimensional [*Durand et al*., 2009a, 2009b] as well as recently three-dimensional [*Favier et al*., 2012] synthetic marine ice sheet setups, all conducted within the MISMIP (Marine Ice Sheet Model Intercomparison Project) [*Pattyn et al*., 2012]. Recently, models with highly resolved three-dimensional applications have begun to appear in the literature [*Goldberg et al*., 2009; *Favier et al*., 2012; *Cornford et al*., 2013]. To date, many prognostic studies on the ice sheet scale have been performed with higher-order models or types of SSA models—either by their complete set of equations in a hybrid model together with SIA or as a special type of sliding boundary condition [*Bueler and Brown*, 2009]. However, most models used to predict sea level rise do not include any grounding line migration [*Bindschadler et al*., 2013; *Levermann et al*., 2012a, 2012b].

[97] *Gladstone et al*. [2012] examined an ensemble of scenarios for the future of Pine Island Glacier (Figure 6) when forced by a regional ocean model driven by the A1B SRES scenario to the year 2200. They were not able to usefully constrain the rate of retreat of the glacier using a flowline model, with full collapse of the glacier possible by 2200. However, they used a relatively simple model. It is likely that three-dimensional flow will influence these results [*Cornford et al*., 2013], and initial simulations with a 3-D Stokes model [*Gudmundsson et al*., 2012] confirm earlier results by *Katz and Worster* [2010], using an $n = 1$ flow law (i.e., a Newtonian fluid; Figure 8), that grounding lines on reverse slopes can be dynamically stable.

[98] While erosion rates beneath ice streams probably amount to only a few millimeters per year [*Cowton et al*., 2012], observational evidence on the Whillans Ice Stream in West Antarctica (Figure 6) supports the expectation that at the grounding line a deposit of sediment may be formed (Figure 16) [*Anandakrishnan et al*., 2007]. This ice stream does not start to float until it descends the downstream side of the sedimentary wedge. The grounding line is therefore situated where locally the bed slopes upward inland, irrespective of the regional bed slope. It should be emphasized that this is the only example of an ice stream where this wedge is known to exist; observational evidence at this resolution is generally hard to acquire. However, in this case at least, the wedge may make the ice stream grounding line stable against rises of sea level of perhaps a few meters [*Alley et al*., 2007].

5.4. Basal Sliding

[99] A topic tightly interlinked with fast outlet, marine-terminated glaciers and ice streams is the physics of basal sliding. Naturally, by its inaccessibility, the basal conditions (the general term for the lower boundary of a land-based ice sheet or glacier that may be some meters thickness of (dilatant) till over hard bedrock, or simply hard rock) is a largely unknown and unmeasured part of the system. In temperate glaciers (i.e., glaciers with temperatures at the pressure melting point) sliding behavior is often intimately related to basal hydrology.

[100] On the continental ice sheets, the fast-flowing ice streams and outlet glaciers owe their speed to basal sliding in addition to internal ice deformation. Outlet glaciers and ice streams comprise only 13% of the Antarctic coastline, but they drain more than 90% of the snow that accumulates in the interior [*Morgan et al*., 1982]. In Greenland, the flux from Jakobshavn, only about 5 km in width near the grounding line, is about 7% of the annual mass loss from the ice sheet [*Rignot and Kanagaratnam*, 2006]. Ice streams are somewhat defined by the subglacial geometry; that is, they tend to be in bedrock troughs. However, it is probable that the supply of water—generated by internal ice deformation or frictional heating, high geothermal heat flux, or subglacial water routing—plays the dominant role in defining the location of an ice stream. Observations on Antarctic ice streams reveal that fast-flowing regions in close proximity may vary in the mechanism of their deformation, but with sliding on the ice-till interface or deformation within the subglacial till being dominant. It is now recognized that the subglacial water system beneath much of Antarctica is linked in complex ways [*Fricker et al*., 2007]. The variation in water supply leads to changes in basal water pressure, which can, in places, be essentially equal to the ice overburden pressure. The difference between the ice overburden pressure and the water pressure is the effective pressure. Since till has been observed to be dilatant, this high water pressure is required for the till to undergo plastic failure since otherwise the overburden pressure would make the till far stronger than the ice above it, effectively creating a hard rock bed. The processes controlling subglacial effective pressure and sediment strength are only partly understood [e.g., *Clarke*, 2005]. To be physically authentic, modeled sliding must, however, depend on the strength of the basal material and on the amount of liquid water present at the ice base. For realistic behavior of ice streams the ice basal temperature and basal water must coevolve [e.g., *Bougamont et al*., 2011], which was a problem

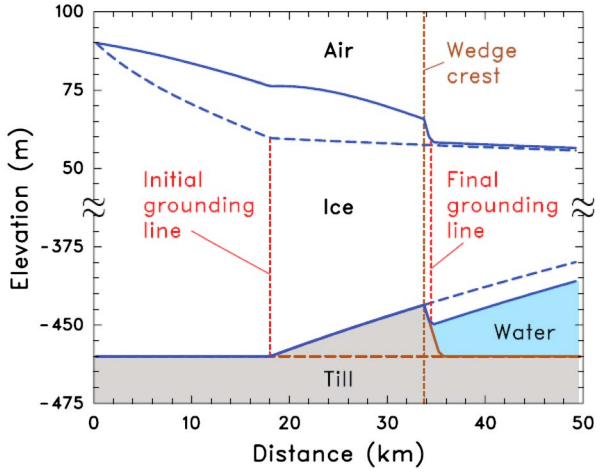

Figure 16. Diagrammatic representation of the Whillans ice stream grounding line. The ice which is firmly grounded is often modeled using the SIA equations (equation (10)), while the floating ice shelf can be modeled with the SSA (equation (11)), with the transition solved using the Schoof equations [*Schoof*, 2007a, 2007b] or a Stokes simulation. Observations of this ice stream grounding line using radar show a sediment wedge deposited by the ice stream, similar features on other ice streams have not yet been found. Dashed lines show the steady ice stream profile in the absence of a grounding line wedge, and solid lines show the wedge and the corresponding steady ice stream profile. The wedge causes the ice to thicken, the grounding line to advance past the wedge crest, and an inflection point to form in the upper surface at the upglacier end of the wedge, which might serve to increase water storage there. The potentially unstable reverse slope grounding line will be changed to a normal slope in the immediate vicinity of the final grounding line. From *Alley et al.* [2007]. Reprinted by permission.

in earlier generations of ice models where often sliding was simply switched on wherever the basal ice was at the pressure melting point. *Schoof* [2005] predicted a sliding law dependence on basal roughness and water pressure which was then verified using a full Stokes model by *Gagliardini et al*. [2007] on a synthetic bed geometry. This sliding law also has some support from laboratory measurements [*Iverson and Petersen*, 2011]. *Schoof* [2009] showed that this law and a variety of other friction laws converged on the Coulomb friction law in appropriate parametric limits. From a practical perspective, this is important as it allows numerical solutions to be computed using smoother friction laws than a classical Coulomb friction law. The Coulomb friction law cannot be used in conjunction with the SIA since the friction law predicts bounded basal drag [*Iken*, 1981; *Schoof*, 2005; *Gagliardini et al*., 2007], which on steeply sloping beds, means that the driving stress cannot be balanced locally by basal drag (as it must be in an SIA). Hence, longitudinal or lateral stresses must become important to ensure force balance on the glacier. *Pimentel et al.* [2010] produced a higher-order model of a valley glacier that takes into account subglacial hydrology and a Coulomb friction law describing glacier sliding with cavitation. The spatial and temporal evolution of subglacial water pressure on Glacier Haut d'Arolla was shown to regulate basal sliding speed through the Coulomb friction sliding law.

[101] The motion of ice streams appears to depend critically on the distribution and nature of regions of high drag (sticky spots) [*Alley*, 1993]. It is not known what controls the present configuration of these features, though presumably they are related to the bed roughness and geometry—either directly as a bedrock bump, or by routing water supply and till properties. How the location of sticky spots varies over time is not known. The observation that Kamb Ice Stream on Antarctica's Siple coast (Figure 6) has become stagnant during the last few centuries [*Retzlaff and Bentley*, 1993] and an adjacent one is slowing down [*Joughin et al*., 2002] suggests that the response of these systems can vary over timescales significant for sea level rise within the coming century. The driving mechanisms for these centennial-scale changes relates to water supply to the beds beneath, and water piracy between, ice streams [*Tulaczyk et al*., 2000; *Anandakrishnan and Alley*, 1997; *Bougamont et al*., 2011]. This is presumably independent of climate forcing since the locations of the ice streams appear to have been the same since the last glacial period [*Anderson and Shipp*, 2001] despite widespread retreat of the grounding line as sea levels rose 120 m. As the surface temperatures in the onset regions of the Antarctic ice streams are far below melting point, changes in climate forcing cannot directly affect the water supply to these ice streams; hence, it must be extremely unlikely that this mechanism will lead to generation of new ice streams in Antarctica.

[102] In Greenland, surface melting occurs to altitudes of about 2000 m [*Tedesco et al*., 2011]. The supply of surface water to the bed is well documented and found to affect ice velocities on seasonal scales [*Zwally et al*., 2002]. However, *Das et al*. [2008] showed that this effect does not seem to affect ice discharge on annual timescales, an important finding which was confirmed by analysis of surface mass balance and GRACE satellite mass loss estimates for Greenland [*van den Broeke et al*., 2009; *Moon et al*., 2012]. *Schoof* [2010] and *Pimentel and Flowers* [2011] showed why these effects occur with a model that combined both a distributed (high pressure) drainage system with switching to a channelized (low pressure) system. Above a critical water flow, a steady water supply slows down a glacier through more efficient subglacial drainage and lower subglacial water pressures. Enhanced ice flow occurs as a result of short-term variations in water supply that lead to temporarily enhanced subglacial water pressure. This has consequences under changing climate for the Greenland ice sheet where we may expect more periods with short-term high water pressures through rain fall events, and a longer season when diurnal melting occurs.

[103] Jakobshavn ice stream is topographically well controlled in a deep bedrock trough (Figures 4 and 5), and hence contains deep, thick, and warm ice that provides a basal water supply. On the other hand, the Northeast Greenland Ice Stream (Figure 4) originates much nearer the ice divide than all other ice streams and seems to be driven by a high geothermal heat flux causing melt rates of up to 15 cm/yr

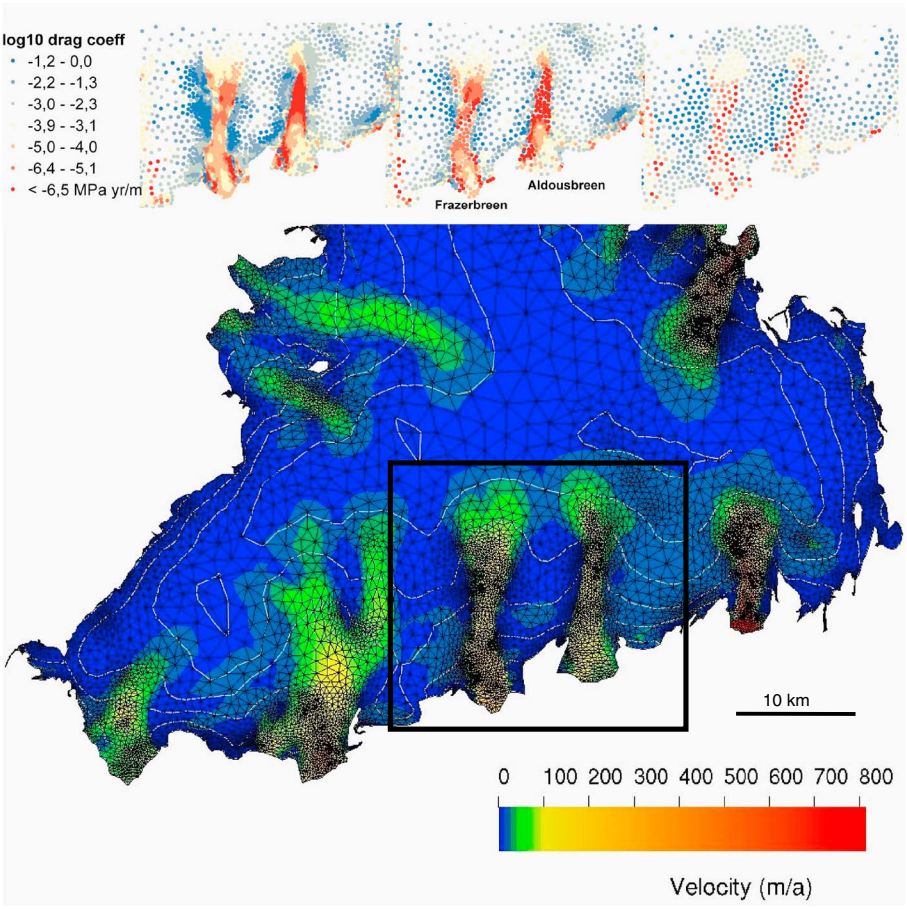

Figure 17. Unstructured finite element grid for part of Vestfonna ice cap (Svalbard) where higher resolution corresponds to higher observed velocities. The coarse grid is clearly evident in the central regions and the dense network of nodes in the faster flowing outlet glaciers. Inset at top is the basal drag coefficient distribution from *Schäfer et al*. [2012] with high drag in blue and low drag in red, derived by three different mesh choices for the two outlet glaciers in the boxed section on the main image. The unstructured mesh shown in the (left) main image, (middle) a coarser mesh, and (right) a regular mesh.

[*Fahnestock et al*., 2001]. The path of the ice stream is likely driven by the path of the water drainage—which in turn is driven by ice sheet topography driving hydraulic potential. The high geothermal heat flux is not likely to change over century timescales, suggesting stability from climate forcing.

[104] Although parts of the physics of basal sliding are becoming understood, the critical issue continues to be lack of information on bedrock conditions that makes it difficult to determine appropriate parameter values to use within a sliding model. Measurements usually exist on the upper surface of the glacier or ice sheet. In recent years, satellite observations have improved in quality and velocity maps and digital elevation models over the ice sheets are available for both ice sheets (Figures 4 and 6). In addition, many of the features of ice streams on ice sheets are also found on smaller ice caps which are much more accessible, for example, Vestfonna and Austfonna on Svalbard. In combination with ice flow models, these data can be used to inversely determine the sliding conditions at the bedrock. As with any inverse method, the utility of the answer provided depends on the physics of the forward model; in this case, the sliding model used will affect the inverse solution found. More rigorously, this information can be found by the use of an adjoint model of a nonlinear Stokes problem. Adjoint models can be obtained by the automatic differentiation of a forward model [e.g., *Heimbach and Bugnion*, 2009], but this procedure is presently available only in "low level" programming languages. Hence, it is not possible to retrieve an automatic derivative of any arbitrary chosen ice sheet model. Nevertheless, three different methods have been proposed that avoid this issue by solely making use of the forward model: (1) Bayesian method [*Raymond and Gudmundsson*, 2009]; (2) Control method using the (self-)adjoint of the linear Stokes problem [*Morlighem et al*., 2010; *Petra et al*., 2012]; (3) An inverse Robin method [*Arthern and Gudmundsson*, 2010].

[105] The latter two are variational methods and minimize a cost function that measures the difference between observations and computed results. The Robin method has been applied to the flowline of a surging glacier [*Jay-Allemand et al*., 2011] and in three dimensions to the whole Greenland ice sheet [*Gillet-Chaulet et al*., 2012] and the Vestfonna ice cap on Svalbard (Figure 17) [*Schäfer et al*.,

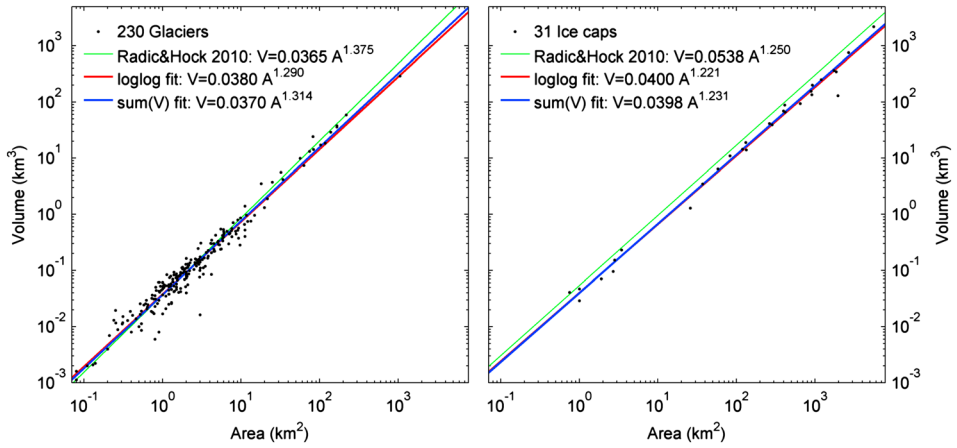

Figure 18. Area volume scaling for glaciers (left) and ice caps (right) from a collection of well studied glaciers and ice caps by *Cogley* [2012]. The y-axis is the same so that the smaller volumes for a given area of ice caps can be seen. The fitted lines are the least squares log volume regression (magenta) and a weighted least absolute volume deviation regression (cyan) [see *Grinsted*, 2013]. The parameters from *Radic and Hock* [2010] with prescribed χ are also shown (green).

2012]. In these approaches, the grid resolution makes important changes in the derived ice flux transported to calving fronts. In many models, uniform meshes are used, whereas recently it has been more common to use unstructured meshes where the element size can be set according to some observations or desirable property, such as surface velocity change. This leads to a focus of processing power and resolution on the more interesting parts of the ice sheet (typically fast flow regimes) at the expense of slow moving, less steep, and less spatially and temporally variable parts (Figure 17).

5.5. Mountain Glaciers

[106] There is a considerable difference in volume loss estimated by the process-based mass balance calculations and the AAR methods (Figure 11). The time constant of glacier loss may influence this, as most ice mass is contained in the large glaciers [*Grinsted*, 2013] with likely longer time constants. Furthermore, since the AAR method produces a percentage estimate of total glacier volume that should be removed to balance climate forcing, it relies on a reliable estimate of total glacier volume. A practical method used to estimate the total volume of all glaciers in the world is volume-area scaling (equation (16)). Recently, novel methods have been developed based on ice physics and flux-balance considerations that can also be applied globally [*Huss and Farinotti*, 2012]. Scaling laws can be physically justified for idealized perfectly plastic glaciers where exponents (χ) of 1.375 and 1.25 have been argued to be appropriate for straight valley glaciers and circular ice caps, respectively [*Bahr et al.*, 1997]. These relationships are designed to capture how the volume of an idealized glacier changes as it grows or shrinks. The idealized assumptions are only approximations, and for real glaciers other exponents may give a more accurate approximation to their behavior. Furthermore, there is no a priori reason to expect that the same scaling constant will be appropriate for all glaciers even if the idealized assumptions were to hold. However, empirical estimates of volume and area support the notion that a universal scaling law can be applied across a wide range of sizes, although the scatter indicates that applying such scaling laws to individual glaciers can only provide estimates with large uncertainties in the range of 50–200% (Figure 18). For real glaciers, we may have situations where it is not obvious how to divide an ice mass into a distinct number of glacier units. For example, several valley glaciers may share the same ice field, or two valley glaciers may meet in a single tongue. The practical problem of how the area is divided among separate units has an impact on the total volume due to the nonlinearity of the scaling law. The division issue can be particularly important for volume estimates based on the new global Randolph Glacier Inventory (RGI) [*Arendt et al.*, 2012] where each glacier unit may not have been carefully divided into distinct units because of the vast number of new glacier outlines the RGI contains. That is, in some regions, individual inventory records may represent large glacier complexes rather than individual glaciers, while some ice caps have been subdivided according to drainage basin. The physical flux-balance approach of *Huss and Farinotti* [2012] is likely less sensitive to glacier complex issues, but requires additional assumptions on the mass balance, and flow of ice.

[107] In Figure 18b we see that the *Radic and Hock* [2010] ice cap volume-area scaling law has a large bias of the order of +50% [*Grinsted*, 2013] relative to observations. The bias may be explained by considering the units of the constant κ (equation (16)) which are length$^{(3-2\chi)}$. The scaling constant determined from one study is thus not applicable to a scaling law relationship using another exponent as was done in, e.g., *Radic and Hock* [2010].

[108] Often the goal of volume-area scaling is to estimate the total volume of all glaciers and ice caps in a large sample (e.g., the whole world). The traditional technique to estimate χ and κ is from a sample of known volume and area glaciers using least squares straight regression in a log-log space. The model arising from this approach is optimized to minimize the relative misfit for a wide range of size classes and is heavily biased toward the small- and medium-sized glaciers

for which most observations are available. Alternatively, we can construct a model where we minimize the absolute volume misfit weighted to reduce any sampling bias in the calibration data set. The resulting alternative model is better suited to estimate total volumes, which are directly related to sea level, as an error in the volume of a large ice mass is more important than an error in a small ice mass [*Grinsted*, 2013].

[109] The mountain glacier sea level component has, to date, only considered mass balance modeling. Process-based mass balance models do not estimate calving loss from marine-terminated glaciers as a function of environment driving forces; but they may simply balance flux that arrives at the glacier front to keep a constant front position. As already mentioned, calving losses are significant for regions with marine-terminating glaciers. None of the mass balance models presently used for aggregated studies of sea level rise were designed to work in regions with summer accumulation as well as ablation, such as that which occurs in Himalayan and tropical glaciers. Energy balance modeling has the potential for more complete mass balance modeling, but at present the number of glaciers with available data is very few. Degree-day factors vary considerably over Tibet, and potentially with time as anthropogenic pollutants such as black carbon are being emitted more in Asia than elsewhere [*Xu et al*, 2009; *Ramanathan and Carmichael*, 2008]. The statistical models used by *Slangen and van der Wal* [2011] and by AR4 do not have the potential to reach a mass balance in equilibrium with a different climate, and therefore a small perturbation will ultimately lead to either complete loss or unrestricted expansion of glaciers. This is unlikely to be important on decadal timescales, though it does indicate an unphysical element in these models.

5.6. Initial Conditions

[110] With all models, a decision must be made on when the preparatory spin-up has produced a realistic state such that a simulation for time evolution may begin. This preparatory state is usually taken to be the preindustrial period before anthropogenic forcing and the industrial revolution began. This is the case for coupled atmosphere-ocean models which require a long time (of the order of 1000 years) for the deep and abyssal ocean to move away from preset initialization temperatures (and observations to test against are sparse) [*Li et al*., 2012]. When projections are made through the 21st century, it is assumed that the models are correctly starting from the pre-industrial conditions. However, some models show drift which is sometimes simply removed in a post processing step [e.g., *Yin*, 2012; *Gupta et al*., 2012]. This probably accounts for much of the scatter in steric sea level rise estimates [*Gupta et al*., 2012].

[111] In ice sheet models typically at the end of the spin-up, model forcing is changed from scaled ice core-derived values of temperature and surface mass balance to a more complete representation of spatial variability from climate models. This transition introduces a step-like change over the ice sheet that the model then diffuses away over some timescale (likely to be decades). When using fully thermomechanically coupled models the temperature evolution is very slow compared with the dynamical behavior. This implies that setting up the correct temperature distribution with an ice sheet model requires many tens of thousands of model years to reach a steady state, and this is not possible in a full Stokes model given present computational limits. A simple way around this is to assume steady state conditions—which can be easily calculated, but which of course never exist in a real ice sheet. Therefore, *Seddik et al*. [2012] in their FS model of Greenland used a shallow ice model to evolve the temperature distribution through a glacial cycle in the ice sheet and then used that thermal distribution as the initialization of the FS model to simulate future evolution. The geometry was fixed, except for a few decades of relaxation. Naturally the geometry and dynamical state of the ice sheet from the SIA model would be different from that produced by the FS with the same thermal structure, hence there are issues involved in matching the models so as not to give an unphysical step change in geometry or ice flow. Thus, the FS model will adjust to the change which will be manifested as a drift in ice volume, and the sea level response can only be interpreted in a relative sense. To arrive at the total sea level contribution, the baseline sea level change from some control run that contains the initialization drift but no forcing must be subtracted.

[112] *Mitrovica et al*. [2001] analyzed patterns of sea level rise globally and inferred that the Greenland ice sheet contributed about 0.6 mm/yr to global sea level over the twentieth century. This is consistent with the missing element of the sea level budget plotted in Figure 3, which was also estimated to be a trend of 0.6 mm/yr prior to 1950. It is not clear when such a contribution may have started, but an assumption has been commonly made in models that ice sheets were in equilibrium with preindustrial or present-day climate forcing [e.g., *Seddik et al*., 2012]. This is due to (1) limitations to available computational power needed for standard ice sheet spin-ups, (2) limited utility of standard spin-up procedures even if the necessary computer resources were available (e.g., a standard spin-up will not produce a modern-day ice sheet that is close enough to the real one to be directly useful for prognostic simulations), and (3) limitations to current formal optimization procedures as applied to ice sheet models (and limits on the available data for use as constraints). The problems with model initialization are thus known, and attempts are being made to tackle them now. A common procedure is to subtract the model results using the preindustrial or present day forcing from the results with the prescribed forcing applied [e.g., *Seddik et al*., 2012; *Bindschadler et al*., 2013] so that hopefully errors in initial conditions will be canceled.

5.7. Model Coupling/Potential Feedbacks

[113] Coarse-resolution ice sheet models forced by atmospheric models have been used to simulate sea level and ice sheet coupling for several decades over a variety of timescales from centennial to glacial-interglacial [e.g., *Philippon et al*., 2006; *Vizcaino et al*., 2008; *Fyke et al*., 2011]. However, these models tend to only have very crude ice sheet dynamics, and

feedbacks typically are simply changes in topography as ice sheets decay under temperature and precipitation forcing. For example, *Fyke et al.* [2011] note "The obvious relationship between ocean temperature and ice shelf melt rates calls for a parameterization that links ice shelf melt rates to coarse modeled ocean temperatures. However, this version of the coupled model does not currently include such a parameterization as a default option."

[114] The importance of high-resolution ocean models was illustrated by the response of the Filchner-Ronne ice shelf to sub-shelf melting over the 21st century simulated by *Hellmer et al*. [2012]. Few such simulations have been done to date, and none have incorporated a two-way response of ice sheet and ice shelf on the atmosphere and ocean in Earth System Models. Potentially important feedbacks occur when freshwater fluxes from the ice sheets may strongly influence the thermohaline circulation of the global ocean [*Stammer et al*., 2011; *Hu et al*., 2011; *Weijer et al*., 2012]. Increased fresh water flux is occurring in Greenland from both accelerated ice discharge and increased surface melting. Beyond a threshold level of freshwater flux, the Atlantic circulation changes become so large that they in turn have an impact on the climate forcing over Greenland. Longer term topographic change in the ice sheets are implicated in circulation changes and moisture supply during the deglaciation [*Kapsner et al*., 1995] that can influence relations between temperature and precipitation. The topographic effect is unlikely to be relevant in the next century [e.g., *Vizcaino et al*., 2008], but the changing moisture source from the Arctic Ocean as the Arctic sea ice declines is certain to be significant. Very high resolution ocean circulation fjord models are required to simulate the response of the Greenland ice streams such as Jakobshavn and Petermann that terminate in long, narrow fjords, and the few observations to date indicate complex three-dimensional flow in the fjord and perhaps underneath the floating ice [*Johnson et al*., 2011]. A feedback effect between sea level and ice sheets not included to date in models involves the gravitational changes at the grounding line as the ice retreats. Though sea level rises globally, there is a local drop in sea level at a rapidly retreating ice margin that can act, on some timescales, as a stabilizing factor for the grounding line on reverse sloping bedrock [*Gomez et al*., 2010].

5.8. Semiempirical Calibration Issues

[115] For semiempirical models, the historical record of climate forcing and the response of sea level are crucial since the future prediction can only capture processes that have occurred during the past "training period." As Figure 1 shows, the choice of calibration data set used over the tide gauge period makes a significant difference to the semiempirical parameters determined and hence to the predicted sea level response. *Grinsted et al*. [2010] estimated that the *Moberg et al*. [2005] forcing data set was much more likely in a Bayesian sense than the *Jones and Mann* [2004] temperature reconstruction. Radiative forcing may be a more reliable indicator than global temperatures since radiative forcing is a less locally determined variable than temperature and hence better determined by fewer observations. However, there are several radiative forcing data sets available, and the volcanic forcing term, in particular, is rather variable among the alternative forcing data sets. This partially reflects the limited spatial information on volcanic forcing which comes largely from ice cores drilled on the polar ice sheets.

[116] In semiempirical models, the long-term response of sea level is hard to separate from a nonclimate response, in an analogous way with spin-up for ice sheet models. The latest Rahmstorf model [*Kemp et al*., 2011a, 2011b; *Rahmstorf et al*., 2011] uses the infinite response term (equation (18)) to model both the nonclimate sea level and the slow response. The *Jevrejeva et al*. [2010] model does not explicitly have that possibility since there is a single response time. Long-term disequilibria must instead be subtracted in a similar manner as nonclimatic sea level variability.

[117] There are clearly differences in projections based on using the multiple response time formulation (equation (18)) or the single response time formulation (equation (20))—as was discussed in section 4.4. The multiple response model shows a difference in projections of up to 25 cm if land water contribution is taken into account during the period of calibration [*Rahmstorf et al*., 2011], while the single response time method is much less sensitive, changing by only a few centimeter changes in projections if land water component was eliminated from calibration sea level time series [*Jevrejeva et al*., 2012b]. The multiresponse time model is also more sensitive to changes in the calibration data set and forcing scenario. For example, using sea level data from *Jevrejeva et al*. [2008], *Rahmstorf et al*. [2011] project 135 cm while using *Church and White* [2011] only 87 cm of sea level rise by 2100. In contrast, the single response time model shows median rises of 103 cm, 90 cm, and 135 cm by 2100 with three different radiative forcings (Figure 1b).

[118] To illustrate the impact of processes with two different response times, Figure 19 shows how fast and slow processes (such as mountain glaciers and Antarctica) may contribute a mixed signal to global sea level when forced by a cooling climate (somewhat like the Little Ice Age, LIA) and then abrupt warming. Sea level reaches a long-term minimum during the nineteenth century, then begins to rise. In the example, both the glaciers and the ice sheets are slowly growing as a response to the steadily cooling LIA conditions. Once the trend is reversed with abrupt warming, the glaciers react fastest. It could be argued that a model fitting the response of global sea level in such an example will be fooled by the quick responder (which can only contribute about 0.6 m sea level), into extrapolating a response for the whole cryosphere (contributing much more sea level). The obvious way to resolve the issue is to see what happens as the glacier reservoir is emptied, though this requires a long period of observations. This issue can actually be resolved in practice by careful consideration of the past sea level and the components of the sea level budget, which provide good constraints on the parameters that are fitted in a semiempirical model (see section 3.1). To do so, however, requires use of as long a model calibration period as possible—that means using the full length of the tide gauge data set and any proxy sea level

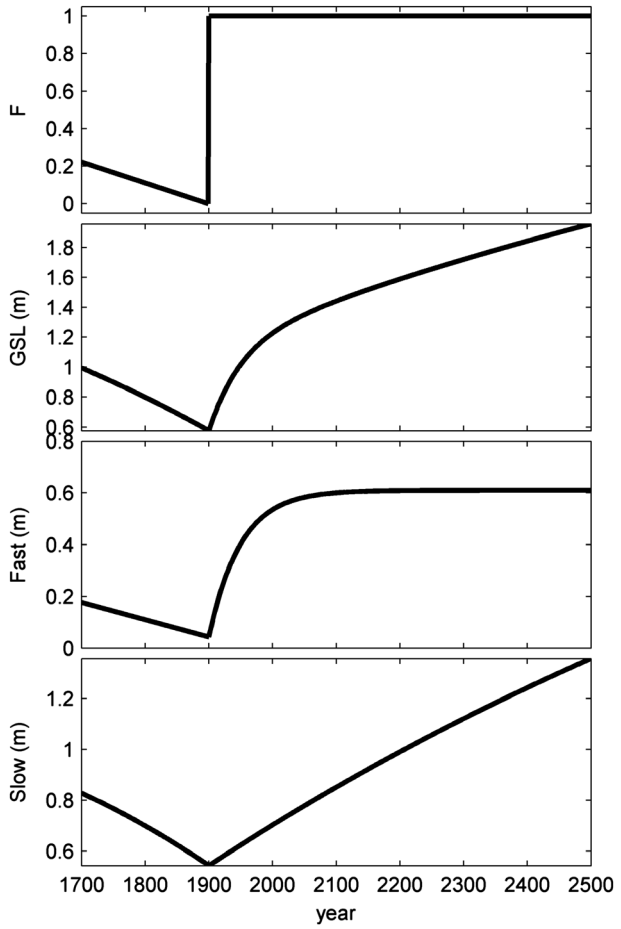

Figure 19. Fast and slow response elements in a simple sea level model forced by an abrupt warming after steady cooling. The parameters chosen for the fast response are a 50 year response time with $a = 0.6$ and $b = 0$ in equation (21), and the slow system has a 1500 year response time $a = 5$ and $b = -2$. F may be interpreted as either a change in global mean temperature (C°) or a change in radiative forcing (W/m^2).

data sets [*Bittermann et al*., 2013]. Tide gauge data extends through the eighteenth and nineteenth centuries when global sea level was in equilibrium with temperatures around the end of the Little Ice Age.

[119] It is crucially important to know if the ice sheets (the slow reservoir in Figure 19) were supplying a significant component of the sea level rise during the twentieth century. If they were not, then the difference in sea level prediction from process models (Figure 1) could be due to only sampling the fast response mountain glaciers in the semiempirical modeling training period. Several lines of evidence suggest that Greenland was contributing to sea level through the twentieth century: *Mitrovica et al*. [2001] suggest 0.6 mm yr^{-1} over the past 100 years; *Wake et al*. [2009] and *Bjørk et al*. [2012] suggest evidence of mass loss from glacier front and mass balance reconstructions; and *Csatho et al*. [2008] detected thinning of Jakobshavn Isbræ during 1902–1913, linking this behavior to the interaction of ice dynamics with changes upstream of Jakobshavn Isbræ. *Jevrejeva et al*. [2012b] examine how mass loss from Greenland if correlated with mountain glacier reconstructions gives reasonable closure to the observed sea level budget (see also Figure 3). Against this evidence for a long term contribution is the observation that through the relatively dense period of observational evidence spanning the period from about 1980, the mass balance of Greenland changed from near zero to strongly negative [*van den Broeke et al*., 2009], which does not of course rule out an earlier period of negative mass balance (which is indeed shown around 1970) [*van den Broeke et al*., 2009]. While there is no evidence that Antarctica was contributing, lack of evidence does not constitute proof that no contribution was being made.

5.9. Semiempirical Parameter Fitting

[120] Uncertainties in sea level observations are controlled by various factors. Instrument error and random noise introduce white noise to each individual tide gauge or proxy. Large-scale atmospheric circulation trends produce spatially correlated and long-period noise characteristics similar to red noise. Inhomogeneous sampling introduces spatial biases, whereby one particular ocean basin (such as the Northeastern Atlantic) may experience regional changes, e.g., in thermohaline overturning circulation, that can dominate sea level on continental scales for decades. While the north Atlantic is overrepresented in the early part of the record, many regions especially in the Southern Hemisphere were unsampled until recent decades.

[121] A simple assessment of the global mean sea level assuming red noise reveals only about 5 degrees of freedom [e.g., *Bartlett*, 1935]. This would severely constrain semiempirical fitting when models contain four or five free parameters. However, there are more sophisticated ways of avoiding overfitting. *Grinsted et al*. [2010] calculated the likelihood of a particular model set of parameters based on the misfit between observed and modeled sea level. This procedure takes into account the serial error covariance in the data. The likelihood function can be written as a multivariate Gaussian distribution:

$$L(m) = \gamma e^{-\frac{1}{2}(S(m)-S_{\mathrm{obs}})^T C^{-1}(S(m)-S_{\mathrm{obs}})}, \qquad (24)$$

where γ is a normalization constant, $\boldsymbol{S}_{\mathrm{obs}}$ and $\boldsymbol{S}(\boldsymbol{m})$ are the vectors of observed and modeled sea level, respectively, and $\boldsymbol{C}$ is the uncertainty covariance matrix (Figure 20) where $\boldsymbol{C}_{ij}$ is the covariance between the global sea level uncertainty at time instants i and j. The negative exponent is a measure of the misfit between model and observations normalized by the observational uncertainties. In *Rahmstorf* [2007a, 2007b], the model misfit was expressed in terms of sea level rise rate rather than sea level itself, and therefore the smoothed the data, reducing further the degrees of freedom. All observations were considered to be independent (after binning) and of equal variance at all times, hence the $\boldsymbol{C}$ matrix of *Rahmstorf* [2007a, 2007b] is simply a constant, that is, only the leading diagonal is nonzero. In *Rahmstorf et al*. [2011] (the same model as in *Kemp et al*. [2011a]) the $\boldsymbol{C}$ matrix is assumed to be defined by a first-order autoregressive model (red noise); that is, the $\boldsymbol{C}$ matrix elements decay to zero rapidly away from the leading diagonal, but the values along the diagonal increase over time due to observational error.

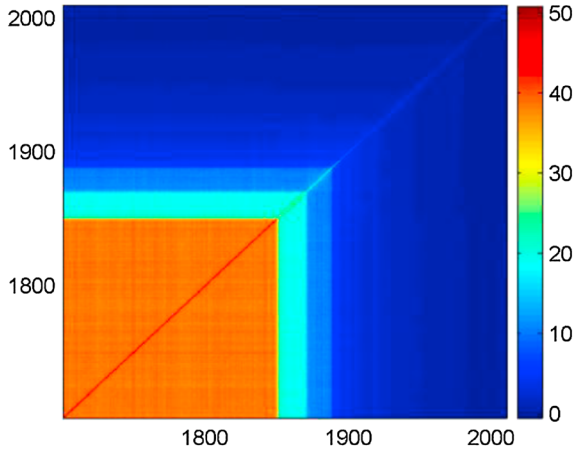

Figure 20. Uncertainty covariance matrix $\boldsymbol{C}$, for the global sea level reconstruction since 1700 of *Jevrejeva et al*. [2009; 2010], color bar in (cm^2). The lowest uncertainties are during the period 1980-1999- the reference period. Uncertainty in early periods reflects tide gauge station observations being only from Europe. The leading diagonal has higher uncertainty than the perpendicular elements immediately adjacent to it, reflecting the decorrelation process whereby errors tend to cancel over time. The dominant characteristic is the persistent correlation in uncertainty reflected in the rectilinear error map and which is due to the lack of sampling (representativity issue) of sufficient ocean basins. Alternatively, the map can be thought of as integrating uncertainty as we go back in time from the present (known sea level); if an error exists at some point in time, it will also be present all preceding times; hence, uncertainty must always increase with time from the baseline period. These errors are larger (that is, more conservative) than the ones used in *Jevrejeva et al*. [2008] and *Rahmstorf et al*. [2011].

This model effectively means errors are decorrelated over decadal time periods, so that century-scale trends are rather well defined. *Grinsted et al*. [2010] made different error assumptions. They assumed a white noise observational error, but then a red noise error to simulate large-scale processes such as circulation changes. However, the dominant error is the representativeness of a tide gauge station. The structure of that error can be estimated using a jack-knife procedure where the impact of removing ocean basins on the global sea level variability is explored. This procedure is only an exploration, since available data are too sparse to define an accurate $\boldsymbol{C}$ matrix and long correlation times—so the far-off diagonal elements in the $\boldsymbol{C}$ matrix were fitted assuming a Markov chain process. Overall, this leads to correlation of errors over longer times than the red noise assumption, and larger uncertainties in long-term trends. An empirical orthogonal function analysis (as used in the sea level reconstruction of *Church and White* [2011]; Figure 3) would of course give regional patterns of sea level that could give an estimate of representativeness—but it would only give a snapshot at one time, hence it would not reveal changing patterns of sea level that result from either climate change or long-period natural variability.

[122] Once the likelihood function is defined, then estimates are produced of the full range of likely model parameters which result in a "reasonable" fit to the observations. Reasonable is defined by the likelihood function, such that acceptable models do not give a much worse misfit than the best guess model (which would be the result of a singular value decomposition). *Jevrejeva et al*. [2012a, 2012b] examined the use of semiempirical model to fit to process-based models of steric sea level. This allows an independent estimate of the confidence of fitting to output from a physical climate model. The resulting projections agree with process-based estimates of future steric sea level within the confidence intervals estimated from the Monte Carlo method.

6. SUMMARY AND OUTLOOK

[123] Much progress has been made in understanding ice flow via process models (Table 2). This is also reflected in the convergence in estimates of sea level rise for the year 2100 (Figure 1). While the state of understanding in 2007 suggested that either process-based models were missing some components or semiempirical models were overestimating sea level due to incorrect assumptions, nowadays the situation is less clear-cut.

[124] Figure 1b shows that process-based model projections are higher today that at the time of IPCC AR4 and that uncertainties in those projections have also increased. As mentioned earlier, no ice sheet models are able to take radiative forcing from RCP scenarios and produce sea level rise estimates except in terms of surface mass balance effects and the thermal expansion of ocean water. However, attempts have been made to approximate the RCP8.5 scenario by the SeaRISE group using a sophisticated surface mass balance combined with arbitrarily changing basal melting [*Bindschadler et al*., 2013; *Levermann et al*., 2012a, 2012b]. The Greenland ice sheet alone has been projected to contribute 22 cm but with a minimum and maximum of 4–66 cm [*Bindschadler et al*., 2013]. This contrasts with total uncertainties of 20 cm estimated for ice sheet dynamics in IPCC AR4 [*Meehl et al*., 2007a, 2007b]. *Bindschadler et al*. [2013] estimated an Antarctic sea level rise component of 7 cm with a maximum of 17 cm, while *Levermann et al*. [2012b] estimated a 90% range of −0.01 to 45 cm using similar SeaRISE forcing but with slightly different models and assumptions as *Bindschadler et al*. [2013]. These new publications show high end estimates of about 1 m from ice sheets under RCP8.5 while AR4 projections (Figure 1) had 5–95% interval rises of 22–48 cm for the less extreme A1B (Figure 1a) without dynamics included. For RCP8.5 we now have a full range of about 82 cm (47–129 cm) for the total sea level budget by 2100.

[125] For semiempirical models, there are clearly differences in projections based on using the multiple response time formulation (equation (18)) or the single response time formulation (equation (20)). The multiresponse time model is more sensitive to changes in the calibration data set and forcing scenario. The single response time model produces lower sea level rise estimates for each calibration forcing data set, but by margins as large as the Monte Carlo-derived confidence intervals for the semiempirical models (Figure 1b), so in that sense they are consistent with each other.

TABLE 2. Progress and Challenges for Sea Level Models

Problem	Importance for Sea Level by 2100	State of Modeling	Reference Section
Calving	Critical for ice sheets with ice shelves, huge for mountain glaciers	No fundamental theory exists, some parameterizations within models	5.2
Sub ice shelf melt	Large via buttressing effect on land ice	High-resolution coupled ocean ice shelf models becoming useful to quantify the buttressing effect	5.1 and 5.7
Coupling to climate models	Large	Presently only one-way coupling, ocean interplay under ice shelves ongoing, simulation of fjords not included in climate models	5.7
Grounding line	Moderate-Large	Theory exists, but resolution required is <1 km is not available from radar mapping, may use statistical methods	5.3
Validation for past and current climate	Moderate	Requires extensive tuning, unclear how well models perform on submillennial timescales	3 and 5.6
Local surface mass balance	Large for mountain glaciers, moderate for ice sheets	Rough topography makes statistical downscaling essential on mountain glaciers, regional models sufficient for ice sheets	5.5
Ice streams	Moderate	Unstructured grids, higher-order, and full Stokes models required and now used	5.3 and 5.4
Basal sliding	Potentially large if it changes with climate	Inversion techniques can determine present basal drag (but not evolution), subglacial hydrology largely excluded in models	5.4
Basal topography change	Minimal	Sedimentation and scouring not included in models, outwash fans could stabilize some grounding lines	5.3
Geothermal heat flux	Minimal	Few data exist, but unlikely to change over century timescales	5.4

[126] It is clear where the key elements of the cryosphere-sea level system lie—often with relatively small regions such as grounding lines, calving fronts, or ice streams, which exert enormous control over the behavior of the whole ice sheet. Some specific forcing, e.g., oceanic circulation change, has been simulated and the resultant impact on ice shelves studied. Similarly, climate warming scenarios have been modeled for mountain glaciers. Yet there are clearly processes which are known to be important [e.g., *Lipscomb et al*., 2009; *Little et al*., 2007] and have been the focus of research efforts, but which are not yet handled well enough either because of missing physics (calving) or lack of computing power and observation data (grounding line dynamics). Similarly, the semiempirical models rely on observations of the past to simulate a different future. There are great difficulties with nonclimate-related processes, and with accounting for the correct noise, and hence how much reliable information can be extracted from the time series available. Furthermore, both observations of the current state of the ice sheets and semiempirical sea level rise models rely implicitly on good values of GIA, especially in the polar regions. These are largely available only from variants on Peltier's global model [*Peltier*, 2004] of postglacial rebound.

[127] Potential ways forward exist in calving relations for the ice shelves, and from marine-terminating mountain glaciers, but they have not yet been coupled to models of atmospheric and oceanic climate driving. Much of the dynamic impact of climate takes place through ocean forcing of floating ice. When IPCC AR4 was released in 2007, much modeling effort had been fixated on the "Zwally Effect" [*Zwally et al*., 2002], and the potential importance of surface melt to ice sheet decay in Greenland. Research and modeling over the past ~5 year shifted the focus toward ice-ocean interactions. The very high resolution required at grounding lines and calving fronts suggests that statistical parameterization of processes related to bed friction and fracture mechanics may be fruitful in future [*Durand et al*., 2011]. The shear number of mountain glaciers also demands statistical methods.

[128] Progress in handling the interaction between surface forcing of climate via introduction of melt water to the bed relies on surface energy balance accuracy, routing of water at the bed, and if the bed is soft, understanding of the interaction between basal till and water supply. Surface energy balance using downscaled regional climate model forcing seems well in hand [*Fettweis et al*., 2013; *Vernon et al*., 2013; *Machguth et al*., 2013]. Basal hydrology allowing for this water supply on glaciers with hard beds may then be reasonably simulated with models allowing high and low pressure systems [*Pimentel and Flowers*, 2011; *Schoof*, 2010]. On soft beds, models based on Darcy flow in the sediment and a pressure-activated channel system allowing both inefficient and efficient components [*Clarke*, 2005; *van der Wel et al*., 2013] are also being actively incorporated into full Stokes flow models. The results from these models will be available within a few years and should give much insight into ubiquitous glacier / climate interactions such as glacier surges and long-term acceleration that may be related to climate forcing or more internally driven variability—a topic of great uncertainty and division among experts at present [*Bamber and Aspinall*, 2013].

[129] Sea level rise of a meter by 2100 is within uncertainty limits of models with "business as usual" forcing (Figure 1)—though expert opinion favors a lower upper limit of around 84 cm [*Bamber and Aspinall*, 2013]. An even higher rate of sea level rise was associated with Meltwater pulse 1a (Figure 2) [*Bard et al*., 1996], but in contrast to the deglaciation, the decay of modern ice sheets may be constrained by transport of large icebergs across the continental shelves of Antarctica and Greenland. Many large Antarctic icebergs remain stranded on shallows after calving in very cold water

for many years before entering the warmer waters. This we speculate could limit the access of warm water to the remaining marine-terminating glaciers, inhibiting mass loss in somewhat an analogous way as the presence of sea ice affects the coastal currents around Antarctica today.

[130] The fundamental limits of semiempirical models are the assumption of linearity between climate of the past and sea level response and that of the future. Nonlocal interactions in the climate system are generally analyzed using linear inverse theory [e.g., *Winkler et al*., 2001]. This is similar to a least squares fit linking the values of various dynamical quantities at one time with their values at some future time. In practice, this involves making the assumption that the dynamics are sufficiently approximated by a linear, stable, stochastic dynamical system. It has been demonstrated [e.g., *Tsonis et al*., 2006] that some nonlinear properties of complex systems cannot be extracted using linear inverse analysis. Hence, the distinction between projections based on process models and semiempirical ones may be an etymological rather than a practical issue. More practically, observational uncertainty due to lack of widespread tide gauge stations and proxy data in the past, combined with ambiguity in formulation of the noise model (Figure 20), leads to increased spread in model parameter estimation and hence in future predictions. To distinguish a combined response from a fast response (Figure 19), the past variability must be constrained with estimates of the individual budget components (and their uncertainties). This ties together semiempirical and process-based models in an iterative way. A complimentary approach could be through use of Bayesian methods, which have recently been applied to Antarctica [*Little et al*., 2013]. These approaches apply Monte Carlo methods to establish a probability density function for, e.g., Antarctica's contribution to sea level rise over the 21st century, by using limited observations or model data to update prior probability distributions.

[131] Perhaps the largest uncertainty in sea level prediction is Antarctica, where past behavior is likely different in its relation to climate forcing than the future—e.g., through lowering sea level by increased precipitation, or raising it by large ice shelf disintegration [*Hellmer et al*., 2012]. If Antarctica is now making a positive contribution to sea level rise, as some recent observations suggest [*Shepherd et al*., 2012; *Rignot et al*., 2008; *Ramillien et al*., 2006; *Cazenave et al*., 2009; *Velicogna and Wahr*, 2006; *Velicogna*, 2009], it is hard to see how a warming will reverse the trend. This is because the increased precipitation expected in warmer conditions will likely be overwhelmed by a dynamic ice loss through calving and loss of ice shelf buttressing effects. Or put another way, the timescales for dynamic changes as a result of accumulation changes are much longer than the timescale for dynamic changes associated with grounding line motion.

[132] Both process and semiempirical models (Figure 1) seem to suggest that prospects for keeping sea level rise below a meter at 2100 rest on keeping temperature below about a 2°C rise [*Schaeffer et al*., 2012]. However, all models show that sea levels will continue to rise beyond 2100, perhaps to 2–3 m by 2300 [*Jevrejeva et al*., 2012a, 2012b; *Schaeffer et al*., 2012]. Possibilities for preventing such rises rest with either dramatic emission cuts in greenhouse gases, including from the developing world [*Wei et al*., 2012], or relying on geoengineering [*Moore et al*., 2010]. It is well worth considering the uncertainties inherent in sea level rise projections (Figure 1), and how they have changed rapidly over the last 5 years before a drastic approach such as geoengineering is considered. Despite evidence that sea level will affect many of the poorer nations disproportionately, and unjustly given their greenhouse gas emissions, international agreement on emission controls continues to be an elusive target.

NOTATION

β	vertical mass balance gradient.
β^2	basal friction parameter.
γ	normalization constant.
$\dot{\boldsymbol{\varepsilon}}$	strain rate tensor.
$\dot{\boldsymbol{\varepsilon}}_1$, $\dot{\boldsymbol{\varepsilon}}_2$	eigenvalues of depth averaged strain rate tensor.
$\dot{\boldsymbol{\varepsilon}}_E$	effective strain rate.
ζ	aspect ratio, thickness/length.
η	ice viscosity.
κ	constant in glacier volume-area scaling.
λ	stress-strain rate constant.
ν	time constant in semiempirical models.
Φ	internal heat source.
ρ	density of ice.
$\boldsymbol{\sigma}$	stress tensor.
$\boldsymbol{\tau}$	deviatoric stress tensor.
τ_E	effective stress.
τ_b	basal shear stress.
τ_{xy}	deviatoric shear stress component applied perpendicular to x direction, acting in y direction, similarly with other stress and strain rate components.
χ	exponent in volume/area scaling.
A	flow law factor.
A_0	flow law Arrhenius factor.
Ais	Antarctic ice sheet sea level budget component.
a	constant in semiempirical models.
a_1	constant in semiempirical models.
a_2	constant in semiempirical models.
B	mass balance of glacier.
b	constant in semiempirical models.
$b_\perp$	local mass balance flux.
$\boldsymbol{C}$	uncertainty covariance matrix.
C_T	mass balance temperature sensitivity.
C_P	mass balance precipitation sensitivity.
c	heat capacity of ice.
$\dot{c}$	calving rate.
E	enhancement factor for ice viscosity.
F	radiative forcing.
Gis	Greenland ice sheet sea level budget component.
$\boldsymbol{g}$	gravitational acceleration.
H	ice thickness.
H_M	ice thickness at calving front.

H_w water depth at calving front.
$\mathbf{I}$ identity matrix.
k thermal conductivity of ice.
k_Φ fracture density coefficient.
k_c calving rate coefficient.
$L(m)$ likelihood function of model.
Mg mountain glacier sea level budget component.
n ice flow law exponent.
p pressure.
Q activation energy in Arrhenius equation.
R gas constant.
S sea level.
S_{eq} equilibrium sea level.
$\boldsymbol{S}(\boldsymbol{m})$ modeled sea level vector.
$\boldsymbol{S}_{\mathbf{obs}}$ observed sea level vector.
S_T thermosteric sea level.
S_{nc} nonclimate-related sea level budget component.
s surface elevation.
T temperature.
T_0 reference temperature in semiempirical models.
$T_{0,0}$ reference temperature for slow response in semiempirical models
T_m absolute temperature.
t time.
$\mathbf{u}$ velocity field vector.
u horizontal velocity component in x direction.
v Horizontal velocity component in y direction.
w vertical velocity component in z direction.
x Cartesian horizontal coordinate.
Y ice shelf width.
Y_0 ice shelf width calving constant.
y Cartesian horizontal coordinate.
z Cartesian vertical coordinate.

[133] **ACKNOWLEDGMENTS.** Work was supported by China's National Key Science Program for Global Change Research (2010CB950504, 2010CB951401, and 2012CB957704) and NSFC 41076125, and is publication 10 of the Nordic Centre of Excellence SVALI, Stability and Variations of Arctic Land Ice funded by the Nordic Top-Level Research Initiative. William Lipscomb, Rupert Gladstone, Martina Schäfer, and Liyun Zhao provided helpful comments on the manuscript. The Editor on this paper was Alan Robock. He thanks Stefan Rahmstorf, Stephen Griffies, and three anonymous reviewers for their review assistance on this manuscript.

REFERENCES

Albrecht, T., and A. Levermann (2012a), Fracture-induced softening for large-scale ice dynamics, paper presented at General Assembly, Eur. Geophys. Union, Vienna.

Albrecht, T., and A. Levermann (2012b), Fracture field for large-scale ice dynamics, *J. Glaciol.*, *58*, 165–176, doi:10.3189/2012JoG11J191.

Alley, R. B. (1993), In search of ice-stream sticky spots, *J. Glaciol.*, *39*(133), 447–454.

Alley, R. B., D. D. Blankenship, C. R. Bentley, and S. T. Rooney (1986), Deformation of till beneath Ice Stream B, West Antarctica, *Nature*, *322*(6074), 57–59.

Alley, R. B., S. Anandakrishnan, T. K. Dupont, B. R. Parizek, and D. Pollard (2007), Effect of sedimentation on ice-sheet grounding-line stability, *Science*, *315*, 1838–1841.

Alley, R. B., H. J. Horgan, I. Joughin, K. Cuffey, T. Dupont, B. Parizek, S. Anandakrishnan, and J. Bassis (2008), A simple law for ice-shelf calving, *Science*, *322*, 1344.

Amundson, J. M., and M. Truffer (2010), A unifying framework for iceberg-calving models. *J. Glaciol.*, *56*, 822–830, doi:10.3189/002214310794457173.

Anandakrishnan, S., and R. B. Alley (1997), Stagnation of Ice Stream C, West Antarctica by water piracy, *Geophys. Res. Lett.*, *24*, 265–268.

Anandakrishnan, S., G. A. Catania, R. B. Alley, and H. J. Horgan (2007), Discovery of till deposition at the grounding line of Whillans Ice Stream, *Science*, *315*(5820), 1835–1838.

Anderson, J. B., and S. S. Shipp (2001), Evolution of the West Antarctic ice sheet, in *The West Antarctic Ice Sheet: Behavior and Environment, Antarct. Res. Ser.*, vol. *77*, edited by R. B. Alley and R. A. Bindschadle, pp. 45–57, AGU, Washington, D. C.

Anthoff, D., R. J. Nicholls, R. S. J. Tol, and A. T. Vafeidis (2006), Global and regional exposure to large rises in sea-level: A sensitivity analysis, *Working Pap., 96*, Tyndall Cent. for Clim. Change Res., Norwich, U. K.

Arendt, A., et al. (2012), Randolph Glacier Inventory [v1.0]: A dataset of global glacier outlines. *Global Land Ice Measurements from Space*, Boulder, Colo. [Available at http://www.glims.org/RGI/]

Arthern, R. J., and G. H. Gudmundsson (2010), Initialization of ice-sheet forecasts viewed as an inverse Robin problem, *J. Glaciol.*, *56*, 527–533.

Astrom, J. A., T. I. Riikila, T. Tallinen, T. Zwinger, D. Benn, J. C. Moore, and J. Timonen (2013), A particle based simulation model for glacier dynamics, *Cryosphere Discuss.*, *7*, 921–941.

Bahr, D. B., M. F. Meier, and S. Peckham (1997), The physical basis of glacier volume-area scaling, *J. Geophys. Res.*, *102*(B9), 20,355–20,362.

Bahr, D. B., M. Dyurgerov, and M. F. Meier (2009), Sea-level rise from glaciers and ice caps: A lower bound, *Geophys. Res. Lett.*, *36*, L03501, doi:10.1029/2008GL036309.

Bamber, J. L., and W. Aspinall (2013) An expert judgement assessment of future sea level rise from the ice sheets, *Nat. Clim. Change*, *3*, 424–427, doi:10.1038/nclimate1778.

Bamber, J. L., R. L. Layberry, and S. P. Gogineni (2001), A new ice thickness and bed data set for the Greenland ice sheet: 1. Measurement, data reduction, and errors, *J. Geophys. Res.*, *106*(D24), 33,773–33,780.

Bamber, J. L., J. L. Gomez-Dans, and J. A. Griggs (2009a), A new 1 km digital elevation model of the Antarctic derived from combined satellite radar and laser data–Part 1: Data and methods, *Cryosphere*, *3*, 101–111.

Bamber, J. L., R. E. M. Riva, B. L. A. Vermeersen, and A. LeBrocq (2009b), Reassessment of the potential sea-level rise from a collapse of the West Antarctic Ice Sheet, *Science*, *324*, 901–903.

Bard, E., et al. (1996), Sea level record from Tahiti corals and the timing of deglacial meltwater discharge, *Nature*, *382*, 241–244.

Bartlett, M. S. (1935), Some aspects of the time-correlation problem in regard to tests of significance, *J. R. Stat. Soc.*, *98*, 536–543.

Bassett, S. E., G. A. Milne, J. X. Mitrovica, and P. U. Clark (2005), Ice sheet and solid Earth influences on far-field sea-level histories, *Science*, *309*, 925–928.

Bassis, J. N. (2011), The statistical physics of iceberg calving and the emergence of universal calving laws, *J. Glaciol.*, *57*(201), 3–16.

Benn, D. I., N. R. J. Hulton, and R. H. Mottram (2007a), "Calving laws," "sliding laws" and the stability of tidewater glaciers, *Ann. Glaciol.*, *46*, 123–130.

Benn, D. I., C. W. Warren, and R. H. Mottram (2007b), Calving processes and the dynamics of calving glaciers, *Earth Sci. Rev.*, *82*, 143–179, doi:10.1016/j.earscirev.2007.02.002.

Berthier, E., T. A. Scambos, and C. A. Shuman (2012), Mass loss of Larsen B tributary glaciers (Antarctic Peninsula) unabated

since 2002, *Geophys. Res. Lett.*, *39*, L13501, doi:10.1029/2012GL051755.

Bindoff, N. L., et al. (2007), Observations: Oceanic climate change and sea level, in *Climate Change 2007: The Physical Science Basis. Contributions of Working Group I to the Fourth Assessment Report of the Intergovernmental Panel on Climate Change*, edited by S. Solomon et al., Cambridge Univ. Press, Cambridge, U. K.

Bindschadler, R. A., et al. (2013), Ice-sheet model sensitivities to environmental forcing and their use in projecting future sea-level (the SeaRISE project), *J. Glaciol.*, *59*(214), 195–224.

Bittermann, K., S. Rahmstorf, M. Perrette, and M. Vermeer (2013), Predictability of twentieth century sea-level rise from past data, *Environ. Res. Lett.*, *8*, 014013, doi:10.1088/1748-9326/8/1/014013.

Bjørk, A. A., K. H. Kjær, N. J. Korsgaard, S. A. Khan, K. K. Kjeldsen, C. S. Andresen, J. E. Box, N. K. Larsen, and S. Funder (2012), An aerial view of 80 years of climate-related glacier fluctuations in southeast Greenland, *Nat. Geosci.*, *5*(6), 427–432.

Blatter, H., R. Greve, and A. Abe-Ouchi (2011) Present state and prospects of ice sheet and glacier modeling, *Surv. Geophys.*, *32*, 555–583, doi:10.1007/s10712-011-9128-0.

Borstad, C. P., A. Khazendar, E. Larour, M. Morlighem, E. Rignot, M. P. Schodlok, and H. Seroussi (2012), A damage mechanics assessment of the Larsen B ice shelf prior to collapse: Toward a physically-based calving law, *Geophys. Res. Lett.*, *39*, L18502, doi:10.1029/2012GL053317.

Bougamont, M., S. Price, P. Christoffersen, and A. J. Payne (2011), Dynamic patterns of ice stream flow in a 3-D higher-order ice sheet model with plastic bed and simplified hydrology, *J. Geophys. Res.*, *116*, F04018, doi:10.1029/2011JF002025.

Braithwaite, R. J. (1990), A simple energy-balance model to calculate ice ablation at the margin of the Greenland ice sheet, *J. Glaciol.*, *36*, 222–228.

Bromwich, D. H., et al. (2013), Central West Antarctica among most rapidly warming regions on Earth, *Nat. Geosci.*, *6*, 139–145, doi:10.1038/ngeo1671.

Brown, C. S., M. F. Meier, and A. Post (1982), Calving speed of Alaska tidewater glaciers, with application to Columbia Glacier, *U.S. Geol. Surv. Prof. Pap.*, 1044–9612, C1–C13.

Bueler, E., and J. Brown (2009), Shallow shelf approximation as a "sliding law" in a thermomechanically coupled ice sheet model, *J. Geophys. Res.*, *114*, F03008, doi:10.1029/2008JF001179.

Burgess, D., M. Sharp, D. Mair, J. Dowdeswell, and T. Benham (2005), Flow dynamics and iceberg calving rates of Devon Ice Cap, Nunavut, Canada, *J. Glaciol.*, *51*, 219–230.

Cazenave, A., and W. Llovel (2010), Contemporary sea level rise, *Annu. Rev. Mar. Sci.*, *2*, 145–173.

Cazenave, A., et al. (2009), Sea level budget over 2003–2008: A reevaluation from GRACE space gravimetry, satellite altimetry and Argo, *Global Planet. Change*, *65*, 83–88, doi:10.1016/j/gloplacha.2008.10.004.

Chambers, D. P., M. A. Merrifield, and R. S. Nerem (2012), Is there a 60-year oscillation in global mean sea level?, *Geophys. Res. Lett.*, *39*, L18607, doi:10.1029/2012GL052885.

Chao, B. F., Y. Wu, and Y. Li (2008), Impact of artificial reservoir water impoundment on global sea level, *Science*, *320*(5873), 212–214.

Church, J. A., and N. J. White (2006), A 20th century acceleration in global sea-level rise, *Geophys. Res. Lett.*, *33*, L01602, doi:10.1029/2005GL024826.

Church, J. A., and N. J. White (2011), Sea-level rise from the late 19th to the early 21st Century, *Surv. Geophys.*, *32*, 585–602.

Church, J. A., et al. (2001), Changes in sea level, in *Climate Change 2001: The Scientific Basis*. *Contribution of Working Group I to the Third Assessment Report of the Intergovernmental Panel on Climate Change*, pp. 639–694, Cambridge Univ. Press, Cambridge, U. K.

Church, J. A., N. J. White, R. Coleman, K. Lambeck, and J. X. Mitrovica (2004), Estimates of the regional distribution of sea-level rise over the 1950 to 2000 period, *J. Clim.*, *17*, 2609–2625.

Church, J. A., N. J. White, L. F. Konikow, C. M. Domingues, J. G. Cogley, E. Rignot, J. M. Gregory, M. A. van den Broeke, A. J. Monaghan, and I. Velicogna (2011), Revisiting the Earth's sea-level and energy budgets from 1961 to 2008, *Geophys. Res. Lett.*, *38*, L18601, doi:10.1029/2011GL048794.

Clark, C. D. (2010), Emergent drumlins and their clones: From till dilatancy to flow instabilities, *J. Glaciol.*, *51*, 1011–1025.

Clarke, G. K. C. (2005), Sublacial processes, *Annu. Rev. Earth Planet. Sci.*, *33*, 247–276.

Cogley, J. G. (2009), Geodetic and direct mass-balance measurements: Comparison and joint analysis, *Ann. Glaciol.*, *50*(50), 96–100.

Cogley, J. G. (2012), The future of the world's glaciers, in *The Future of the World's Climate*, edited by A. Henderson-Sellers and K. McGuffie, pp. 197–222, Elsevier, Amsterdam, doi:10.1016/B978-0-12-386917-3.00008-7.

Colville, E. J., A. E. Carlson, B. L. Beard, R. G. Hatfield, J. S. Stoner, A. V. Reyes, and D. J. Ullman (2011), Sr-Nd-Pb isotope evidence for ice-sheet presence on southern Greenland during the last interglacial, *Science*, *333*, 620–623.

Cornford, S. L., D. F. Martin, D. T. Graves, D. F. Ranken, A. M. Le Brocq, R. M. Gladstone, A. J. Payne, E. G. Ng, and W. H. Lipscomb (2013), Adaptive mesh, finite volume modeling of marine ice sheets, *J. Comput. Phys.*, *232*, 529–549, doi:10.1016/j.jcp.2012.08.037.

Cowton, T., P. Nienow, I. Bartholomew, A. Sole1, and D. Mair, (2012), Rapid erosion beneath the Greenland ice sheet, *Geology*, *40*(4), 343–346, doi:10.1130/G32687.1.

Crowley, T. J., S. K. Baum, K. Y. Kim, G. C. Hegerl, and W. T. Hyde (2003), Modeling ocean heat content changes during the last millennium, *Geophys. Res. Lett.*, *30*(18), 1932, doi:10.1029/2003GL017801.

Csatho, B., T. Schenk, C. J. van der Veen, and W. B. Krabill (2008), Intermittent thinning of Jakobshavn Isbræ, West Greenland, since the Little Ice Age, *J. Glaciol.*, *53*(184), 131–144.

Cuffey, K. M., and W. S. B. Paterson (2010), *The Physics of Glaciers*, 4th ed., Elsevier, Amsterdam.

Dahl-Jensen, D., K. Mosegaard, N. Gundestrup, G. D. Clow, S. J. Johnsen, A. W. Hansen, and N. Balling (1998), Past temperature directly from the Greenland Ice Sheet, *Science*, *282*, 268–271.

Dahl-Jensen, D., et al. (2013), Eemian interglacial reconstructed from a Greenland folded ice core, *Nature*, *493*, 489–494, doi:10.1038/nature11789.

Das, S. B., I. Joughin, M. D. Behn, I. M. Howat, M. A. King, D. Lizarralde, and M. P. Bhatia (2008), Fracture propagation to the base of the Greenland ice sheet during supraglacial lake drainage, *Science*, *320*(5877), 778–781, doi:10.1126/science.1153360.

Deschamps, P., N. Durand, E. Bard, B. Hamelin, G. Camoin, A. L. Thomas, G. M. Henderson, J. Okuno, and Y. Yokoyama (2012), Ice-sheet collapse and sea-level rise at the Bolling warming 14,600 years ago, *Nature*, *483*, 559–564, doi:10.1038/nature10902.

Ding, Q., E. J. Steig, D. S. Battisti, and J. M. Wallace (2012), Influence of the Tropics on the Southern Annular Mode, *J. Clim.*, *25*, 6330–6348, doi:10.1175/JCLI-D-11-00523.1.

Dinniman, M. S., J. M. Klinck, and E. E. Hofmann (2012), Sensitivity of circumpolar deep water transport and ice shelf basal melt along the West Antarctic peninsula to changes in the winds, *J. Clim.*, *25*, 4799–4816.

Docquier, D., L. Perichon, and F. Pattyn (2011), Representing grounding line dynamics in numerical ice sheet models: Recent advances and outlook, *Surv. Geophys.*, *32*, 417–435, doi:10.1007/s10712-011-9133-3.

Domingues, C. M., J. A. Church, N. J. White, P. J. Gleckler, S. E. Wijffels, P. M. Barker, and J. R. Dunn (2008), Improved estimates of upper-ocean warming and multi-decadal sea level rise, *Nature*, *453*, 1090–1093.

Douglas, B. C. (1992), Global sea level acceleration, *J. Geophys. Res.*, *97*(C8), 12,699–12,706.

Dowdeswell, J. A., T. J. Benham, T. Strozzi, and O. Hagen (2008), Iceberg calving flux and mass balance of the Austfonna ice cap

on Nordaustlandet, Svalbard, *J. Geophys. Res.*, *113*, F03022, doi:10.1029/2007JF000905.

Drouet, A. S., D. Docquier, G. Durand, R. Hindmarsh, F. Pattyn, O. Gagliardini, and T. Zwinger (2012), Grounding line transient response in marine ice sheet models, *Cryosphere Discuss.*, *6*, 3903–3935, doi:10.5194/tcd-6-3903-2012.

Dupont, T. K., and R. B. Alley (2005), Assessment of the importance of ice-shelf buttressing to ice-sheet flow, *Geophys. Res. Lett.*, *32*, L04503, doi:10.1029/2004GL022024.

Durand, G., O. Gagliardini, T. Zwinger, E. Le Meur, and R. Hindmarsh (2009a), Full Stokes modeling of marine ice sheets: influence of the grid size, *Ann. Glaciol.*, *52*, 109–114.

Durand, G., O. Gagliardini, B. de Fleurian, T. Zwinger, and E. LeMeur (2009b), Marine ice sheet dynamics: Hysteresis and neutral equilibrium, *J. Geophys. Res.*, *114*, F03009, doi:10.1029/2008JF001170.

Durand, G., O. Gagliardini, L. Favier, T. Zwinger, and E. le Meur (2011), Impact of bedrock description on modeling ice sheet dynamics, *Geophys. Res. Lett.*, *38*, L20501, doi:10.1029/2011GL048892.

Ekman, M. (1988), The world's longest continuous series of sea level observations, *Pure Appl. Geophys.*, *127*, 73–77.

Fahnestock M, W. Abdalati, I. Joughin, J. Brozena, and P. Gogineni (2001), High geothermal heat flow, basal melt, and the origin of rapid ice flow in central Greenland, *Science*, *294*(5550), 2338–2342, doi:10.1126/science.1065370.

Favier, L., O. Gagliardini, G. Durand, and T. Zwinger (2012), A three-dimensional full stokes model of the grounding line dynamics: Effect of a pinning point beneath the ice shelf, *Cryosphere*, *6*, 101–112, doi:10.5194/tc-6-101-2012.

Fettweis, X., B. Franco, M. Tedesco, J. van Angelen, J. Lenaerts, M. van den Broeke, and H. Gallée (2013) Estimating the Greenland ice sheet surface mass balance contribution to future sea level rise using the regional atmospheric climate model MAR, *Cryosphere*, *7*, 469–489.

Fleming, K., P. Johnston, D. Zwartz, Y. Yokoyama, K. Lambeck, and J. Chappell (1998), Refining the eustatic sea-level curve since the Last Glacial Maximum using far- and intermediate-field sites, *Earth Planet. Sci. Lett.*, *163*(1-4), 327–342, doi:10.1016/S0012-821X(98)00198-8.

Fricker, H. A., T. Scambos, R. Bindschadler, and L. Padman (2007), An active subglacial water system in West Antarctica mapped from space, *Science*, *315*(5818), 1544–1548.

Fyke, J. G., A. J. Weaver, D. Pollard, M. Eby, L. Carter, and A. Mackintosh (2011), A new coupled ice sheet/climate model: description and sensitivity to model physics under Eemian, Last Glacial Maximum, late Holocene and modern climate conditions, *Geosci. Model Dev.*, *4*, 117–136.

Gagliardini, O., D. Cohen, P. Råback, and T. Zwinger (2007), Finite element modeling of subglacial cavities and related friction law, *J. Geophys. Res.*, *112*, F02027, doi:10.1029/2006JF000576.

Gagliardini, O., G. Durand, T. Zwinger, R. C. A. Hindmarsh, and E. Le Meur (2010), Coupling of ice-shelf melting and buttressing is a key process in ice-sheets dynamics, *Geophys. Res. Lett.*, *37*, L14501, doi:10.1029/2010GL043334.

Gehrels, W. R., et al. (2005), Onset of recent rapid sea-level rise in the western Atlantic Ocean, *Quat. Sci. Rev.*, *24*, 2083–2100, doi:10.1016/j.quascirev.2004.11.016.

Gehrels, W. R., B. P. Horton, A. C. Kemp, and D. Sivan (2011), Two millennia of sea level data: The key to predicting change, *Eos Trans. AGU*, *92*(35), 289–290.

Giesen, R. H., and J. Oerlemans (2012), Global application of a surface mass balance model using gridded climate data, *Cryosphere Discuss.*, *6*, 1445–1490.

Giesen, R. H., and J. Oerlemans (2013), Climate-model induced differences in the 21st century global and regional glacier contributions to sea-level rise, *Clim. Dyn.*, doi:10.1007/s00382-013-1743-7.

Gillet-Chaulet, F., O. Gagliardini, H. Seddik, M. Nodet, G. Durand, C. Ritz, T. Zwinger, R. Greve, and D. Vaughan (2012), Greenland Ice Sheet contribution to sea-level rise from a new-generation ice-sheet model, *Crysophere Discuss*, *6*, 1561–1576.

Gladstone, R. M., A. J. Payne, and S. L. Cornford (2010), Parameterising the grounding line in flow-line ice sheet models, *Cryosphere*, *4*, 605–619, doi:10.5194/tc-4-605-2010.

Gladstone, R. M., V. Lee, J. Rougier, A. J. Payne, H. Hellmer, A. Le Brocq, A. Shepherd, T. L. Edwards, J. Gregory, and S. L. Cornford (2012), Calibrated prediction of Pine Island Glacier retreat during the 21st and 22nd centuries with a coupled flowline model, *Earth Planet. Sci. Lett.*, *333–334*, 191–199.

Gleckler, P. T., T. M. L. Wigley, B. D. Santer, J. M. Gregory, K. AchutaRao, and K. E. Taylor (2006), Krakatoa's signature persists in the ocean, *Nature*, *439*, 675, doi:10.1038/439675a.

Goldberg D., D. M. Holland, and C. Schoof (2009), Grounding line movement and ice shelf buttressing in marine ice sheets, *J. Geophys. Res.*, *114*, F04026, doi:10.1029/2008JF001227.

Gomez, N., J. X. Mitrovica, P. Huybers, and P. U. Clark (2010), Sea level as a stabilizing factor for marine-ice-sheet grounding lines, *Nat. Geosci.*, *3*, 850–853, doi:10.1038/ngeo1012.

Good, P., J. M. Gregory, and J. A. Lowe (2011), A step-response simple climate model to reconstruct and interpret AOGCM projections, *Geophys. Res. Lett.*, *38*, L01703, doi:10.1029/2010GL045208.

Goosse, H., E. Deleersnijder, T. Fichefet, and M. H. England (1999), Sensitivity of a global coupled ocean-sea ice model to the parameterization of vertical mixing, *J. Geophys. Res.*, *104*(6), 13,681–13,695.

Goosse, H., H. Renssen, A. Timmermann, and R. S. Bradley (2005), Internal and forced climate variability during the last millennium: A model-data comparison using ensemble simulations, *Quat. Sci. Rev.*, *24*, 1345–1360.

Gornitz, V. (2001), Impoundment, groundwater mining, and other hydrologic transformations: Impacts on global sea level rise, in *Sea Level Rise, History and Consequences*, edited by B. C. Douglas, M. S. Kearney, and S. P. Leatherman, pp. 97–119, *International Geophysics Series*, vol. 75, 232 p., Academic Press, New York.

Gouretski, V., and K. P. Koltermann (2007), How much is ocean really warming?, *Geophys. Res. Lett.*, *34*, L01610, doi:10.1029/2006GL027834.

Gregory, J. M., J. A. Lowe, and S. F. B. Tett (2006), Simulated global mean sea level change over the last half-millennium, *J. Clim.*, *19*(18), 4576–4591.

Gregory, J. M., et al. (2012), Twentieth-century global-mean sea-level rise: Is the whole greater than the sum of the parts?, *J. Clim.*, doi:10.1175/JCLI-D-12-00319.1.

Greve, R., and H. Blatter (2009), *Dynamics of Ice Sheets and Glaciers*, Adv. in Geophys. and Environ. Mech. and Math., Springer, Heidelberg.

Griffies, et al., (2011), The GFDL CM3 Coupled Climate Model: Characteristics of the ocean and sea ice simulations, *J. Clim.*, *24*(13), doi:10.1175/2011JCLI3964.1.

Griffies, S. M., and R. J. Greatbatch (2012), Physical processes that impact the evolution of global mean sea level in ocean climate models, *Ocean Model.*, *51*, 37–72.

Grinsted, A. (2013), An estimate of global glacier volume, *Cryosphere*, *7*, 141–151, doi:10.5194/tc-7-141-2013.

Grinsted, A., J. C. Moore, and S. Jevrejeva (2007), Observational evidence for volcanic impact on sea level and the global water cycle, *Proc. Natl. Acad. Sci. U. S. A.*, *104*(50), 19,730–19,734, doi:10.1073/pnas.0705825104.

Grinsted, A., J. C. Moore, and S. Jevrejeva (2010), Reconstructing sea level from paleo and projected temperatures 200 to 2100AD, *Clim. Dyn.*, *34*, 461–472.

Grinsted, A., S. Jevrejeva, and J. C. Moore (2011), Comment on the subsidence adjustment applied to the Kemp et al. proxy of North Carolina relative sea level, *Proc. Natl. Acad. Sci. U. S. A.*, *108*, E781–E782.

Gudmundsson, G. H., J. Krug, G. Durand, L. Favier, and O. Gagliardini (2012), The stability of grounding lines on

retrograde slopes, *The Cryosphere*, *6*, 1497–1505, doi:10.5194/tc-6-1497-2012.

Gupta, A. S., L. C. Muir, J. N. Brown, S. J. Phipps, P. J. Durack, D. Monselesan, and S. E. Wijffels (2012), Climate drift in the CMIP3 models. *J. Clim.*, *25*, 4621–4640.

Headly, M. A., and J. P. Severinghaus (2007), A method to measure Kr/N_2 ratios in air bubbles trapped in ice cores, and its application in reconstructing past mean ocean temperature, *J. Geophys. Res.*, *112*, D19105, doi:10.1029/2006JD008317.

Hegerl, G. C., F. W. Zwiers, P. Braconnot, N. P. Gillett, Y. Luo, J. A. Marengo Orsini, N. Nicholls, J. E. Penner, and P. A. Stott (2007), Understanding and attributing climate change, in *Climate Change 2007: The Physical Science Basis. Contribution of Working Group I to the Fourth Assessment Report of the Intergovernmental Panel on Climate Change*, edited by S. Solomon et al., pp. 663–745, Cambridge Univ. Press, Cambridge, U. K.

Heimbach, P., and V. Bugnion (2009), Greenland ice-sheet volume sensitivity to basal, surface and initial conditions derived from an adjoint model, *Ann. Glaciol.*, *50*(52), 67–80.

Hellmer, H., H. F. Kauker, R. Timmermann, J. Determann, and J. Rae (2012), Twenty-first-century warming of a large Antarctic ice-shelf cavity by a redirected coastal current, *Nature*, *485*(7397), 225–228, doi:10.1038/nature11064.

Hindmarsh, R. C. A. (2012), An observationally validated theory of viscous flow dynamics at the ice-shelf calving front, *J. Glaciol.*, *58*, 375–387, doi:10.3189/2012JoG11J206.

Hock, R., M. de Woul, V. Radiac, and M. Dyurgerov (2009), Mountain glaciers and ice caps around Antarctica make a large sea-level rise contribution, *Geophys. Res. Lett.*, *36*, L07501, doi:10.1029/2008GL037020.

Holland, D., R. Thomas, B. de Young, M. Ribergaard, and B. Lyberth (2008), Acceleration of Jakobshavn Isbræ triggered by warm subsurface ocean waters, *Nat. Geosci.*, *1*, 659–664, doi:10.1038/ngeo316.

Horton R., et al. (2008), Sea level rise projections for current generation CGCMs based on the semi-empirical method, *Geophys. Res. Lett.*, *35*, L02715, doi:10.1029/2007GL032486.

Hu A., G. A. Meehl, W. Han, and J. Yin (2011), Effect of the potential melting of the Greenland Ice Sheet on the meridional overturning circulation and global climate in the future, *Deep Sea Res. II*, *58*, 1914–1926.

Huntington, T. G. (2008), Can we dismiss the effect of changes in land-based water storage on sea level rise?, *Hydrol. Processes*, *22*, 717–723.

Huss, M., and D. Farinotti (2012), Distributed ice thickness and volume of all glaciers around the globe, *J. Geophys. Res.*, *117*, F04010, doi:10.1029/2012JF002523.

Hutter, K. (1983), *Theoretical Glaciology*, Kluwer, Dordrecht.

Huybrechts, P. (1998), Report of the Third EISMINT Workshop on Model Intercomparison, p. 120, European Science Foundation, Strasbourg.

Iken, A. (1981), The effect of subglacial water pressure on the sliding velocity of a glacier in an idealized numerical model, *J. Glaciol.*, *27*, 407–422.

Intergovernmental Panel on Climate Change (IPCC) (2007), Summary for policymakers, in *Climate Change 2007: The Physical Science Basis*. Contribution of Working Group I to the Fourth Assessment Report of the Intergovernmental Panel on Climate Change, edited by S. Solomon et al., pp. 1–18Cambridge Univ. Press, Cambridge, U. K.

Ishii, M., and M. Kimoto (2009), Reevaluation of historical ocean heat content variations with time-varying XBT and 15 MBT depth bias corrections, *J. Oceanogr.*, *65*, 287–299.

Iverson, N. R., and B. B. Petersen (2011), A new laboratory device for study of subglacial processes: First results on ice-bed separation during sliding, *J. Glaciol.*, *57*, 1135–1146.

Jacob, T., J. Wahr, W. T. Pfeffer, and S. Swenson (2012), Recent contributions of glaciers and ice caps to sea level rise, *Nature*, *482*, 514–518, doi:10.1038/nature10847.

Jacobs, S., A. Jenkins, C. Giulivi, and P. Dutrieux (2011), Stronger ocean circulation and increased melting under Pine Island Glacier ice shelf, *Nat. Geosci.*, *4*, 519–523.

Jay-Allemand, M., F. Gillet-Chaulet, O. Gagliardini, and M. Nodet (2011), Investigating changes in basal conditions of variegated glacier prior to and during its 1982–1983 surge, *The Cryosphere*, *5*, 659–672, doi:10.5194/tc-5-659-2011.

Jevrejeva, S., J. C. Moore, and A. Grinsted (2004), Oceanic and atmospheric transport of multi-year ENSO signatures to the polar regions, *Geophys. Res. Lett.*, *31*, L24210, doi:10.1029/2004GL020871.

Jevrejeva, S., A. Grinsted, J. C. Moore, and S. Holgate (2006), Nonlinear trends and multi-year cycle in sea level records, *J. Geophys. Res.*, *111*, C09012, doi:10.1029/2005JC003229.

Jevrejeva, S., J. C. Moore, A. Grinsted, and P. L. Woodworth (2008), Recent global sea level acceleration started over 200 years ago?, *Geophys. Res. Lett.*, *35*, L08715, doi:10.1029/2008GL033611.

Jevrejeva, S., A. Grinsted, and J. C. Moore (2009), Anthropogenic forcing dominates sea level rise since 1850, *Geophys. Res. Lett.*, *36*, L20706, doi:10.1029/2009GL040216.

Jevrejeva, S., J. C. Moore, and A. Grinsted (2010), How will sea level respond to changes in natural and anthropogenic forcings by 2100?, *Geophys. Res. Lett.*, *37*, L07703, doi:10.1029/2010GL042947.

Jevrejeva, S., J. C. Moore, and A. Grinsted (2012a), Sea level projections with new generation of scenarios for climate change, *Global Planet. Change*, *80*, 14–20, doi.org/10.1016/j.gloplacha. 2011.09.006.

Jevrejeva, S., J. C. Moore, and A. Grinsted (2012b), Potential for bias in 21st century sea level projections from semiempirical models, *J. Geophys. Res.*, *117*, D20116, doi:10.1029/2012JD017704.

Johannessen, O. M., K. Khvorostovsky, M. W. Miles, and L. P. Bobylev (2005), Recent ice-sheet growth in the interior of Greenland, *Science*, *310*, 1013–1016.

Johnson, H. L., A. Münchow, K. K. Falkner, and H. Melling (2011), Ocean circulation and properties in Petermann Fjord, Greenland, *J. Geophys. Res.*, *116*, C01003, doi:10.1029/2010JC006519.

Jones, P. D., and M. E. Mann (2004), Climate over past millennia, *Rev. Geophys.*, *42*, RG2002, doi:10.1029/2003RG000143.

Joughin, I., S. Tulaczyk, R. Bindschadler, and S. F. Price (2002), Changes in West Antarctic ice stream velocities: Observation and analysis, *J. Geophys. Res.*, *107*(B11), 2289, doi:10.1029/2001JB001029.

Joughin, I., B. E. Smith, I. M. Howat, T. Scambos, and T. Moon (2010), Greenland flow variability from ice-sheet-wide velocity mapping, *J. Glaciol.*, *56*(197), 415–430, doi:10.3189/002214310792447734.

Jouvet, G., M. Picasso, J. Rappaz, M. Huss, and M. Funk (2011), Modelling and numerical simulation of the dynamics of glaciers including local damage effects, *Math. Model. Nat. Phenom.*, *6*, 263–280, doi:10.1051/mmnp/20116510.

Kapsner, W. P., R. B. Alley, C. A. Shuman, S. Anandakrishnan, and P. M. Grootes (1995), Dominant influence of atmospheric circulation on snow accumulation in Greenland over the past 18,000 years, *Nature*, *373*, 52–54, doi:10.1038/373052a0.

Karstensen, J., P. Schlosser, D. W. R. Wallace, J. L. Bullister, and J. Blindheim (2005), Water mass transformation in the Greenland Sea during the 1990s, *J. Geophys. Res.*, *110*, C07022, doi:10.1029/2004JC002510.

Kaser, G., J. G. Cogley, M. B. Dyurgerov, M. F. Meier, and A. Ohmura (2006), Mass balance of glaciers and ice caps: Consensus estimates for 1961–2004, *Geophys. Res. Lett.*, *33*, L19501, doi:10.1029/2006GL027511.

Katz, R. F., and M. G. Worster (2010), Stability of ice-sheet grounding lines, *Proc. R. Acad. A*, *466*, 1597–1620, doi:10.1098/rspa.2009.0434.

Kemp, A., B. Horton, J. Donnelly, M. Mann, M. Vermeer, and S. Rahmstorf (2011a), Climate related sea level variations over the past two millennia, *Proc. Natl. Acad. Sci. U. S. A.*, *108*, 11,017–11,022.

Kemp, A., B. Horton, J. Donnelly, M. Mann, M. Vermeer, and S. Rahmstorf (2011b), Reply to Grinsted et al.: Estimating land subsidence in North Carolina, *Proc. Natl. Acad. Sci. U. S. A.*, 108, E783.

Kevorkian, J., and J. D. Cole (1981), *Multiple Scale and Singular Perturbation Methods*, Springer-Verlag, New York.

Khan, S. A., J. Wahr, M. Bevis, I. Velicogna, and E. Kendrick (2010), Spread of ice mass loss into northwest Greenland observed by GRACE and GPS, *Geophys. Res. Lett.*, *37*, L06501, doi:10.1029/2010GL042460.

King, M. A., R. J. Bingham, P. Moore, P. L. Whitehouse, M. J. Bentley, and G. A. Milne (2012), Lower satellite-gravimetry estimates of Antarctic sea-level contribution, *Nature*, *491*, 586–589, doi:10.1038/nature11621.

Kirchner, N., K. Hutter, M. Jakobsson, and R. Gyllencreutz (2011), Capabilities and limitations of numerical ice sheet models: A discussion for Earth-scientists and modelers, *Quat. Sci. Rev.*, *30*, 3691–3704.

Konikow, L. F. (2011), Contribution of global groundwater depletion since 1900 to sea-level rise, *Geophys. Res. Lett.*, *38*, L17401, doi:10.1029/2011GL048604.

Kopp, R. E., F. J. Simons, J. X. Mitrovica, A. C. Maloof, and M. Oppenheimer (2009), Probabilistic assessment of sea level during the last interglacial stage, *Nature*, *462*, 863–867, doi:10.1038/nature08686.

Lambeck, K., and J. Chappell (2001), Sea level change through the last glacial cycle, *Science*, *292*(5517), 679–686.

Lambeck, K., F. Antonioli, A. Purcell, and S. Silenzi (2004), Sea-level change along the Italian coast for the past 10,000 yr, *Quat. Sci. Rev.*, *23*, 1567–1598.

Le Treut, H., R. Somerville, U. Cubasch, Y. Ding, C. Mauritzen, A. Mokssit, T. Peterson, and M. Prather (2007), Historical overview of climate change, in *Climate Change 2007: The Physical Science Basis Contribution of Working Group I to the Fourth Assessment Report of the Intergovernmental Panel on Climate Change*, edited by S. Solomon et al., pp. 100–108, Cambridge University Press, Cambridge, U. K.

Leclercq, P. W., J. Oerlemans, and J. G. Cogley (2011), Estimating the glacier contribution to sea-level rise over the period 1800—2005, *Surv. Geophys.*, *32*, 519–535, doi:10.1007/s10712-011-9121-7.

Lemke, P., et al (2007), Observations: Changes in snow, ice and frozen ground, in *Climate Change 2007: The Physical Science Basis Contribution of Working Group I to the Fourth Assessment Report of the Intergovernmental Panel on Climate Change*, p. 374, Cambridge Univ. Press, Cambridge U. K.

Lettenmaier, D. P., and P. C. D. Milly (2009), Land waters and sea level, *Nat. Geosci.*, *2*(7), 452–454.

Levermann, A., T. Albrecht, R. Winkelmann, M. A. Martin, M. Haseloff, and I. Joughin (2012a), Kinematic first-order calving law implies potential for abrupt ice-shelf retreat, *Cryosphere*, *6*, 273–286, doi:10.5194/tc-6-273-2012.

Levermann, A., et al. (2012b), Projecting Antarctic ice discharge using response functions from SeaRISE ice-sheet models, *Cryosphere Discuss.*, *6*, 3447–3489.

Levitus, S., J. Antonov, and T. Boyer (2005), Warming of the world ocean, 1955–2003, *Geophys. Res. Lett.*, *32*, L02604, doi:10.1029/2004GL021592.

Levitus, S., J. I. Antonov, T. P. Boyer, R. A. Locarnini, H. E. Garcia, and A. V. Mishonov (2009), Global ocean heat content 1955–2008 in light of recently revealed instrumentation problems, *Geophys. Res. Lett.*, *36*, L07608, doi:10.1029/2008GL037155.

Levitus, S., et al. (2012), World ocean heat content and thermosteric sea level change (0–2000), 1955–2010, *Geophys. Res. Lett.*, L10603, doi:10.1029/2012GL05110.

Li, J., and H. J. Zwally (2011), Modeling of firn compaction for estimating ice-sheet mass change from observed ice-sheet elevation change, *Ann. Glaciol.*, *52*, 1–7.

Li, C., J. S. von Storch, and J. Marotzke (2012), Deep-ocean heat uptake and equilibrium climate response, *Clim Dyn.*, *40*, 1071–1086, doi:10.1007/s00382-012-1350-z.

Lipscomb, W., R. Bindschadler, E. Bueler, D. Holland, J. Johnson, and S. Price (2009), A community ice sheet model for sea level prediction: Building a next-generation community ice sheet model; Los Alamos, New Mexico, 18–20 August 2008, *Eos Trans. AGU*, *90*(3), 23, doi:10.1029/2009EO030004.

Little, C. M., et al. (2007), Toward a new generation of ice sheet models, *Eos Trans. AGU*, *88*(52), 578, doi:10.1029/2007EO520002.

Little, C. M., M. Oppenheimer, and N. M. Urban (2013), Upper bounds on twenty-first-century Antarctic ice loss assessed using a probabilistic framework, *Nat. Clim. Change*, doi:10.1038/nclimate1845.

MacAyeal, D. R. (1989), Large-scale flow over a viscous basal sediment: Theory and application to Ice Stream E, Antarctica, *J. Geophys. Res.*, *94*(B4), 4017–4087.

Machguth, H., P. Rastner, T. Bolch, N. Mölg, L. Sandberg Sørensen, G. Aðalgeirsdottir, J. van Angelen, M. van den Broeke, and X. Fettweis (2013), The future sea-level rise contribution of Greenland's glaciers and ice caps, *Environ. Res. Let.*, *8*, 025005.

Marzeion, B., A. H. Jarosch, and M. Hofer (2012), Past and future sea-level change from the surface mass balance of glaciers, *Cryosphere*, *6*, 1295–1322.

Massom, R. A., A. B. Giles, H. A. Fricker, R. C. Warner, B. Legresy, G. Hyland, N. Young, and A. D. Fraser (2010), Examining the interaction between multi-year landfast sea ice and the Mertz Glacier Tongue, East Antarctica: Another factor in ice sheet stability?, *J. Geophys. Res.*, *115*, C12027, doi:10.1029/2009JC006083.

Meehl, G. A., C. Covey, T. Delworth, M. Latif, B. McAvaney, J. F. B. Mitchell, R. J. Stouffer, and K. E. Taylor (2007a), The WCRP CMIP3 multi-model dataset: A new era in climate change research, *Bull. Am. Meteorol. Soc.*, *88*, 1383–1394.

Meehl, G. A., et al. (2007b), Global climate projections, in *Climate Change 2007: Contribution of Working Group I to the Fourth Assessment Report of the IPCC*, edited by S. Solomon et al., Univ. Press, Cambridge, U. K.

Meier, M. F., M. B. Dyurgerov, U. K. Rick, S. O'Neel, W. T. Pfeffer, R. S. Anderson, S. P. Anderson, and A. F. Glazovsky (2007), Glaciers dominate eustatic sea-level rise in the 21st century, *Science*, *317*, 1064–1067.

Mernild, S. H., and W. H. Lipscomb (2012), Imbalance and accelerated melting of glaciers and ice caps, *Geophys. Res. Abstr.*, *14*, EGU2012-11851.

Mernild, S. H., W. H. Lipscomb, D. B. Bahr, V. Radić, and M. Zemp (2013), Global glacier retreat: A revised assessment of committed mass losses and sampling uncertainties, *Cryosphere Discuss.*, *7*, 1987–2005, doi:10.5194/tcd-7-1987-2013.

Milly, P. C. D., A. Cazenave, and M. C. Gennero (2003), Contribution of climate-driven change in continental water storage to recent sea level rise, *Proc. Natl. Acad. Sci. U. S. A.*, *100*, 13,158–13,161.

Milly, P. C. D., et al. (2010), Terrestrial water-storage contributions to sea level rise and variability, in *Understanding Sea level Rise and Variability*, edited by J. A. Church et al., Wiley-Blackwell, Oxford, UK, doi:10.1002/9781444323276.ch8.

Milne, G. A., A. J. Long, and S. E. Bassett (2005), Modelling Holocene relative sea-level observations from the Caribbean and South America, *Quat. Sci. Rev.*, *24*(10-11), 1183–1202, doi:10.1016/j.quascirev.2004.10.005.

Milne, G. A., W. R. Gehrels, C. W. Hughes, and M. E. Tamisiea (2009), Identifying the causes of sea-level change, *Nat. Geosci.*, *2*(7), 471–478.

Mitrovica, J. X., M. E. Tamisiea, J. L. Davis, and G. A. Milne (2001), Recent mass balance of polar ice sheets inferred from patterns of global sea-level change, *Nature*, *409*, 1026–1029.

Moberg, A., D. M. Sonechkin, K. Holmgren, N. M. Datsenko, and W. Karlén (2005), Highly variable Northern Hemisphere temperatures reconstructed from low- and high-resolution proxy data, *Nature*, *433*, 613–617.

Moon, T., I. Joughin, B. Smith, and I. Howat (2012), 21st-century evolution of Greenland outlet glacier velocities, *Science*, *336*(6081), 576–578.

Moore, J. C., S. Jevrejeva, and A. Grinsted (2010), Efficacy of geoengineering to limit 21st century sea-level rise, *Proc. Natl. Acad. Sci. U. S. A.*, *107*, 15,699–15,703, doi:10.1073/pnas.1008153107.

Moore, J. C., S. Jevrejeva, and A. Grinsted (2011), The historical sea level budget, *Ann. Glaciol.*, *52*(59), 8–14.

Morgan, V. I., T. H. Jacka, G. J. Akerman, and A. L. Clarke (1982), Outlet glacier and mass-budget studies in Enderby, Kemp and Mac. Robertson lands, Antarctica, *Ann. Glaciol.*, *3*, 204–210.

Morlighem, M., E. Rignot, H. Seroussi, E. Larour, H. Dhia, and D. Aubry (2010), Spatial patterns of basal drag inferred using control methods from a full-Stokes and simpler models for Pine Island Glacier, West Antarctica, *Geophys. Res. Lett.*, *37*, L14502, doi:10.1029/2006JF000576.

Muszynski, I., and G. E. Birchfield (1987), A coupled marine ice stream-ice-shelf model, *J. Glaciol.*, *33*(113), 3–15.

Nerem, R. S., D. Chambers, E. W. Leuliette, G. T. Mitchum, and B. S. Giese (1999), Variations in global mean sea level associated with the 1997–1998 ENSO event: Implications for measuring long term sea level change, *Geophys. Res. Lett.*, *26*(19), 3005–3008.

Ngo-Duc, T., K. Laval, J. Polcher, A. Lombard, and A. Cazenave (2005), Effects of land water storage on global mean sea level over the past half century, *Geophys. Res. Lett.*, *32*, L09704, doi:10.1029/2005GL022719.

Nicholls, K. W. (1997), Predicted reduction in basal melt rates of an Antarctic ice shelf in a warmer climate, *Nature*, *388*, 460–462.

Nick, F. M., C. J. Van der Veen, A. Vieli, and D. I. Benn (2010), A physically based calving model applied to marine outlet glaciers and implications for the glacier dynamics, *J. Glaciol.*, *56*(199), 781–794, doi:10.3189/002214310794457344.

Oerlemans, J. (1989), A projection of future sea level, *Clim. Change*, *15*, 151–174.

Oerlemans, J. (2005), Extracting a climate signal from 169 glacier records, *Science*, *308*, 675–677.

Oerlemans, J., M. Dyurgerov, and R. S. W. van de Wal (2007), Reconstructing the glacier contribution to sea-level rise back to 1850, *Cryosphere*, *1*(1), 59–65.

Ohmura, A., and N. Reeh (1991), New precipitation and accumulation maps for Greenland, *J. Glaciol.*, *37*, 140–148.

Pardaens, A. K., J. A. Lowe, S. Brown, R. J. Nicholls, and D. de Gusmão (2011), Sea-level rise and impacts projections under a future scenario with large greenhouse gas emission reductions, *Geophys. Res. Lett.*, *38*, L12604, 10.1029/2011GL047678.

Parker, B. (2011), The tide predictions for D-Day, *Phys. Today*, *64*(9), 35–40, doi:10.1063/PT.3.1257.

Paterson, A. B., and N. Reeh (2001), Thinning of the ice sheet in northwest Greenland over the past forty years, *Nature*, *414*, 60–62.

Pattyn, F., et al. (2012), Results of the Marine Ice Sheet Model Intercomparison Project, MISMIP, *Cryosphere Discuss.*, *6*, 267–308, doi:10.5194/tcd-6-267-2012.

Peltier, W. R. (1998), Postglacial variations in the level of the sea: Implications for climate dynamics and solid-earth geophysics, *Rev. Geophys.*, *36*(4), 603–689, doi:10.1029/98RG02638.

Peltier, W. R. (2004), Global glacial isostasy and the surface of the ice-age Earth: The ICE-5G (VM2) model and GRACE, *Annu. Rev. Earth Planet. Sci.*, *32*, 111–149, doi:10.1146/annurev.earth.32.082503.144359.

Peltier, W. R., and R. G. Fairbanks (2006), Global glacial ice volume and Last Glacial Maximum duration from an extended Barbados sea level record, *Quat. Sci. Rev.*, *25*, 3322–3337.

Petra, N., H. Zhu, G. Stadler, T. Hughes, J. R. Thomas, and O. Ghattas (2012), An inexact Gauss-Newton method for inversion of basal sliding and rheology parameters in a nonlinear Stokes ice sheet model, *J. Glaciol.*, *58*, 889–903.

Pfeffer, W. T., J. T. Harper, and S. O'Neel (2008), Kinematic constraints on glacier contributions to 21st-century sea-level rise, *Science*, *321*(5894), 1340–1343.

Philippon, G., G. Ramstein, S. Charbit, M. Kageyama, C. Ritz, and C. Dumas (2006), Evolution of the Antarctic Ice Sheet throughout the last deglaciation: A study with a new coupled climate-North and South Hemisphere ice sheet model, *Earth Planet. Sci. Lett.*, *248*, 750–758.

Pimentel, S., and G. E. Flowers (2011), A numerical study of hydrologically driven glacier dynamics and subglacial flooding, *Proc. R. Soc. A*, *2011*(467), 537–558, doi:10.1098/rspa.2010.0211.

Pimentel, S., G. E. Flowers, and C. G. Schoof (2010), A hydrologically coupled higher-order flow-band model of ice dynamics with a Coulomb friction sliding law, *J. Geophys. Res.*, *115*, F04023, doi:10.1029/2009JF001621.

Pokhrel, Y., N. Hanasaki, P. J-F. Yeh, T. J. Yamada, S. Kanae, and T. Oki (2012), Model estimates of sea-level change due to anthropogenic impacts on terrestrial water storage, *Nat. Geosci*. *5*, 389–392, doi:10.1038/ngeo1476.

Pollard, D., and R. M. DeConto (2009), Modelling West Antarctic ice sheet growth and collapse through the past five million years, *Nature*, *458*, 329–332.

Price, S. F., A. J. Payne, I. M. Howat, and B. E. Smith (2011), Committed sea-level rise for the next century from Greenland ice sheet dynamics during the past decade, *Proc. Natl. Acad. Sci. U. S. A.*, *108*, 8978–8983, doi:10.1073/pnas.1017313108.

Pritchard, H. D., S. R. M. Ligtenberg, H. A. Fricker, D. G. Vaughan, M. R. van den Broeke, and L. Padman (2012), Antarctic ice sheet loss driven by basal melting of ice shelves, *Nature*, *484*, 502–505, doi:10.1038/nature10968.

Purkey, S. G., and G. C. Johnson (2010), Warming of global abyssal and deep Southern Ocean waters between the 1990s and 2000s: Contributions to global heat and sea level rise budgets, *J. Clim.*, *23*(23), 6336–6351, doi:10.1175/2010JCLI3682.1.

Radic, V., and R. Hock (2010), Regional and global volumes of glaciers derived from statistical upscaling of glacier inventory data, *J. Geophys. Res.*, *115*, F01010, doi:10.1029/2009JF001373.

Radic, V., and R. Hock (2011), Regionally differentiated contribution of mountain glaciers and ice caps to future sea-level rise, *Nat. Geosci.*, *4*, 91–94.

Rahmstorf, S. (2007a), A semiempirical approach to projecting future sea-level rise, *Science*, *315*, 368–370.

Rahmstorf, S. (2007b), Response to comments on "A semiempirical approach to projecting future sea-level rise," *Science*, *317*, 1866d.

Rahmstorf, S., M. Perrette, and M. Vermeer (2011), Testing the robustness of semiempirical sea level projections, *Clim. Dyn.*, *39*, 861–875, doi:10.1007/s00382-011-1226-7.

Ramanathan, V., and G. Carmichael (2008), Global and regional climate changes due to black carbon, *Nat. Geosci.*, *1*, 221–227.

Ramillien, G., et al. (2006), Interannual variations of ice sheets mass balance from GRACE and sea level, *Global Planet. Change*, *53*, 198–208.

Raper, S. C. B., and R. J. Braithwaite (2006), Low sea level rise projections from mountain glaciers and icecaps under global warming, *Nature*, *439*(2006), 311–313.

Raper, C. S. B., J. M. Gregory, and R. J. Stouffer (2002), The role of climate sensitivity and ocean heat uptake on AOGCM transient temperature and thermal expansion response, *J. Clim.*, *15*, 124–130.

Raymond, M. J., and G. H. Gudmundsson (2009), Estimating basal properties of ice streams from surface measurements: A nonlinear Bayesian inverse approach applied to synthetic data, *Cryosphere*, *3*, 265–278, doi:10.5194/tc-3-265-2009.

Retzlaff, R., and C. R. Bentley (1993), Timing of stagnation of Ice Stream C, West Antarctica, from short-pulse radar studies of buried surface crevasses, *J. Glaciol.*, *39*, 553–561.

Rignot, E., and P. Kanagaratnam (2006), Changes in the velocity structure of the Greenland *Ice* Sheet, *Science*, *311*(5763), 986–990, doi:10.1126/science.1121381.

Rignot, E. B., et al. (2008), Antarctic ice mass loss from radar interferometry and regional climate modelling, *Nat. Geosci.*, *1*, 106–110.

Rignot, E., J. Mouginot, and B. Scheuchl (2011), Ice flow of the Antarctic ice sheet, *Science*, *333*, 1427–1430, doi:10.1126/science.1208336.

Ritz, C., V. Rommelaere, and C. Dumas (2001), Modeling the evolution of Antarctic ice sheet over the last 420,000 years: Implications for altitude changes in the Vostok region, *J. Geophys. Res.*, *106*, 31,943–31,964.

Riva, R. E. M., B. C. Gunter, T. J. Urban, B. L. A. Vermeersen, R. C. Lindenbergh, M. M. Helsen, J. L. Bamber, R. de Wal, M. R. van den Broeke, and B. E. Schutz (2009), Glacial isostatic adjustment over Antarctica from combined ICESat and GRACE satellite data, *Earth Planet. Sci. Lett.*, *288*(3–4), 516–523, doi:10.1016/j.epsl.2009.10.013.

Roemmich, D., et al. (2010), Global ocean warming and Sea level rise, in *Understanding Sea Level Rise and Variability*, edited by J. Church et al., Wiley-Blackwell, Oxford, UK, doi:10.1002/9781444323276.ch6.

Rohling, E. J., K. Grant, M. Bolshaw, A. P. Roberts, M. Siddall, C. H. Hemleben, and M. Kucera (2009), Antarctic temperature and global sea level closely coupled over the past five glacial cycles, *Nat. Geosci.*, *2*, 500–504, doi:10.1038/ngeo557.

Ross, N., R. G. Bingham, H. F. J. Corr, F. Ferraccioli, T. A. Jordan, A. Le Brocq, D. M. Rippin, D. Young, D. D. Blankenship, and M. J. Siegert (2012), Steep reverse bed slope at the grounding line of the Weddell Sea sector in West Antarctica, *Nat. Geosci.*, *5*, 393–396, doi:10.1038/ngeo1468.

Scambos, T. A., J. A. Bohlander, C. A. Shuman, and P. Skvarca (2004), Glacier acceleration and thinning after ice shelf collapse in the Larsen B embayment, Antarctica, *Geophys. Res. Lett.*, *31*, L18402, doi:10.1029/2004GL020670.

Schaeffer, M., W. Hare, S. Rahmstorf, and M. Vermeer (2012), Long-term sea-level rise implied by 1.5°C and 2°C warming levels, *Nat. Clim. Change*, *2*, 867–870, doi:10.1038/NCLIMATE1584.

Schäfer, M., T. Zwinger, P. Christoffersen, F. Gillet-Chaulet, K. Laakso, R. Pettersson, V. A. Pohjola, T. Strozzi, and J. C. Moore (2012), Sensitivity of basal conditions in an inverse model: Vestfonna Ice-Cap, Nordaustlandet/Svalbard, *Cryosphere*, *6*, 771–783.

Schneider, D. P., C. Deser, and Y. Okumura (2011), An assessment and interpretation of the observed warming of West Antarctica in the austral spring, *Clim. Dyn.*, *38*, 323–347, doi:10.1007/s00382-010-0985-x.

Schoof, C. (2005), The effect of cavitation on glacier sliding, *Proc. R. Soc. A*, *461*, 609–627, doi:10.1098/rspa.2004.1350.

Schoof, C. (2007a), Ice sheet grounding line dynamics: Steady states, stability and hysteresis, *J. Geophys. Res.*, *112*, F03S28, doi:10.1029/2006JF000664.

Schoof, C. (2007b), Marine ice sheet dynamics, part 1. The case of rapid sliding, *J. Fluid Mech.*, *573*, 27–55.

Schoof, C. (2009), Coulomb friction and other sliding laws in a higher order glacier flow model, *Math. Models Methods Appl. Sci.*, *20*(1), 157–189.

Schoof, C. (2010), Ice sheet acceleration driven by melt supply variability, *Nature*, *468*, 803–806, doi:10.1038/nature09618.

Schoof, C. (2011), Marine ice sheet dynamics, part 2. A Stokes flow contact problem, *J. Fluid Mech.*, *679*, 122–255.

Schoof, C., and R. C. A. Hindmarsh (2010), Thin-film flows with wall slip: An asymptotic analysis of higher order glacier flow models, *Q. J. Mech. Appl. Math.*, *63*(1), 73–114, doi:10.1093/qjmam/hbp025.

Seddik, H., R. Greve, T. Zwinger, and L. Placidi (2011), A full-Stokes ice flow model for the vicinity of Dome Fuji, Antarctica, with induced anisotropy and fabric evolution, *The Cryosphere*, *5*, 495–508, doi:10.5194/tc-5-495-2011.

Seddik, H., R. Greve, T. Zwinger, F. Gillet-Chaulet, and O. Gagliardini (2012), Simulations of the Greenland ice sheet 100 years into the future with the full Stokes model Elmer/Ice, *J. Glaciol.*, *58*(209), 427–440.

Shepherd A., et al. (2012), A reconciled estimate of ice-sheet mass balance, *Science*, *338*, 1183–1189, doi:10.1126/science.1228102.

Sivan, D., et al. (2004), Ancient coastal wells of Caesarea Maritima, Israel, an indicator for sea level changes during the last 2000 years, *Earth Planet. Sci. Lett.*, *222*, 315–330, doi:10.1016/j.epsl.2004.02.007.

Slangen, A. B. A., and R. S. W. van de Wal (2011), An assessment of uncertainties in using volume-area modelling for computing the twenty-first century glacier contribution to sea-level change, *Cryosphere*, *5*, 673–686, doi:10.5194/tc-5-673-2011.

Slangen, A. B. A., C. A. Katsman, R. S. W. van de Wal, L. L. A. Vermeersen, and R. E. M. Riva (2011), Towards regional projections of twenty-first century sea-level change based on IPCC SRES scenarios, *Clim. Dyn.*, doi:10.1007/s00382-011-1057-6.

Sokolov, A. P., C. E. Forest, and P. H. Stone (2003), Comparing oceanic heat uptake in AOGCM transient climate change experiments, *J. Clim.*, *16*, 1573–1582.

Solomon, S., G. Plattner, R. Knutti, and P. Friedlingstein (2009), Irreversible climate change due to carbon dioxide emissions, *Proc. Natl. Acad. Sci. U. S. A.*, *106*, 1704–1709.

Sørensen, L. S., S. B. Simonsen, K. Nielsen, P. Lucas-Picher, G. Spada, G. Adalgeirsdottir, R. Forsberg, and C. S. Hvidberg (2011), Mass balance of the Greenland ice sheet (2003–2008) from ICESat data—The impact of interpolation, sampling and firn density, *Cryosphere*, *5*, 173–186, doi:10.5194/tc-5-173-2011.

Stammer, D., N. Agarwal, P. Herrmann, A. Köhl, and C. R. Mechoso (2011), Response of a coupled ocean–atmosphere model to Greenland ice melting, *Surv. Geophys.*, *32*, 621–642, doi:10.1007/s10712-011-9142-2.

Steig, E. J., Q. Ding, D. S. Battisti, and A. Jenkins (2012), Tropical forcing of Circumpolar Deep Water Inflow and outlet glacier thinning in the Amundsen Sea Embayment, West Antarctica, *Ann. Glaciol.*, *53*, 19–28, doi:10.3189/2012AoG60A110.

Tedesco, M., X. Fettweis, M. R. van den Broeke, R. S. W. van de Wal, C. J. P. P. Smeets, W. J. van de Berg, M. C. Serreze, and J. E. Box (2011), The role of albedo and accumulation in the 2010 melting record in Greenland, *Environ. Res. Lett.*, *6*, 014005.

Tett, S. F. B., R. Betts, T. J. Crowley, J. Gregory, T. C. Johns, A. Jones, T. J. Osborn, E. Ostrom, D. L. Roberts, and M. J. Woodage (2007), The impact of natural and anthropogenic forcings on climate and hydrology since 1550, *Clim. Dyn.*, *28*(1), 3–34.

Thoma, M., A. Jenkins, D. Holland, and S. Jacobs (2008), Modelling Circumpolar Deep Water intrusions on the Amundsen Sea continental shelf, Antarctica, *Geophys. Res. Lett.*, *35*, L18602, doi:10.1029/2008GL034939.

Thomas, R. H., E. J. Rignot, K. Kanagaratnam, W. B. Krabill, and G. Casassa (2004), Force-perturbation analysis of Pine Island Glacier, Antarctica, suggests cause for recent acceleration, *Ann. Glaciol.*, *39*, 133–138, doi:10.3189/172756404781814429.

Thomas, I. D., et al. (2011), Widespread low rates of Antarctic glacial isostatic adjustment revealed by GPS observations, *Geophys. Res. Lett.*, *38*, L22302, doi:10.1029/2011GL049277.

Timmermann, R., Q. Wang, and H. H. Hellmer (2012), Ice shelf basal melting in a global finite-element sea ice–ice shelf–ocean model, *Ann. Glaciol.*, *53*, 303–314.

Toker, E., D. Sivan, E. Stern, B. Shirman, M. Tsimplis, and G. Spada (2012), Evidence for centennial scale sea level variability during the Medieval Climate Optimum (Crusader Period) in Israel, eastern Mediterranean, *Earth Planet. Sci. Lett.*, *315–316*, 51–61.

Tsonis, A. A., K. L. Swanson, and P. J. Roebber (2006), What do networks have to do with climate?, *Bull. Am. Meteorol. Soc.*, *87*(5), 585–595.

Tulaczyk, S. M., B. Kamb, and H. F. Engelhardt (2000), Basal mechanics of Ice Stream B, West Antarctica. II. Undrained-plastic-bed model, *J. Geophys. Res.*, *105*(B1), 483–494.

Unal, Y. S., and M. Ghil (1995), Interannual an interdecadal oscillation patterns in sea level, *Clim. Dyn.*, *11*, 255–278

Van den Broeke, M., J. Bamber, J. Ettema, E. Rignot, E. Schrama, W. J. van de Berg, E. van Meijgaard, I. Velicogna, and B. Wouters (2009), Partitioning recent Greenland mass loss, *Science*, *326*(5955), 984–986, doi:10.1126/science.1178176.

Van der Veen, C. J. (1999), *Fundamentals of Glacier Dynamics*, 462 pp., A. A. Balkema, Rotterdam, Netherlands.

Van Dyke, M. D. (1964), *Perturbation Methods in Fluid Mechanics*, Academic Press, New York.

Van Veen, J. (1945), Bestaat er een geologische bodemdaling te Amsterdam sedert 1700?, *Tijdschr. K. Ned. Aardrijksk. Genoot*., LXII, 2–36.

Vaughan, D. G. (2008) West Antarctic Ice Sheet collapse the fall and rise of a paradigm, *Clim. Change*, *91*, 65–79.

Velicogna, I. (2009), Increasing rates of ice mass loss from the Greenland and Antarctic ice sheets revealed by GRACE, *Geophys. Res. Lett.*, *36*, L19503, doi:10.1029/2009GL040222.

Velicogna, I., and J. Wahr (2006), Measurements of time-variable gravity show mass loss in Antarctica, *Science*, *311*(5768), 1754–1756, doi:10.1126/science.1123785.

Vermeer, M., and S. Rahmstorf (2009), Global sea level linked to global temperature, *Proc. Natl. Acad. Sci. U. S. A.*, *106*, 21,527–21,532.

Vernon, C. L., J. L. Bamber, J. E. Box, M. R. van den Broeke, X. Fettweis, E. Hanna, and P. Huybrechts (2013), Surface mass balance model intercomparison for the Greenland ice sheet, *Cryosphere*, *7*, 599–614.

Vieli, A., and A. Payne (2005), Assessing the ability of numerical ice sheet models to simulate grounding line migration, *J. Geophys. Res.*, *110*, F01003, doi:10.1029/2004JF000202.

Vinther, B. M., et al. (2009), Holocene thinning of the Greenland Ice Sheet, *Nature*, *461*(17), 385–388.

Vizcaino, M., et al. (2008), Long-term ice sheet-climate interactions under anthropogenic greenhouse forcing simulated with a complex Earth System Model, *Clim. Dyn.*, *31*, 665–690.

Von Storch, H., E. Zorita, and J. F. Gonzalez-Rouco (2008), Relationship between global mean sea-level and global mean temperature in a climate simulation of the past millennium, *Ocean Dyn.*, *58*(3-4), 227–236.

Wada, Y., L. P. H. van Beek, C. M. van Kempen, J. W. T. M. Reckman, S. Vasak, and M. F. P. Bierkens (2010), Global depletion of groundwater resources, *Geophys. Res. Lett.*, *37*, L20402, doi:10.1029/2010GL044571.

Wada, Y., L. P. H. van Beek, F. C. Sperna Weiland, B. F. Chao, Y.-H. Wu, and M. F. P. Bierkens (2012), Past and future contribution of global groundwater depletion to sea-level rise, *Geophys. Res. Lett.*, *39*, L09402, doi:10.1029/2012GL051230.

Wake, L. M., P. Huybrechts, J. E. Box, E. Hanna, I. Janssens, and G. A. Milne (2009), Surface mass-balance changes of the Greenland ice sheet since 1866, *Ann. Glaciol.*, *50*, 178–184, doi:10.3189/172756409787769636.

Walter, F., S. O'Neel, D. McNamara, W. T. Pfeffer, J. N. Bassis, and H. A. Fricker (2010), Iceberg calving during transition from grounded to floating ice: Columbia Glacier, Alaska, *Geophys. Res. Lett.*, *37*, L15501, doi:10.1029/2010GL043201.

Warrick, R. A., C. Le Provost, M. F. Meier, J. Oerlemans, and P. L. Woodworth (1996), Changes in sea level, in *Second Assessment Report of IPCC*, edited by J. J Houghton et al., pp. 362–405, Cambridge Univ. Press, Cambridge.

Weertman, J. (1974), Stability of the junction of an ice sheet and an ice shelf, *J. Glaciol.*, *13*, 3–11.

Wei, T., et al. (2012), Developed and developing world responsibilities for historical climate change and CO_2 mitigation, *Proc. Natl. Acad. Sci. U. S. A.*, *109*(32), 12911–12915, doi/10.1073/pnas.1203282109.

Weijer, W., M. E. Maltrud, M. W. Hecht, H. A. Dijkstra, and M. A. Kliphuis (2012), Response of the Atlantic Ocean circulation to Greenland Ice Sheet melting in a strongly-eddying ocean model, *Geophys. Res. Lett.*, *39*, L09606, doi:10.1029/2012GL051611.

van der Wel, N., P. Christoffersen, and M. Bougamont (2013), The influence of subglacial hydrology on the flow of Kamb Ice Stream, West Antarctica, *J. Geophys. Res. Earth Surf.*, *118*, 97–110, doi:10.1029/2012JF002570.

World Glacier Monitoring Service (2009), *Glacier Mass Balance Bulletin No. 10 (2006–2007)*, edited by W. Haeberli et al., 96 pp., Zurich, Switzerland.

Whitehouse, P. L., M. J. Bentley, and A. M. Le Brocq (2012a), A deglacial model for Antarctica: Geological constraints and glaciological modelling as a basis for a new model of Antarctic glacial isostatic adjustment, *Quat. Sci. Rev.*, *32*, 1–24.

Whitehouse, P. L., M. J. Bentley, G. A. Milne, M. A. King, and I. D. Thomas (2012b), A new glacial isostatic adjustment model for Antarctica: calibrated and tested using observations of relative sea-level change and present-day uplift rates, *Geophys. J. Int.*, *190*(3), 1464–1482, doi:10.1111/j.1365-246X.2012.05557.x.

Wingham, D. J., D. W. Wallis, and A. Shepherd (2009), Spatial and temporal evolution of Pine Island Glacier thinning, 1995–2006, *Geophys. Res. Lett.*, *36*, L17501, doi:10.1029/2009GL039126.

Winkelmann, R., and A. Levermann (2012), Linear response functions to project contributions to future sea level, *Clim. Dyn.*, *40*, 2579–2588, doi:10.1007/s00382-012-1471-4.

Winkelmann, R., A. Levermann, K. Frieler, and M. A. Martin (2012), Uncertainty in future solid ice discharge from Antarctica, *Cryosphere Discuss.*, *6*(2012), 673–714, doi:10.5194/tcd-6-673-2012.

Winkler, C. R., M. Newman, and P. D. Sardeshmukh (2001), A linear model of wintertime low-frequency variability. Part I: Formulation of forecast skill, *J. Clim.*, *14*, 4474–4494.

Woodworth, P. L. (1999), High waters at Liverpool since 1768: The UK's longest sea level record, *Geophys. Res. Lett.*, *26*(11), 1589–1592.

Wu, X. P., M. B. Heflin, H. Schotman, B. L. A. Vermeersen, D. A. Dong, R. S. Gross, E. R. Ivins, A. Moore, and S. E. Owen (2010), Simultaneous estimation of global present-day water transport and glacial isostatic adjustment, *Nat. Geosci.*, *3*(9), 642–646, doi:10.1038/ngeo938.

Xu, B., et al. (2009), Black soot and the survival of Tibetan glaciers, *Proc. Natl. Acad. Sci. U. S. A.*, *106*(52), 22,114–22,118.

Yang, Z., K. O. Emery, and X. Yui (1989), Historical development and use of thousand year old tide prediction tables, *Limnol. Oceanogr.*, *34*, 953–957.

Yin, J. (2012), Century to multi-century sea level rise projections from CMIP5 models, *Geophys. Res. Lett.*, *39*, L17709, doi:10.1029/2012GL052947.

Yin, J., J. T. Overpeck, S. M. Griffies, A. Hu, J. L. Russell, and R. J. Stouffer (2011), Different magnitudes of projected suburface ocean warming around Greenland and Antarctica, *Nat. Geosci.*, *4*, 524–528, doi:10.1038/NGEO1189.

Zwally, H., and M. B. Giovinetto (2011), Overview and assessment of Antarctic ice-sheet mass balance estimates: 1992–2009, *Surv. Geophys.*, *32*, 351–376.

Zwally, H. J., W. Abdalati, T. Herring, K. Larson, J. Saba, and K. Steffen (2002), Surface melt-induced acceleration of Greenland ice-sheet flow, *Science*, *297*(5579), 218–222, doi:10.1126/science.1072708.

Zwally, H. J., et al. (2011), Greenland ice sheet mass balance: Distribution of increased mass loss with climate warming; 2003–07 versus 1992–2002, *J. Glaciol.*, *57*, 88–102.

Zwinger, T., and J. C. Moore (2009), Diagnostic and prognostic simulations with a full Stokes model accounting for superimposed ice of Midtre Lovenbreen, Svalbard, *Cryosphere*, *3*, 217–229.

Zwinger, T., R. Greve, O. Gagliardini, T. Shiraiwa, and M. Lyly (2007), A full Stokes-flow thermo-mechanical model for firn and ice applied to the Gorshkov crater glacier, Kamchatka, *Ann. Glaciol.*, *45*, 29–37.